

*Rolled up microtubes for the capture,
guidance and release of single spermatozoa*

Dissertation

zur Erlangung des akademischen Grades

Doctor rerum naturalium

(Dr. rer. nat.)

vorgelegt am 03.03.2016

der Fakultät für Mathematik und Naturwissenschaften

der Technischen Universität Dresden

von Veronika Magdanz

geboren am 18.04.1985 in Rathenow

Tag der Verteidigung: 24.10.2016

Die Dissertation wurde in der Zeit von April 2012 bis Februar 2016 am Leibniz Institut
für Festkörper- und Werkstoffforschung Dresden e.V. angefertigt.

Gutachter: Prof. Dr. Stefan Diez

Prof. Dr. Oliver G. Schmidt

Parts of this thesis have been published in the following peer reviewed journal articles and reprinted figures are copyrighted by the respective publisher as indicated. Reuse is in accordance with the author rights granted in the Copyright Transfer Agreements.

V. Magdanz, S. Sanchez, O. G. Schmidt: *Development of a sperm-flagella driven micro-bio-robot*. *Advanced Materials* 2013, vol. 25, 45, pp. 6581-6588.

V. Magdanz, G. Stoychev, L. Ionov, S. Sanchez, O. G. Schmidt: *Stimuli-responsive microjets with reconfigurable shape*. *Angewandte Chemie International Edition* 2014, vol. 53, 10, pp. 2673-2677.

V. Magdanz, M. Guix, O. G. Schmidt: *Tubular micromotors: from microjets to spermbots*. *Robotics and Biomimetics* 2014, vol.1, 11, pp. 1-10.

V. Magdanz, O. G. Schmidt: *Spermrobots: Potential impact for drug delivery and assisted reproductive technologies (Editorial)*. *Expert Opinion on Drug Delivery* 2014, vol. 11, 8, Informa Healthcare, pp. 1125-1129.

I. S. M. Khalil, **V. Magdanz**, S. Sanchez, O. G. Schmidt, S. Misra: *Biocompatible, accurate, and fully autonomous: A sperm-driven micro-bio-robot*. *Journal of Micro-Bio Robotics* 2014, vol. 9, 3-4, pp. 79-86.

V. Magdanz, M. Medina-Sanchez, Y. Chen, M. Guix, O. G. Schmidt: *How to Improve Spermrobot Performance*. *Advanced Functional Materials* 2015, vol. 25, 18, pp. 2763-2770.

V. Magdanz, M. Guix, F. Hebenstreit, O. G. Schmidt: *Dynamic polymeric microtubes for the remote-controlled capture, guidance and release of sperm cells*. *Advanced Materials* 2016, vol. 28, 21, pp. 4084-4089.

Back Cover design by Thomas Sasse

Collage from press releases in response to the publication in *Advanced Materials* 2013, vol. 25, 45, pp. 6581-6588:

New Scientist, 13.12.2013: „How do you control a spermbot? Try a magnetic field“

Daily News, 13.12.2013: „Scientists create ‘robotic sperm’ controlled by magnets“

Tech Times, 15.12.2013: „Scientists create spermbot...what?!?“

Diari de Girona, 06.10.2015: “Spermbot”

The Week, The idea factory by Emily Shire, 13.12.2013: “How sperm could one day cure cancer”

Batanga, accessed 03.02.2016: “Spermbots: espermatozoides robot controlados magnetismo”

The independent, 25.05.2014: “Scientist create ‘robotic sperm’ to help with fertilization and drug delivery”

International Science Times, 13.12.2013: „‘Spermbot’ could be used to fertilize eggs, deliver targeted medicine in humans“

ExtremeTech, 16.12.2013: „Spermbots: Remote-controlled sperm, for guaranteed delivery“

Gurumed, 14.12.2013: „SpermBot ou comment capturer un spermatozoide pour le controler a l’interieur du corps?“

El Mundo, 02.02.2014: “El (e)nano robot cargado con un espermatozoide que las embaraza”

GMA News Online, 13.12.2013: “Scientists create magnetic ‘mecha-sperm’ for drug delivery, fertilization”

Fertility Law Group, 11.03.2014: “Spermbots and Nanoparticles offer high-tech infertility solutions”

Physics News, 13.12.2013: “Robo-sperm could be the drug delivery mechanism of the future”

EMDT, 20.12.2013: “Researchers build sperm drive for micro-robots”

Motherboard, 13.12.2013: “Sperm-powered micro-robots could offer a new method of fertilization”

Prima Zoom, accessed 03.02.2016: “Robotické spermie jsou tady. Vedci vytvořili něco pozoruhodného”

Wikistrike, 16.12.2013: “Des scientifiques inventent le spermot, un robot biunique a base de sperme”

Phys.org, 17.01.2014: “Sperm-bots are made to move in desired direction”

Le Figaro, 13.12.2013: “Spermots: des spermatozoides ‘robots’ pour lutter contre l’infertilité”

BBC Persian, 22.12.2013

Mail Online, 25.05.2014 “Birth of the robo-sperm: Scientist create first cyborg sperm that can be remote-controlled using magnets”

DiarioAbierto.es, 20.01.2014: “Spermots, la fertilidad por control remoto”

Fox News Network, 15.12.2013: “New strides against infertility”

Discover Magazine, 12.12.2013 “Robo-sperm could be the drug delivery mechanism of the future”

Berliner Zeitung, “Deutsche Forscher entwickeln Spermien mit Fernsteuerung”

SELBSTSTÄNDIGKEITSERKLÄRUNG

Hiermit erkläre ich an Eides statt, dass ich die am heutigen Tag eingereichte Dissertation zum Thema „Rolled up microtubes for the capture, guidance and release of single spermatozoa“ unter der Betreuung von Herrn Prof. Dr. Stefan Diez und Herrn Prof. Dr. Oliver G. Schmidt in der Zeit von April 2012 bis Februar 2016 am Institut für Integrative Nanowissenschaften des Leibniz Instituts für Festkörper- und Werkstoffforschung, IFW Dresden, selbstständig erarbeitet habe. Hiermit versichere ich, dass ich die vorliegende Arbeit ohne zulässige Hilfe Dritter und ohne Benutzung anderer Hilfsmittel angefertigt habe und Zitate kenntlich gemacht habe. Die Dissertation wurde in dieser oder ähnlicher Form an keiner anderen Stelle weder im Inland noch im Ausland zum Zwecke eines Promotionsverfahrens eingereicht. Es wurde von mir bisher kein Promotionsverfahren an anderer Stelle beantragt. Ich erkenne die Promotionsordnung der Fakultät für Mathematik und Naturwissenschaften der Technischen Universität Dresden vom 23.02.2011 an.

Dresden, den 03.03.2016

Veronika Magdanz

ABSTRACT

The search for autonomously moving, highly functional and controllable microdevices is a purpose of current micro/nanobiotechnology research, especially in the area of biomedical applications, for which reason, biocompatible solutions are in demand. In this thesis, a novel type of hybrid microswimmer is fabricated by the combination of rolled up thin nanomembranes with bovine spermatozoa. The microbiorobot presented here uses the powerful motion of the sperm flagella as a propulsion source for the magnetic microtube. This work demonstrates how the microswimmer performs its motion and how several factors such as temperature, radius of the microtube, penetration of the cell inside the microtube and length of the tube have influence on its performance. Directional control mechanisms are offered by external magnetic fields and are presented to be useful for the on-chip separation of the microbiorobots from a mixture of cells and microtubes. Two surface modification methods are presented as means to improve the coupling efficiency between the microtubes and the sperm cells. By these surface functionalizations, the extracellular matrix protein fibronectin is attached on the inner microtube walls and serves as binding agent for the spermatozoa. Finally, a remote release mechanism for the sperm cells is demonstrated by the incorporation of thermoresponsive material into the microtubes, which makes them fold and unfold upon small temperature changes. This work discusses the potential of such microswimmers for the application in assisted reproduction techniques and gives an outlook on future perspectives.

TABLE OF CONTENTS

SELBSTSTÄNDIGKEITSERKLÄRUNG	0
ABSTRACT	1
TABLE OF CONTENTS	3
1 MOTIVATION AND GOALS	5
1.1 MINIATURIZATION: “THERE IS PLENTY OF ROOM AT THE BOTTOM...”	5
1.2 SPERMBOTS: POTENTIAL IMPACT	7
2 BACKGROUND AND STATE-OF-THE-ART	11
2.1 MICROBIOROBOTICS	11
2.2 SPERM MORPHOLOGY AND THEIR JOURNEY TO THE EGG	15
2.3 INFERTILITY AND ASSISTED REPRODUCTION TECHNIQUES.....	19
2.4 SINGLE CELL RELEASE	22
2.5 STIMULI-RESPONSIVE MATERIALS	25
3 MATERIAL AND METHODS	29
3.1 ROLLED UP TECHNOLOGY	29
3.2 TREATMENT OF BOVINE SPERMATOZOA	32
3.2.1 <i>Preparation of Spermibots</i>	32
3.2.2 <i>Speed Measurements</i>	33
3.2.3 <i>Separation On Chip</i>	33
3.3 SURFACE MODIFICATION OF MICROTUBES.....	34
3.3.1 <i>Surface Chemistry</i>	35
3.3.2 <i>Microcontact printing</i>	39
3.4 POLYMER TUBE FABRICATION.....	44
3.4.1 <i>Synthesis of photosensitive monomer 4-Acryloylbenzophenone</i>	44
3.4.2 <i>Synthesis of poly (N-isopropylacrylamide-co-Acryloylbenzophenone)</i>	46
3.4.3 <i>Photolithography of polymeric films</i>	48
3.5 VIABILITY TESTS.....	51
4 RESULTS AND DISCUSSION	53
4.1 CHARACTERIZATION OF SPERMBOTS	55
4.2 TEMPERATURE INFLUENCE.....	60
4.3 MAGNETIC CONTROL	62
4.4 SEPARATION ON CHIP	68

4.5	EFFECT OF DECREASED MICROTUBE LENGTH	72
4.6	COUPLING EFFICIENCY	74
4.7	THERMORESPONSIVE POLYMERIC MICROTUBES FOR CELL RELEASE	80
4.8	SPERM VIABILITY TESTS	94
5	SUMMARY AND CONCLUSIONS.....	97
6	OUTLOOK.....	101
7	LIST OF FIGURES	107
8	LIST OF TABLES	113
9	ABBREVIATIONS	115
10	CURRICULUM VITAE	117
11	LIST OF PUBLICATIONS	119
	JOURNAL ARTICLES	119
	CONTRIBUTIONS TO COLLECTED EDITIONS/PROCEEDINGS	121
12	ACKNOWLEDGEMENTS	123
13	REFERENCES	125

1 MOTIVATION AND GOALS

1.1 MINIATURIZATION: “THERE IS PLENTY OF ROOM AT THE BOTTOM...”

Richard Feynman mentioned in his lecture “There is plenty of room at the bottom” that it would be a wild and interesting idea to “swallow the surgeon”;^[1] that this tiny person would move around inside the body, find out what the problem is and do the surgery on the inside, without cutting through the skin.

This visionary idea of miniaturization of a surgeon has fascinated humans ever since. Science fiction picked up this topic, particularly in the 1966 movie “Fantastic Voyage”^[2] in which a medical crew with a submarine is miniaturized so that it can maneuver through the human blood and brain vessels to perform surgery in order to cure an injury of the brain. Certainly, also researchers have been intrigued by this idea and a huge effort is being made by the nano-and microrobotics research communities worldwide to see the vision of miniaturization of medical operations come true in the future. The miniaturization of a highly functional and complex system involves different aspects. First of all, the environmental conditions for the motion on the micro-and nanoscale are different than on the macroscale. In order to move forward on the microscale, where inertial forces play no role and forces caused by friction are predominant phenomena,^[3] a swimmer needs to be able to perform a non-reciprocal motion so that it moves forward. Therefore,

macroscopic designs of motors and machines can not necessarily be adapted for microscopic motion and researchers are called to create novel approaches that enable efficient movement on the microscale. Furthermore, the control mechanisms of such microswimmers need to be adjusted because positioning, manipulation and steering are far more challenging on the small scale. The performance of robotic tasks such as sensing need to offer microscale resolution, which is another challenging task in the development of autonomous mobile microdevices.^[4] These devices can be defined as microbiorobots, because they move on the microscale, use biological power sources and are created to perform robotic tasks.

The development of a new microbiorobot by combining single sperm cells with rolled-up microtubes leads to the creation of “spermbots” and is the main motivation of this work. The following sections 1 and 2 shall give an introduction to the specific potential of such microbiorobots and how this new approach is embedded in the field of microbiorobotics. Due to the specific potential of spermbots for reproductive medicine, background information on infertility and assisted reproduction techniques is given in section 2.2.

1.2 SPERMBOTS: POTENTIAL IMPACT

Magnetic microtubes offer a method for the capture and remote control of motile cells. One vision of using spermbots is to guide single motile sperm cells to the oocyte location and achieve assisted fertilization *in vivo*, as visualized schematically in Figure 1. This is especially appealing in cases that chemotactic or thermotactic response of spermatozoa is dysfunctional, very few motile sperm are being produced (oligozoospermia, involved in about 15 % of male infertility cases^[5]) or sperm cells simply do not find the oocyte location on their own for unknown reasons. Spermbot-assisted fertilization might be less invasive and more natural than existing artificial reproduction techniques and therefore might result in higher success rates. One major difference will be that the oocytes can remain *in vivo* in their natural environment and selected sperm cells are brought to the fertilization site. An overview of the state-of-the-art artificial reproduction techniques will be given in section 2.2. Up to date, there is still much unknown about how spermatozoa reach the egg in the reproductive system. The guided microtube-sperm motor might serve as an explorative or diagnostic tool that gives insight about the sperm journey through the female reproductive system. Spermbots could be utilized for fallopian tube diagnostics or even treatment of female infertility conditions, or to explore the reasons for unknown infertility, because they likely offer less intrusive procedures than catheters. Yet, this all remains hypothetical and the following requirements are very important to pursue such an

approach. First, the capture of single spermatozoa is a pre-requisite. Secondly, the guidance of the spermatozoa in a remote-controlled way needs to be achieved. As a third step, after guidance to the target location, the single spermatozoon has to be released. Furthermore, tracking and visualization techniques that allow spatial and temporal resolution of the spermbots during *in vivo* applications of the spermbots have to be developed. In addition, the biocompatibility and immune response of the involved materials need to be studied and, finally, the fertilization capability of the released sperm cell has to be guaranteed. The fertilization success will depend on the quality of sperm selection prior to capturing the cells and sperm maturation, as it occurs during the *in vivo* passage to the oocyte.

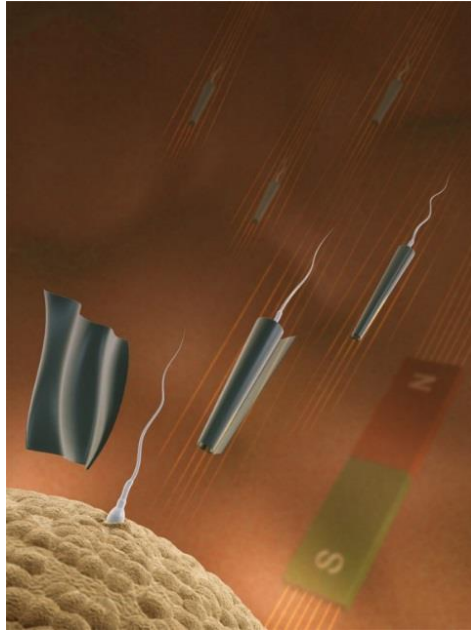


Figure 1: Schematic image of the vision of spermbots for assisted fertilization techniques. Modified from [6].

All these requirements are important but exceed the frame of this thesis. However, the achievement of these goals is the emphasis of this initial work. This work focuses on fulfilling the first three requirements: the capture, remote-controlled motion and release of a single sperm cell.

The work presented here demonstrates the first example of combining a single motile cell with a microtube to create a microbiorobot which can be guided to defined positions by an external magnetic field. The sperm cell can enter the microtube and is trapped in the tube cavity. In order to characterize this microbiorobot, the influence of tube radius, tube length, penetration length of cell inside the microtube as well as external factors such as temperature are evaluated. Moreover, the remote-controlled

separation of a selected microbiorobot in a lab-on-a-chip device is demonstrated. Furthermore, the coupling efficiency is described and two surface modification methods are suggested to increase the coupling success between sperm cells and microtubes. Finally, the thermo-triggered release of the sperm cells is achieved at physiological conditions by the use of temperature-responsive microtubes. Cell viability tests prove the biocompatibility of the involved materials.

2 BACKGROUND AND STATE-OF-THE-ART

2.1 MICROBIOROBOTICS

As mentioned in the introduction, the development of highly functional autonomous microdevices, also referred to as ‘microbiorobots’, is an emerging research field that mainly aims at biomedical applications by the use of remote-controlled microdevices driven by biological power sources. This field brings together knowledge from engineering, material science, physics, chemistry, biology and medicine. The purpose of microbiorobotics is either to mimic the behavior of biological components or to use whole cells or their components to create functional microdevices.^[4]

There have been plenty of approaches to develop artificial micromotors of various designs which are driven by chemical fuels,^[7-12] surface tension gradients,^[13,14] ultrasound,^[15,16] magnetic^[17-19] or electric fields.^[20,21] The use of micromotors towards biomedical operations such as sensing, drug delivery, theranostics or micro-surgery has led to interesting progress such as the drilling into tissue and cells, ^[22-24] and the isolation of cancer cells, DNA and proteins.^[8] Other fascinating advances are the demonstration of the operation of an artificial micromotor inside the stomach of a mouse ^[25] or the motion of rod shaped nanomotors inside living cells by ultrasound.^[15] However, the efficient operation in physiological environments and the avoidance of

toxic fuels remain the main challenges for potential biomedical applications of artificial micromachines.

Magnetic swimmers were created to mimic biological flagella in shape and dimension and therefore propel efficiently in low-Reynolds-numbers regimes. Artificial bacterial flagella^[17,18] and flexible magnetic swimmers^[26,27] are examples of such swimmers and can tolerate a large range of conditions. They are helical^[17,18] or flexible^[26,27] elements that propel by non-reciprocal motion. Both kinds of artificial magnetic swimmers do not have an on-board power source and are only actuated and steered if a continuously rotating magnetic field is applied. Flexible magnetic microswimmers require an oscillating transverse field in order to be actuated. Recently, microhelices were used to capture immotile spermatozoa and propel them by a rotating magnetic field.^[28] This application is especially appealing for cases of male infertility due to motion deficiencies of the spermatozoa.

Biological motors such as flagella or cilia as components in micro-actuators are especially intriguing because they have evolved over millions of years to function efficiently on the nano- and microscale in viscous media. The basis of these biological motors consists of biomolecular motor proteins such as myosin, kinesin and dynein which form different complexes that convert chemical energy into mechanical work.^[29] Although molecular motors offer great efficiency for tasks on the nanoscale, their *in vitro* lifetime is limited and their liberty of action is restricted by tracks (e.g. actin filaments) or surface attachments that

are required for their forward motion. However, cargo transport, self-assembly or analyte transport, just to name a few applications, have been demonstrated successfully on the nanoscale with the use of biomolecular motors.^[30 , 31] The first example of integrating a biomolecular motor in a nanodevice was the combination of the enzyme complex F1-ATPase, which is a rotary molecular motor, attached to a nickel post and a nanopropeller^[32] wherein the molecular motor leads to the rotation of the nanopropeller.

Another approach to make use of biological motors is to implement whole cells as actuators. Bacteria and contractile muscle cells have been harnessed as propulsion sources in various approaches for the development of bio-hybrid systems that may perform robotic tasks on the microscale in the future.^[33-41]

Muscle-powered microdevices were first developed based on an assembly of cardiomyocytes, i.e. beating heart cells, and fabricated microstructures that build the scaffold which the contracting cells attach to.^[36] In a similar fashion, cardiomyocytes were cultured along a polydimethylsiloxane filament and created a slender tail that performs a bending wave by the synchronous contraction of the cells.^[33]

Motile bacteria have also been explored for their potential in developing microbiorobots. They have been utilized in creating disk-shaped motors that turn due to the geometrical design in which bacteria get stuck and push in the corners of the disk and lead to a rotational motion similar to a ratchet.^[37] Furthermore, bacteria demonstrated the ability to act as

bacterial carpets that move fluid or push microparticles forward.^[38,39] Microorganisms are especially attractive as components in microrobots because of their sensing and taxis abilities that offer various directional control mechanisms.^[40] For instance, magnetotactic bacteria are being explored for their potential as microcarriers in blood vessels and for cancer therapy.^[41,42] Apart from magnetotaxis,^[43] chemotaxis,^[44] pH-taxis^[45] and electrokinetic control^[46] have been applied as directional control mechanisms of bacterial microrobots. All microbiorobots have in common that they do not need an external power source for their actuation, though on the other hand their activity range is restricted to physiological conditions (temperature and pH tolerance of microorganisms and spermatozoa).

However, none of these approaches offer the selective encapsulation of a single motile sperm cell and directed control over its motility. The motivation for using sperm cells as driving force is not primarily to develop a more efficient microbiorobot (compared to existing hybrid robots) but rather to aspire towards a medical application that involves the controlled guidance of a single sperm cell to an egg cell.

Compared to other types of microparticles (e.g. spheres), rolled-up tubes are advantageous because they consist of carefully designed thin nanomembranes^[12] and thus consist of light-weight structures that serve as multi-functional carriers or scaffolds for cell guidance. Furthermore, the physical confinement of the cell inside the tube cavity avoids the complex biochemical functionalization of the inner tube surface to bind

specifically to sperm membrane proteins without altering the cell motility, in this particular case sperm activity.^[47] In addition, the mechanical trapping method inside a magnetic microtube can be applied to any motile flagellated or ciliated cell.

2.2 SPERM MORPHOLOGY AND THEIR JOURNEY TO THE EGG

At this point, after explaining the potential of spermrobots for assisted reproduction and the background in microbiorobotics, it is appropriate to explain some information on sperm morphology and the migration of spermatozoa *in vivo* to the oocyte where fertilization takes place.

Although there is a huge range in size and shape of the reproductive cells between species, the mechanisms of sexual reproduction are highly conserved. Here, the focus will be on bovine sperm cells, spermatozoa from bulls, since sperms solely from this species are used in this work. All mammalian sperm cells consist of a head, a midpiece and a flagellum. Figure 2 displays a schematic illustration of their morphology. The bovine sperm cells are about 60 – 70 μm long including the sperm head which is around 10 μm long and 5 μm in diameter.^[48] The head has an oval, flat shape and is about 1 μm in thickness. The head contains very crucial components for fertilization. The genetic information is contained in the head as condensed haploid chromosomal DNA which will contribute the male genetic information for the embryo during fertilization. The acrosome is located on the surface of the sperm head

and is a vital part for the fusion with the egg cell. This organelle contains hydrolytic enzymes that are released when the sperm attaches to the zona pellucida, the outer layer of the oocyte. The midpiece contains a large amount of mitochondria which supply the cell with the needed power for flagella beating and other cell activities by generating ATP.^[49]

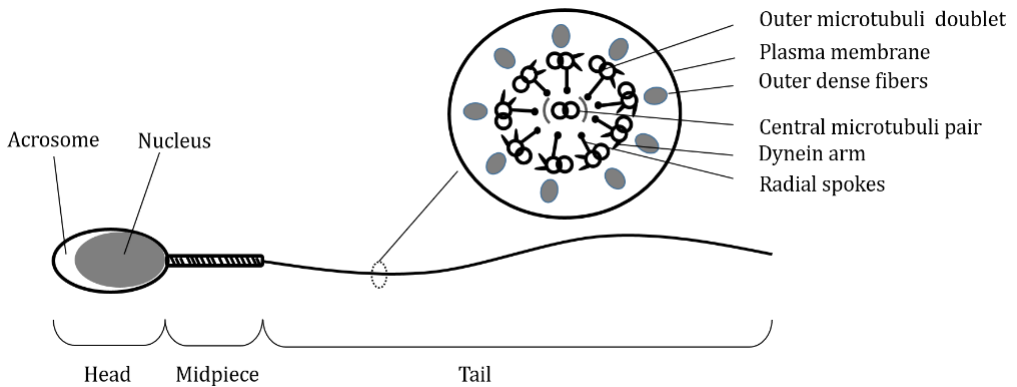


Figure 2: Schematic image of morphology of a bovine sperm cell. The sperm cell consists of a head, midpiece and tail. The inset shows the detailed view of a cross section of the tail.

The sperm tail is the flexible element of the sperm cell which is essential for its motion. The inset in Figure 2 illustrates a cross section of the sperm tail. The tail, as the rest of the cell, are surrounded by the plasma membrane. There are nine outer dense fibers in the tail that are associated with the microtubule doublets and that play a role as stiffening components of the flagella.^[50] The nine outer microtubule doublets as well as the central pair of microtubule are the active elements of the tail.^[49] The motion of the flagella is induced by the sliding of the microtubule pairs towards neighbouring pairs by the force

of dynein arms. Dynein arms are molecular motor proteins which act as linkers between the different microtubule pairs and attach and detach from the microtubule at different times by the conversion of the chemical energy (ATP) into mechanical work. These linkers transform the sliding into a bending motion of the tail.^[49,51]

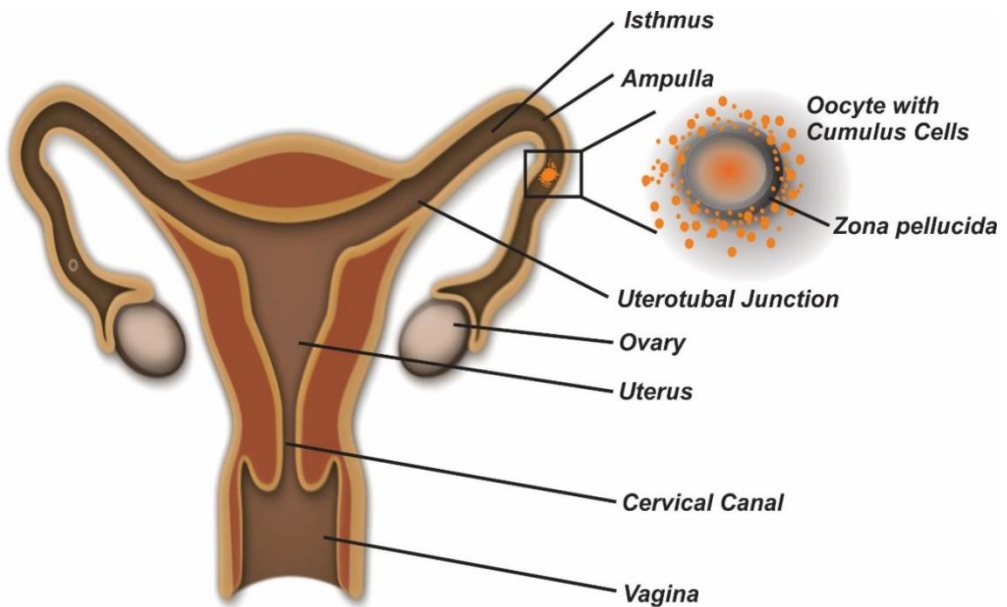


Figure 3: Female reproductive tract. Modified from ^[52].

During their journey to the fertilization site, mammalian sperm cells have to travel a long distance through the female tract to the oocytes. Sperm cells have to pass various obstacles *in vivo*: the vagina, cervix, uterus, uterotubal junction, oviduct (comprising the isthmus and ampulla), the cumulus cells and the zona pellucida which is surrounding the egg (see schematic in Figure 3).^[52-54] The vagina displays an acidic

pH of 5 or lower in humans and is quite hostile for sperm cells. Sperm cells start swimming into the cervical canal where they have to pass through narrow channels filled with mucus into the uterus.^[53] Smooth muscle contractions are thought to support the sperm transport through the uterus to the uterotubal junction. Again, the uterotubal junction displays a barrier for the sperm cells due to the folds filled with viscous mucus.^[53] The following isthmus is a storage site where sperm remain until the egg ovulates.^[54] The spermatozoa bind to the cilia of the oviductal epithelium. The release from the epithelium is associated with capacitation and hyperactivation of the sperm cells. Capacitation is a process that is required by all mammalian sperm cells to become fertile. This ripening process of the spermatozoa prepares them for fertilization and includes the shedding of proteins from the sperm surface and a change in flagellar beating with increased amplitude whereby the cells can release from the attachment sites in the isthmus.^[53] The mechanism of sperm storage and gradual release of sperm cells upon ovulation avoids that more than one sperm fertilizes an egg (polyspermy) which is fatal for embryonic development. In addition, it is thought to be a selection mechanism because sperm cells that are not able to capacitate will not detach from the storage site. This control step is bypassed *in vitro*, where thousands of sperm cells are required for fertilization.^[54] Once the activated sperm cells are in the ampulla, they are attracted by thermotaxis and chemotaxis (gradients of temperature up to 2 °C and chemicals) to the oocyte and surrounding cumulus cells.^[53] Sperm cells adhere and penetrate the zona pellucida by hyaluronidase and protease

activity as well as vigorous sperm motility. The zona pellucida is a thick membrane and displays a “species-specific barrier”.^[54] In order to fuse with the oocyte, sperm cells perform the acrosome reaction. The reaction is supposedly triggered by the contact of the sperm membrane with the zona pellucida, by cumulus cells, or by progesterone, depending on the species.^[54] After passing through the zona pellucida, the sperm cell fuses with the plasma membrane of the oocyte. Although the journey starts off with millions of sperm cells, at this point only very few sperm cells are assumed to reach the location of the oocyte.^[55] Finally, the fertilization is completed when the pronucleus of the sperm cell is formed and fuses with the female pronucleus.^[56]

2.3 INFERTILITY AND ASSISTED REPRODUCTION TECHNIQUES

Infertility is a growing health issue that affects 48.5 million couples worldwide ^[57] and is defined as a disease of the reproductive system^[58] that affects males and females equally. The main causes for female infertility are disorders of the reproductive organs (ovulatory disorders, tubal obstruction, endometriosis, ovulatory dysfunction, uterine and/or cervical factors etc.^[59]). The reason for male infertility can be generalized as low sperm quality, which can be due to low sperm count (oligospermia), poor or no motility of spermatozoa (asthenospermia) and/or abnormal morphology (teratospermia) of sperm cells^[60] and leads to the inability to fertilize an oocyte. It is known that infertility

increases with advanced age and is promoted by unhealthy lifestyles (smoking, alcohol, drug abuse, unhealthy nutrition, no exercise).[61,62]

Human assisted reproduction techniques as means to treat infertility had their first milestone with the birth of Louise Brown in 1978; the first baby conceived by *in vitro* fertilization.[63, 64] However, human reproduction remains a field that is not very well understood and there are still plenty of open questions about fundamental steps that lead to successful fertilization. Possible first steps for treating infertility involve hormonal stimulation and intrauterine insemination (injecting sperms into the uterus during ovulation), which are low-cost and minimally invasive procedures that are suitable in case of cervical factor subfertility, mild-moderate male subfertility and unexplained infertility.[65] If these steps are not successful, *in vitro* fertilization (IVF) or intracytoplasmic sperm injection (ICSI) are possible next steps. IVF and ICSI require the isolation of oocytes and spermatozoa from the human body and the triggering of fertilization *in vitro* by maturing oocytes, adding spermatozoa to the oocytes (in case of ICSI injecting single sperm cells inside the oocyte) and culturing the embryos *in vitro*. Finally, the zygotes are transferred back into the female body for delivery. ICSI and IVF are especially appealing in case of sperm donation or when no motile sperm cells are present, but also in case of tubal blockage. It is also frequently used in cases of unexplained infertility, which accounts for 25 - 30 % of all couples.[66]

These methods are currently the best state-of-the-art artificial reproduction techniques and reach a live birth rate of 30 – 40 %. In addition to the relatively low success rate, challenges of existing artificial reproduction techniques are the increased stress that the couples are exposed to due to the invasive procedure, high costs and an increased rate of miscarriage and birth defects. Besides, ethical ramifications are involved in the *in vitro* reproduction techniques such as the trade of donor sperm and eggs, embryo screening for the purpose of gender selection and diagnosis of inheritable diseases.^[67]

A question that arises from the current state-of-the-art procedures for assisted reproduction is: Is there a more natural procedure possible? The statistics by the German IVF registry 2013 show, starting with 100 % treatments, a successful *in vitro* fertilization rate of 95 % of all treatment cases. The transfer displays a success rate of 94 %, however, only 31 % of the treatments lead to a clinical pregnancy.^[68] Studies show that the low success rate of IVF and ICSI is due to the stress the oocytes and embryos are exposed to during the *in vitro* procedures, which include up to 20 washing and transfer steps.^[69] Instead, might it be possible to offer an assisted *in vivo* reproduction procedure that circumvents the isolation of oocytes from the female body? This is where the spermbots and their potential applications come into play, as discussed in section 1.2.

It should be noted that for patients suffering from oligospermia (having only small amounts of sperm cells), IVF often does not lead to successful

fertilization. It is known that the number of required spermatozoa for *in vitro* fertilization is quite high (a ratio of several thousand sperm cells to one oocyte) compared to the number of sperm cells that reach the oocyte location *in vivo*.^[70] This means that fertilization *in vitro* is far less efficient than in the oviduct where as few as 100 sperm are found present. This indicates that the mimicking of *in vivo* conditions could lower the required sperm-oocyte ratio and increase fertilization rates. The controlled guidance of few sperm cells to the oocyte in the reproductive system, as envisioned by the use of the spermrobots, could lead to successful fertilization with a low sperm-egg ratio.

2.4 SINGLE CELL RELEASE

This work will also demonstrate a cell release mechanism of single cells from dynamic polymeric microtubes. Single cell capture and release is especially of interest in the field of single cell analysis. Various platforms have been developed with complex features for single cell isolation, purification and analysis of different cell properties.^[71-73] Capture and release methods are for instance required for the detection and subsequent analysis of circulating tumor cells. As an example, thermoresponsive polymer brushes have been used to capture and release circulating tumor cells from a blood sample.^[74] These on-chip devices contain static capture and release mechanisms which are either

based on biochemical interactions between the target cells and the surface such as binding to aptamers or antibodies [74,75] or on the mechanical or electrical trapping of cells on-chip.[71]

In contrast, the purpose of this work is, in respect to developing new assisted fertilization techniques, the capture of a motile sperm cell, guidance to a certain location and release of the cell in a remotely controlled way without harming the cell. There are only very few approaches known which can be referred to as state-of-the-art in this field. One approach in the field of animal reproduction is to embed sperm cells into alginate gels.[76,77] These calcium alginate gel capsules maintain the sperm cells in a non-capacitating stage and prolong the fertile period of the spermatozoa during artificial intrauterine insemination and make the time of ovulation less critical. The capsules release sperm cells over time by enzymatic degradation of the shell, providing the extended presence of fertile sperm cells in the animal uterus and thereby increasing fertilization rates.

Approaches to single cell release with grippers have been demonstrated in Gracias' group in several ways. These microgrippers show potential for surgical applications such as biopsy and other robotic tasks. Microgrippers were fabricated from metallic, oxide and also from polymeric materials. They are tetherless devices that fold upon thermal or chemical triggers.[78] Metallic thin films that form rigid panels with flexible joints are used as milliscale grippers for biopsy.[79] In another approach, these metallic grippers were combined with bio-polymeric

hinges that can only be degraded by enzymatic activity and therefore self-fold upon exposure to these enzymes.^[80] With the use of self-folding silicon monoxide/dioxide grippers the capture of single mouse fibroblast cells and red blood cells was demonstrated.^[81] The cells were captured while the structures were still attached to the surface and subsequently released to withdraw the encapsulated cell from its location. These single cell grippers are thought to have potential in utilization for single cell analysis (e.g. genomics, proteomics), diagnostics, therapeutics and surgery. Recently, a type of soft microgripper was developed by the same group based on the hydrogel poly(N-isopropylacrylamide-co-acrylic acid) (PNIPAM-co-AAc) that folds and unfolds by swelling and deswelling in aqueous solution. It was demonstrated that this type of gripper is able to excise cells from a tissue clump or deliver drugs in the pig stomach.^[82] Besides, the thermoresponsive polymer poly(N-isopropylacrylamide) has been used to form self-folding capsules and microtubes that can encapsulate and release yeast cells upon a temperature stimulus.^[83]

Nevertheless, there are no known methods that can remotely control the capture, guidance and release of single sperm cells. The approach in this work includes the fabrication and optimization of thermoresponsive polymeric microtubes that are tailored to capture single sperm cells, guide their motion and release them at physiological temperatures. It is a crucial step to perform the controlled delivery of the cell at a desired location and will be an important progress towards the development of new assisted fertilization techniques.

2.5 STIMULI-RESPONSIVE MATERIALS

Stimuli-responsive materials can change properties depending on the environmental conditions that they are surrounded by. The stimulus that causes these changes can be temperature, pH, light, chemical or biological agents or a signal by an electric or magnetic field.^[84,85] This external signal leads to changes in the conformation, the chemical composition or the solubility of the material. Stimuli-responsive materials are able to undergo these changes rapidly and reversibly many times. They are often considered as “smart” materials and are of interest for diverse applications ranging from the biomedical field (drug delivery, diagnostics, tissue engineering) to the microrobotic field (biosensors, microelectromechanical systems) and advanced material applications (coatings and textiles).^[84] There are many natural polymers that are stimuli-responsive materials, such as gelatin which goes through a sol-gel transition in response to temperature. One very popular artificial stimuli-responsive polymer which has been well investigated over the last decades is poly(N-isopropylacrylamide) (PNIPAM). It has a sol-gel transition temperature close to physiological temperatures (30-35°C) and is known for its sharp temperature response. The temperature-response of PNIPAM is based on the reversible phase transition from a hydrophilic swollen state at temperatures below its lower critical solution temperature (LCST) to a collapsed hydrophobic state at temperatures above its LCST which is based on its inverse solubility in water. PNIPAM polymer networks have a high water content and hence

large volume at room temperature in aqueous solution (see Figure 4 on the left). Hydrogen bonding to the network is favored and leads to the uptake of water. Due to their sensitivity to temperature, the volume of the films shrinks drastically when the polymer is heated above its LCST. The LCST describes the temperature at which the phase transition occurs. The hydrogel collapses and expels the water from its network and becomes hydrophobic at temperatures above its LCST, as displayed schematically in Figure 4 on the right.

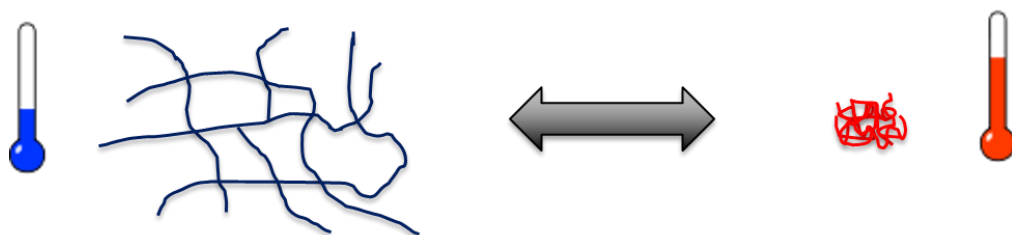


Figure 4: PNIPAM network below (left) and above (right) the lower critical solution temperature.

When a bilayer of two materials with different swelling properties is formed, one being PNIPAM, the swelling and collapsing can be used to apply a geometrical change from two-dimensional films to three-dimensional structures.^[86] Poly(N-isopropylacrylamide) has been fabricated on the molecular level as single chains, macroscopic gels, microgels, latexes, thin films, membranes, coatings and fibers.^[87] The most common methods to synthesize the polymer PNIPAM are free radical initiation in organic solutions or redox initiation in aqueous media.^[87]

PNIPAM is the polymer of choice in this work because of its sharp temperature response which offers shape modulation of two-dimensional films into three-dimensional rolled up microtubes. The thermoresponsive polymer PNIPAM has been used widely for the design of microactuators, drug carriers and micromotors due to its stimuli-response which can be utilized for folding two-dimensional films into complex three-dimensional microstructures that are reconfigurable and multifunctional.^[85-90] The key features and why PNIPAM is so attractive are the sharp thermoresponse at near physiological temperatures, biocompatibility and transparency. Many protocols exist that describe the modification of PNIPAM in order to adjust its swelling temperature by the addition of comonomers such as acrylic acid that change the hydrophobicity of the polymer network.^[91]

3 MATERIAL AND METHODS

3.1 ROLLED UP TECHNOLOGY

The spermbot is created by combining sperm cells with magnetic microtubes, which are fabricated by rolling up thin ferromagnetic layers. The technology of strain engineering for rolling up thin films is well established for several material systems and was previously reported.^[92] Using rolled-up technology, parameters regarding desired materials, nanofilm thickness and template size can be adjusted in a way that the resulting microtubes have a certain diameter, wall thickness, shape, length and advanced functionality.^[92-94] This technology has been employed in various fields, ranging from small scale energy storage devices,^[95-97] nanoelectronics^[94] to photonics^[98,99] and sensors.^[100,101]

Figure 5 shows a schematic of the process for fabricating microtubes *via* the rolled-up technology. In the first step, a substrate is patterned with photoresist using spin-coating and photolithography processes to obtain a structured sacrificial layer (see Figure 5A). In the second step, electron beam evaporation machines are used to deposit thin layers of different materials (e.g. Ti, Fe) onto the substrate. This deposition is carried out at an angle of 75° to obtain an evaporation shadow on one side of the structures, as shown in Figure 5B. This evaporation shadow, where no material was deposited, serves as starting point for the solvent

in the following etching step to remove the sacrificial layer (see Figure 5C). The strain gradients in the thin films that were introduced during the material deposition by applying different deposition rates leads to the immediate conversion of the flat films into rolled-up three-dimensional architectures. By this means, microtubes of certain length (predetermined by the patterning) and radius (predetermined by the film thickness and deposition rate) are fabricated.

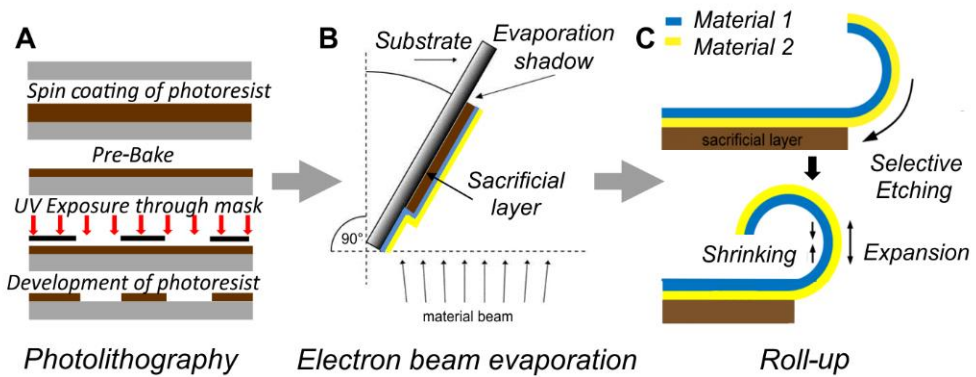


Figure 5: Rolled-up technology for the fabrication of microtubes from thin nanomembranes. Modified from reference [102].

In detail, rolled-up magnetic microtubes for sperm capture and guidance are fabricated as follows: A glass substrate is coated with photoresist AR-P 3510, exposed to UV light for 7 seconds through a photomask with $50 \mu\text{m}^2$ squares and developed with an AR 300-35 : water (1:1) solution. Subsequently, 10 nm layers of titanium (3 \AA/s) and iron (1 \AA/s) are deposited at an angle of 75° onto the substrate using electron beam evaporation. The substrate is immersed in acetone and the layers roll up immediately when the photoresist layer is removed.

These microtubes are dried using the critical point dryer or immediately washed in sperm medium for subsequent cell capture. Microtubes with a diameter slightly larger than the sperm head (5-8 μm) and a length of 50 μm (or 20 μm respectively, for experiments in section 3.3 and 4.5) were fabricated. Figure 6 illustrates the nanomembranes before and after the rolling up process. The evaporation shadows are visible as dark lines on the left side of each square on the array in the left image in Figure 6.

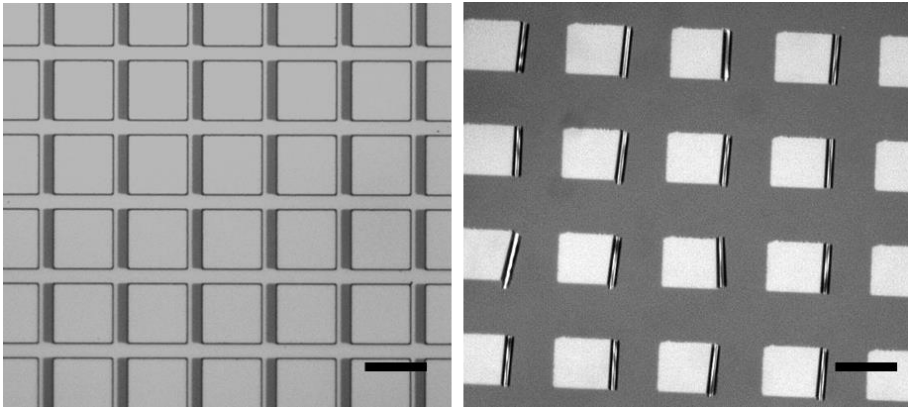


Figure 6: 50x50 μm nanomembranes before (left) and after (right) rollup. The dark area beside each square in the left image displays the evaporation shadow. The right image displays the resulting 50 μm long microtubes.

3.2 TREATMENT OF BOVINE SPERMATOZOA

3.2.1 PREPARATION OF SPERMBOTS

The spermbots were formed by capturing spermatozoa from bulls inside rolled up microtubes. Bovine spermatozoa were chosen due to their easy availability and similar morphology to human sperm. The interaction between bovine spermatozoa and microtubes were investigated by adding microtubes that were released from their substrate and washed 3 times with SP-TALP (modified Tyrode's Albumin-Lactate-Pyruvate Medium, CaissonLabs), into a solution of bovine sperm cells in SP-TALP. The sperm cell solution was prepared as follows: The cryopreserved bovine semen straws (kindly provided by Masterrind GmbH) were withdrawn from the liquid nitrogen storage tank, thawed for 5 minutes in the incubator at 38°C and diluted in 2 mL SP-TALP medium. A washing step was performed by centrifuging the sperm sample at 300g for 5 minutes. The supernatant was removed and the pellet was resuspended in 2 mL fresh SP-TALP. After addition of microtubes to the sample the cells and tubes were observed under the optical microscope. For magnetic guidance a neodymium magnet was used with a magnetic field intensity of 22 mT at a distance of 2 cm from the sample. The temperature experiments were carried out under the same conditions while using a Peltier Element for heating and cooling the sample to the desired temperature.

In order to take scanning electron microscope images, sperm cells were fixed on glass substrates by incubating the cell solution with 2% glutaraldehyde solution for 30 minutes. The samples were subsequently washed three times with PBS and a final rinsing step with water was carried out. To create a conducting surface, the glass wafers were coated with 20 nm chromium using a sputter coater. The scanning electron microscope images were taken with an NVision SEM/FIB 40 machine from Zeiss.

3.2.2 SPEED MEASUREMENTS

The videos were recorded with a Phantom Miro eX2 high-speed camera from VisionResearch mounted onto an inverted microscope. For the tracking of cell paths the video analyzing software ImageJ was used with the plugin MTrack2. The length of trajectories of sperm cells were measured by the use of the ImageJ software and with the known frame rate the speed of tracked cells could be determined.

3.2.3 SEPARATION ON CHIP

For the separation experiments, a μ -Slide Chemotaxis^{2D} from ibidi® was used. At first, SP-TALP medium was filled into one of the 80 μ L chambers. The bovine sperm cells were prepared as described in previous paragraphs. A solution containing Ti/Fe microtubes and bovine sperm cells was filled into the second 80 μ L chamber. Afterwards, the middle channel was filled with clean SP-TALP medium. The inlets and

outlets were closed with plugs and the chip was placed under the microscope with a permanent magnet mounted on a stand underneath the sample holder. The separation process was recorded at room temperature with 5x magnification with 1 frame per second using a Zeiss Axiocam camera.

3.3 SURFACE MODIFICATION OF MICROTUBES

The goal in this part of the work was to attach sperm cell binding agents, for example fibronectin (FN), on the inner tube lining and thereby enable sperm cell adhesion. In order to do so, two surface modification methods were conducted: surface chemistry and microcontact printing technology. For both methods, the initial sample preparation was identical: a glass substrate patterned with photoresist was prepared using photolithography. Afterwards, nanomembranes are deposited using electron beam evaporation. The deposition of nanomembranes can be varied to obtain the desired functionalities. Fe introduces a ferromagnetic layer for subsequent external magnetic control. Ti offers a good adhesion layer onto the glass substrate and Au or SiO₂ are useful as top layers for surface functionalization, as described in the following paragraph. The different outcomes of the two modification approaches are discussed in Section 4.6.

3.3.1 SURFACE CHEMISTRY

The rolled-up technology offers the possibility of choosing the desired inner nanomembrane materials for the microtubes. It was demonstrated previously that the inner surface of rolled up microtubes can be modified by covalently bonding proteins onto them.^[103-105] In these cases, the inner tube material was silicon dioxide or gold. In case of silicon dioxide as an active layer for functionalization, the first step is the surface activation by oxygen plasma or piranha treatment (25 % H₂SO₄ and 15 % H₂O₂ for 1h) and subsequent silanisation with 2 % carboxyethylsilanetriol for 3 – 4 hours at 37°C, with the intention of having exposed carboxylic groups. This surface modification creates an anionic, hydrophilic coating. In the first step of surface modification *via* linker chemistry on gold, a self-assembling monolayer (SAM) of thiols was allowed to form over 24 hours by incubation of thiolated molecules ending with carboxylic groups (11-mercapto-undecanoic acid) on the surface of the rolled-up microtubes. This thiol forms a uniform layer by adsorption of the thiol head groups onto the gold. In this way, the carboxylic ends of the acid are exposed for the next coupling step.

The carbodiimide 1-ethyl-3-(3-dimethylaminopropyl)carbodiimide (EDC) is a zero-length crosslinking agent and forms an activated ester with the carboxylic group of the thiol and the amino-group of the biomolecule (in this case FN). The primary amine N-hydroxysuccinimide (NHS) is used to stabilize the reactive ester-intermediate and form the amide bonds.^[106,107]

When hyaluronic acid was functionalized, APTES ((3-aminopropyl) triethoxysilane) was used for the SAM formation, which has ending amino groups that will bind to the carboxylic groups present in the hyaluronic acid in a covalent way. In case of fluorescein hyaluronic acid functionalization, 2 % APTES was incubated for 1-2 hours on the substrate with rolled up microtubes. The samples were washed three times with water and then immersed in EDC and NHS in a 1:1 mixture with a final concentration of 0.1 M and 0.025 M, and 20 μ L of fibronectin (1 mg/mL) or fluorescein hyaluronic acid (1 mg/mL), respectively. The sample was incubated overnight at room temperature and afterwards washed three times in water.

Finally, this linker chemistry leads to covalent bonding between the surface and the proteins. The detailed procedure of functionalizing microtubes *via* surface chemistry is schematically displayed in Figure 7.

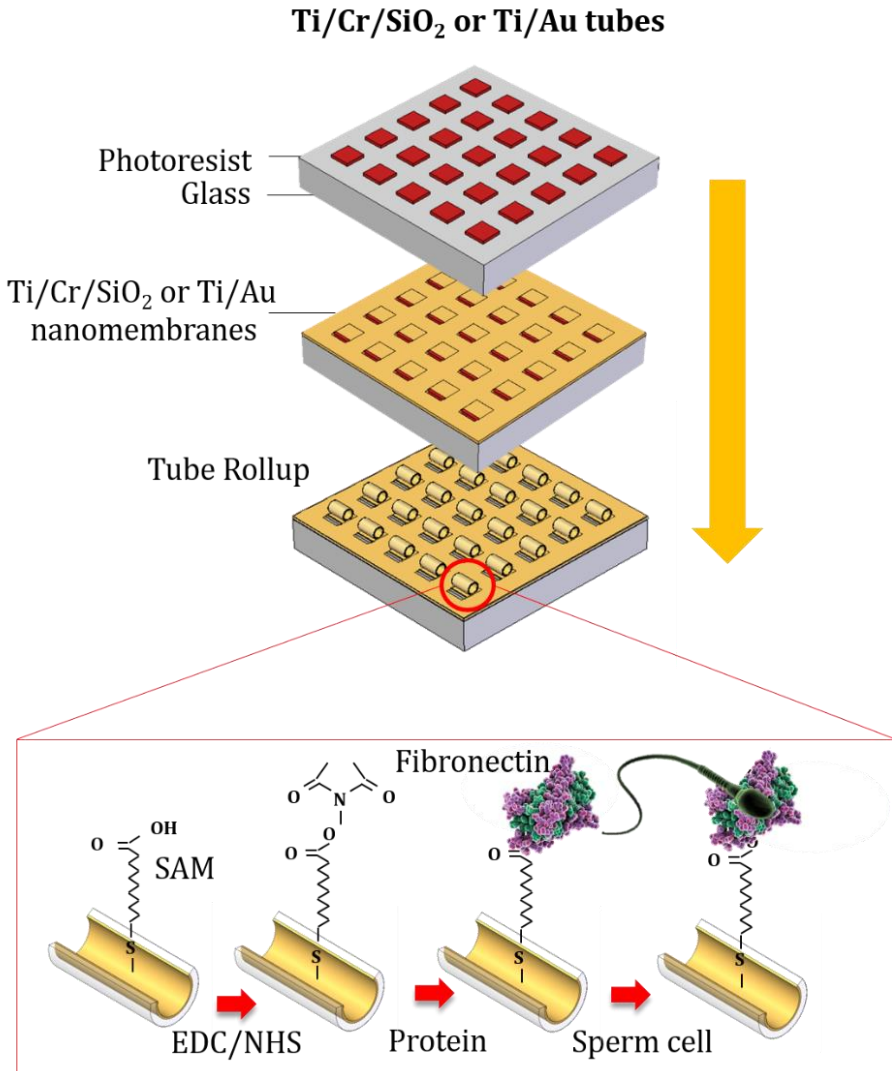


Figure 7: Schematic of surface chemistry functionalization. The gold or silicon dioxide surfaces using EDC-NHS chemistry. The inset shows the formation of a self-assembling monolayer (SAM) onto the gold or SiO₂ surface, linking to EDC and NHS and binding of fibronectin (target protein), then fibronectin binds to receptors of the sperm cell membrane. Schematic modified from reference [108].

Fluorescein hyaluronic acid was chosen as a model biomolecule for functionalization on the surface to characterize the distribution of the biomolecules *via* fluorescence microscopy without further modification. In order to visualize the functionalization of FN further steps of modification with first and second fluorescently labelled antibody would have been necessary. Figure 8 shows in the top row the bright field image of the rolled up microtubes.

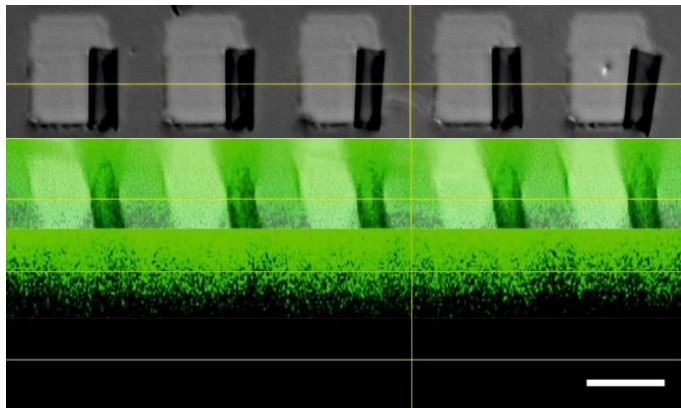


Figure 8: Fluorescein-hyaluronic acid functionalized microtubes. The top image shows 20 μm long rolled up microtubes that are functionalized with fluorescent hyaluronic acid using the EDC/NHS chemistry. The second image shows the overlaid differential interference contrast image and the green fluorescent image in the orthogonal view of the Z-stack. The image below shows only the Z-stack of the green fluorescent channel. The bottom image in is the fluorescent image of the control sample with non-functionalized rolled up microtubes. Scale bar is 20 μm . Modified from [108].

In the second and third row of Figure 8 images of the fluorescent signal of hyaluronic acid that was functionalized *via* the EDC/NHS method are shown. The evenly spread fluorescent signal illustrates that the biomolecule is distributed uniformly on the glass surface. The surface chemistry approach with EDC/NHS is well suited for attaching the biomolecule on a large area in a uniform manner.

3.3.2 MICROCONTACT PRINTING

The second method of surface modification to attach FN inside the microtubes is performed by microcontact printing. This technique is a form of soft-lithography, which was introduced for the first time by G. M. Whitesides and A. Kumar at Harvard University^[109] in 1996 and was also applied for binding sperm cells onto glass or polystyrene surfaces printed with FN.^[147] The microcontact printing method involves the printing of the target protein directly on the nanomembranes before the roll-up of the microtubes (see schematic in Figure 9).

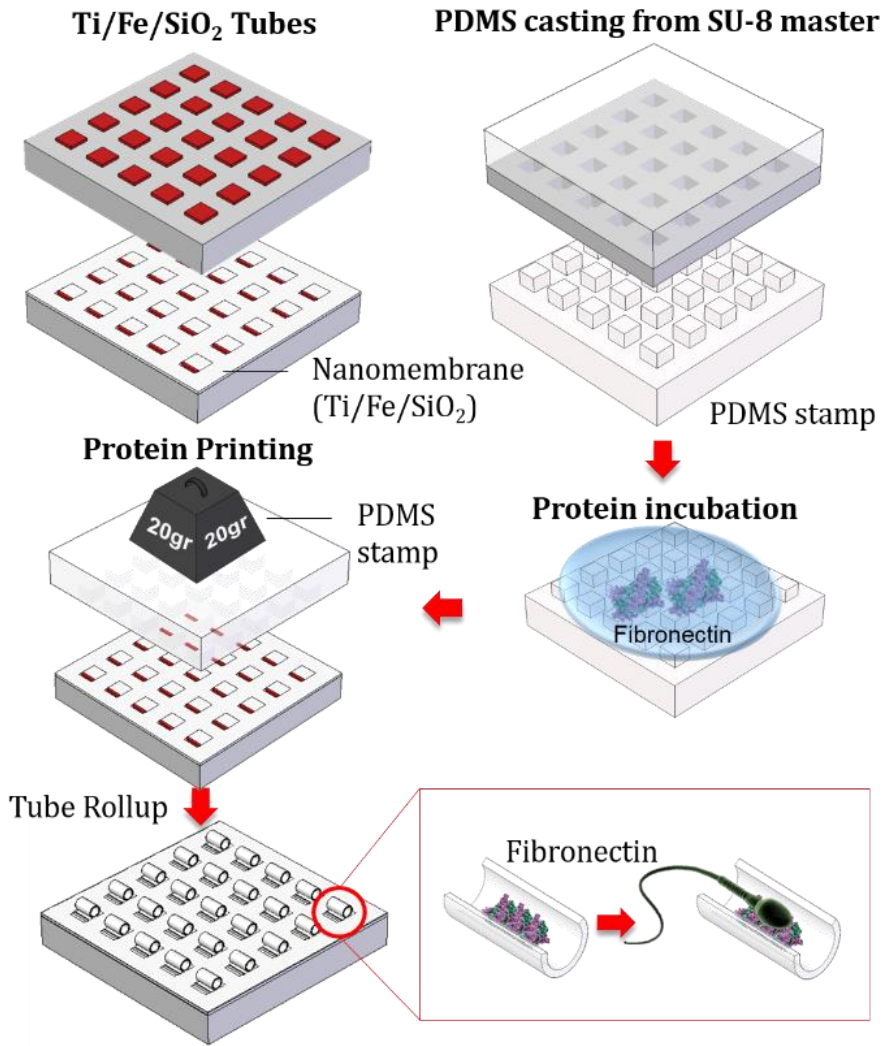


Figure 9: Schematic procedure of microcontact printing onto nanomembranes. Taken from reference [108].

Here, the microcontact printing was performed on the array of deposited nanomembranes (compare with section 3.1) before their rollup. Stamps made from Polydimethylsiloxane (PDMS) with squared pillars (with

geometries of 20 X 20 μm^2 and 50 X 50 μm^2 , height 10 μm), see Figure 10, were prepared by a mold that was fabricated using soft-lithography. A SU8 master was fabricated by standard photolithography methods. Then the PDMS (Sylgard 184, Dow Corning, Germany) pre-polymer was mixed with the curing agent at a ratio of 10:1 (w/w) and air bubbles were removed by degassing in a desiccator. Subsequently, the PDMS was poured onto the SU8 master and baked overnight at 65°C. Afterwards, this PDMS stamp was peeled off and soaked in a FN solution (1 mg / mL) or fluorescein hyaluronic acid (1 mg / mL) for 40 minutes, dried with a nitrogen gun and transferred onto the nanomembrane array using the lambda aligner (FINEPLACER® lambda, USA). The scanning electron microscopic image of the PDMS stamp on the left in Figure 10 displays the shape of the pillars that are used to stamp the target molecule onto the substrate. The image on the right shows how the PDMS stamp soaked in fluorescein hyaluronic acid prints squares that have the same size as the pillars onto a glass slide and only leaves prints where the stamp was touching the substrate.

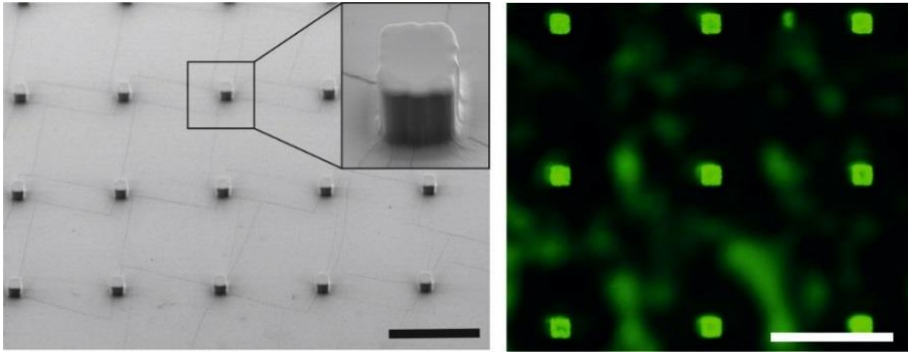


Figure 10: Left: Scanning electron microscopic image of the PDMS stamp used for microcontact printing with $20 \times 20 \mu\text{m}$ pillars. Inset shows magnification of a single pillar structure. Right: fluorescent image of microcontact print of PDMS stamp onto a glass substrate. The stamp was incubated with fluorescein-hyaluronic acid. The green spots show where the stamp was pressed onto the glass substrate and adsorbed the biomolecule. Images modified from reference [108].

After correct alignment of the stamp onto the nanomembranes array, the biomolecule was transferred to the array by applying a uniform weight (20 grams) onto the stamp for 40 minutes. Subsequently, the nanomembranes were rolled up into tubes by immersing them in ethanol for a few seconds, thereby removing the sacrificial layer of photoresist from underneath the nanomembranes.

Again, fluorescein hyaluronic acid was used as a model to observe the distribution of the biomolecules on the surface after the microcontact printing. Figure 11 shows the bright field and fluorescent images of the nanomembrane array before rollup. The fluorescent images proof that the biomolecule is printed in a concentrated way only on top of the

nanomembranes, where the stamp was touching the surface. The control sample in the bottom row of Figure 11 contains non-functionalized nanomembranes before rollup. The weak fluorescent signal derives from the autofluorescence of the photoresist^[110] that is present underneath the nanomembranes.

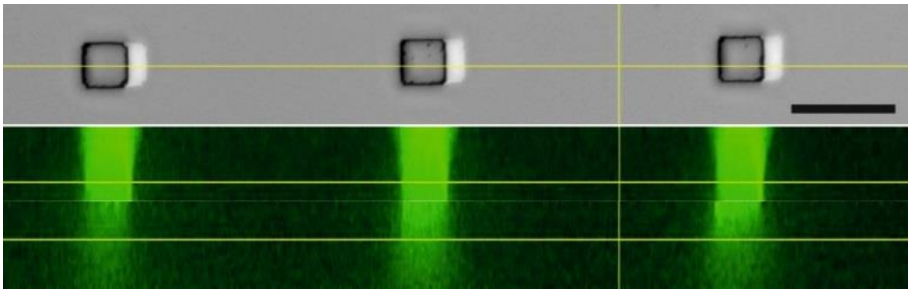


Figure 11: Microcontact printing. The top image shows the bright field image of $20 \times 20 \mu\text{m}^2$ nanomembranes before roll-up that have been printed with fluorescent hyaluronic acid. The second image shows the fluorescent signal of the Z-stack in the green fluorescent channel. The 3rd image shows the control sample with of non-functionalized nanomembranes. The weak fluorescent signal comes from the autofluorescence of the photoresist present underneath the nanomembranes. Scale bar $50 \mu\text{m}$. Modified from ^[108].

Microcontact printing leads to a high quality deposition of the biomolecule in a localized and patterned way.^[111,112] During this procedure, the target molecule attaches *via* surface adhesion on the silicon dioxide surface.

After the surface modification with FN by the use of these two techniques, finally, the sperm cells were incubated on the sample

containing the modified tubes for 30 minutes at 37 °C and 5 % CO₂. Afterwards, the coupling efficiency was evaluated by microscopic analysis. Arrays were analyzed regarding the number of microtubes containing spermatozoa in relation to the total number of microtubes (at least 200 microtubes).

3.4 POLYMER TUBE FABRICATION

Polymeric microtubes were fabricated from thin films of the thermoresponsive polymer poly(N-isopropylacrylamide) (PNIPAM). The polymerization was performed as free radical initiation of the N-isopropylacrylamide monomers in an organic solvent. With the attempt of making this hydrogel photopatternable, it is copolymerized with a photosensitive monomer called 4-acryloylbenzophenone (ABP). The synthesis of this photosensitive chemical was described by Xiao et al [113] and the reported protocol was followed closely. The procedure of how to fabricate microtubes from photopatternable PNIPAM was adapted from existing procedures.[83,88,114]

3.4.1 SYNTHESIS OF PHOTSENSITIVE MONOMER 4-ACRYLOYLBENZOPHENONE

The esterification of 4-benzophenone with acryloylchloride delivers the chemical acryloylbenzophenone which is photosensitive.[113] Figure 12 displays the chemical reaction equation of the synthesis of

acryloylbenzophenone. This chemical is later on used in the polymerisation to create photosensitive polymer films that can be crosslinked and thereby patterned using photolithography.

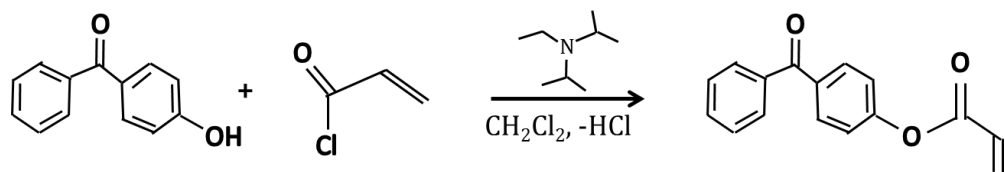


Figure 12: 4-benzophenone and acryloylchloride react to 4-acryloylbenzophenone in methylene chloride and N,N-diisopropylethylamine.

Briefly, acryloylbenzophenone was synthesized as follows: 10 g 4-hydroxy-benzophenone (0.05 mol) and 9.65 mL (0.14 mol) N,N-diisopropylethylamine in 40 mL methylene chloride were added to a 500 mL three-necked round bottom flask equipped with a magnetic stirrer and a thermometer. 0.5 mol of acryloylchloride (4.51 mL) in 10 mL methylene chloride were filled into an addition funnel and added dropwise to the reagents in the three-necked flask. The reaction mixture was stirred on ice for 3-4 hours until all acryloylchloride was added. Subsequently, the methylene chloride was removed by rotary evaporation (400 mbar, 40°C). Then the mixture was allowed to stand overnight. The mixture was washed twice with 20 g of methylene chloride. Afterwards, the reaction solution was extracted twice with 1 mol/l hydrochloric acid, 1 mol/l sodium bicarbonate solution, and deionized water, then dried overnight over anhydrous sodium sulfate.

The resulting agent was passed through a silica gel column with chloroform as eluent. A thin layer chromatography was performed in parallel with each obtained fraction of the column. The fractions that contained the purified product were combined, evaporated in the rotary evaporator and dried overnight.

¹H NMR (500 MHz, CHLOROFORM-d as solvent) was performed at the NMR service of the TU Dresden and confirmed the purified product 4-acryloylbenzophenone (identified peaks: ppm 6.062 (dd, J=10.40, 0.95 Hz, 1 H) 6.340 (dd, J=17.34, 10.72 Hz, 1 H) 6.644 (dd, J=17.18, 1.10 Hz, 1 H) 7.262 (dt, J=8.83, 2.50 Hz, 2 H) 7.483 (td, J=7.30, 1.60 Hz, 2 H) 7.589 (tt, J=7.25, 1.26 Hz, 1 H) 7.797 (dt, J=7.88, 1.90 Hz, 2 H) 7.865 (dt, J=8.83, 2.20 Hz, 2 H).

3.4.2 SYNTHESIS OF POLY (*N*-ISOPROPYLACRYLAMIDE-CO-ACRYLOYLBENZOPHENONE)

The obtained photosensitive monomer 4-acryloylchloride was mixed with N-isopropylacrylamide (NIPAM) and azobisisobutyronitrile (AIBN) as radical initiator of the polymerization. The components were dissolved in 6 mL 1,4 dioxane and oxygen was removed by bubbling nitrogen through the solution for 20 minutes. The vial containing the polymerization mixture was sealed tightly and placed in a thermoshaker at 70 °C and 250 rpm for 24 hours. The mixture was then precipitated in 75 mL diethylether under stirring. The precipitate was filtered off and dried. This procedure delivered the polymer poly(N-

isopropylacrylamide-co-acryloylbenzophenone) (PNIPAM-co-ABP), as shown in the reaction equation in Figure 13.

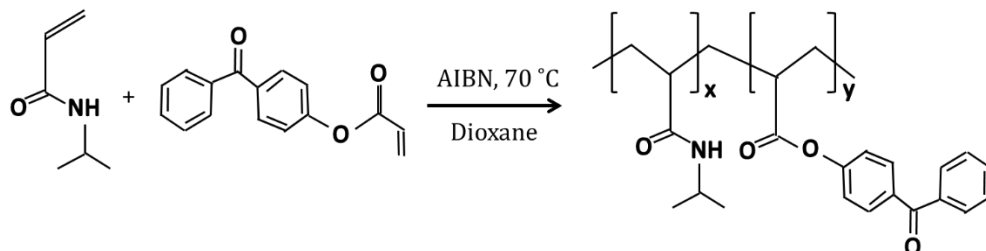


Figure 13: N-isopropylacrylamide polymerizes with 4-acryloylbenzophenone to poly(N-isopropylacrylamide-co-acryloylbenzophenone) in dioxane with AIBN as radical starter.

A similar polymerisation reaction was carried out in ethanol when acrylic acid was added as comonomer, resulting in the polymer poly(N-isopropylacrylamide-co-acryloylbenzophenone-co-acrylic acid) (PNIPAM-co-ABP-AAc). The exact recipes of the polymerization mixtures are listed in Table 1. These procedures were adapted from existing protocols [83,88,114]

Table 1: Conditions and molar concentrations of components for polymerizations.

	PNIPAM-co-ABP	PNIPAM-co-ABP-AAc
N-isopropylacrylamide	1 g	0.65 g
4-Acryloylbenzophenone	50 mg	20 mg
AIBN	14 mg	12 mg
Acrylic Acid	-	20 mg
Solvent	6 mL 1,4-Dioxane	3 mL Ethanol
Conditions	70°C, 24h, 250 rpm	70°C, 24h, 250 rpm
Lower critical solution temperature (LCST)	28 °C	37 °C

3.4.3 PHOTOLITHOGRAPHY OF POLYMERIC FILMS

The patterning of the thermoresponsive, photopatternable PNIPAM-co-ABP and PNIPAM-co-ABP-AAc was done by standard photolithography with a mask aligner MA6 (SÜSS Microtec) generating deep UV light (254 nm). The exposure time of the polymer was adjusted each time to the layer thickness and concentration of the polymer and was between 25-50 seconds. The UV radiation creates a radical on the acryloylbenzophenone molecules and leads to the crosslinking of the

PNIPAM. The substrates consisting of glass or silicon wafer were prepared by thorough cleaning with acetone and isopropanol (2 minutes sonication in each solvent) and subsequent cleaning with oxygen plasma for 1 minute. The samples were coated with TI-prime (4500 rpm, 30s) and heated for 2 minutes at 120 °C. In order to add a sacrificial layer to enhance the rolling and detachment of the polymer tubes later on, 10 nm of germanium were deposited by electron beam deposition before continuation with the process. Different layer thicknesses were obtained by spin-coating solutions with varying concentrations of PNIPAM-co-ABP-AAc in ethanol ranging from 2.5 % to 20 % polymer weight to solvent volume ratio onto the wafer at 3000 rpm for 30 seconds. The samples were placed in the mask aligner underneath a quartz mask with the desired patterns (e.g. 20 μm transparent circles) and exposed to deep UV light in the hard contact mode for the chosen exposure time. Subsequently, the polymer films were developed by rinsing them with dichloromethane for 6 seconds.

The resulting layer thickness for each tested polymer concentration from 5 - 20 % (w/v) in ethanol was measured. Figure 14 gives detail about the obtained layer thicknesses depending on the polymer concentration. The film thicknesses were obtained from profile measurements with a Dektak profilometer and the given data curve includes the standard error of the mean.

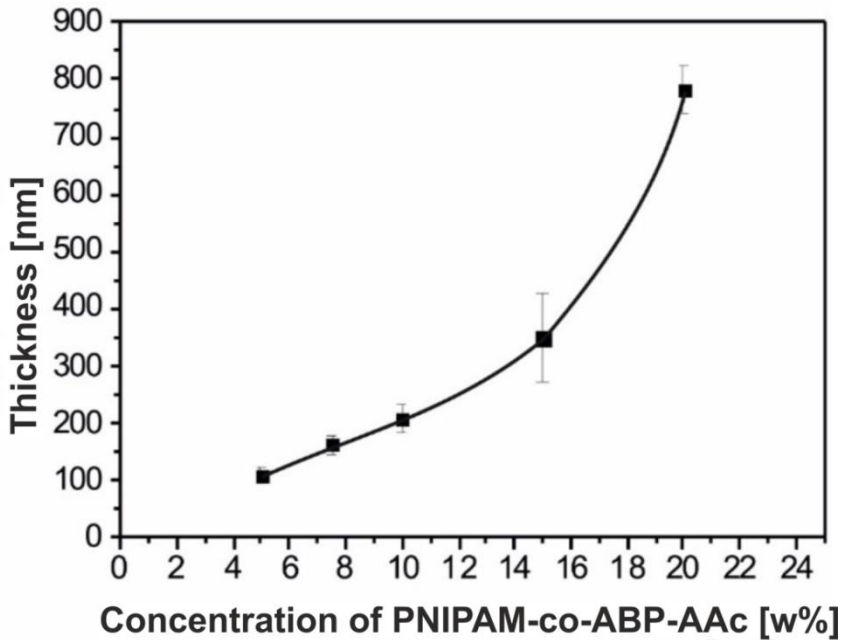


Figure 14: Thicknesses of spin-coated PNIPAM-co-ABP-AAc layers depending on the concentration of PNIPAM-co-ABP-AAc (w/v%) in ethanol.

The substrates with the developed polymer films were then placed in an Electron Beam machine (Edwards E beam) and thin films of e.g. 2 nm Ti and 10 nm of Fe were deposited at an angle of 75° for the formation of the passive layer.

3.5 VIABILITY TESTS

Sperm viability tests were conducted with the LIVE/DEAD® Sperm Viability Kit from Life Technologies. This kit contains the dye SYBR 14 which stains live sperm cells green and propidium iodide which stains dead cells red. The staining mechanism relies on the fact that both dyes are DNA intercalating agents whereas propidium iodide is excluded from live cells because it cannot permeate intact cell membranes. The sperm sample was thawed and washed as described in section 3.2.1. SYBR 14 was added in a dilution of 1:50 to the sperm sample and incubated for 5 – 10 minutes. Subsequently, propidium iodide was added in a 1:20 dilution. The sample was incubated on the different materials for a total of one hour before the fluorescence microscopy of the stained spermatozoa was conducted.

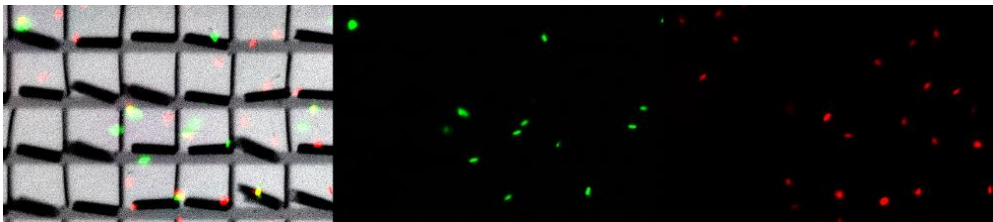


Figure 15: Live/dead staining of bovine spermatozoa. The left image is an overlaid image of bright field and the fluorescent channel with spermatozoa on an array of microtubes. The middle image displays fluorescently labelled cells in the green channel (alive) and the image on the right displays labelled cells (dead) in the red channel.

Figure 15 displays a representative image of the fluorescently labelled sperm cells. The fluorescent imaging was done with an excitation wavelength of 470 nm and an emission wavelength of 509 nm in the green channel (middle image in Figure 15) and 540 nm excitation and 580 nm emission wavelength in the red channel (right image), respectively.

4 RESULTS AND DISCUSSION

Through the combination of the rolled up microtubes with single motile sperm cells a new kind of hybrid microrobot was developed. This chapter describes the obtained spermbots – how they function, how their performance was improved and how they can be manipulated by external control mechanisms. It was observed that the spermbot performance is dependent on various factors such as the initial velocity of the spermatozoon, temperature, length and radius of the microtubes. The characterization of these aspects is focus of the first part of this section in order to gain a better understanding of the spermbots.

Spermatozoa are very powerful microswimmers and are able to interact with rolled-up magnetic microtubes in a way that they enter one opening and become mechanically caught inside the tubes and start pushing them forward. Generally, all mammalian sperm cells display similar anatomy with a head, midpiece and tail, but the size and shape varies largely from species to species. Sperm cells from bulls were used because their size and morphology is similar to human sperm cells. A bovine sperm head is about 10 μm long and 5 μm in diameter but flat and only about 1 μm thick.^[115] It possesses a flagella of about 60 μm in length. A representative microscopic image of a bull sperm cell used in the experiments described here is shown in Figure 16. Spermatozoa are

perfectly adapted to swimming in viscous media on the microscale and thus are promising as a driving force of microrobots.

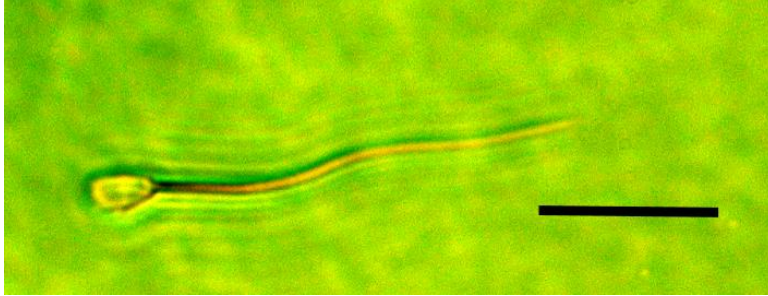


Figure 16: Optical image of a bovine spermatozoon. Scale bar 20 μm .

After addition of bovine spermatozoa to the released rolled up microtubes (50 μm long, 5-8 μm in diameter), the capturing of spermatozoa inside the microtubes takes place randomly. The coupling process is illustrated in Figure 17.

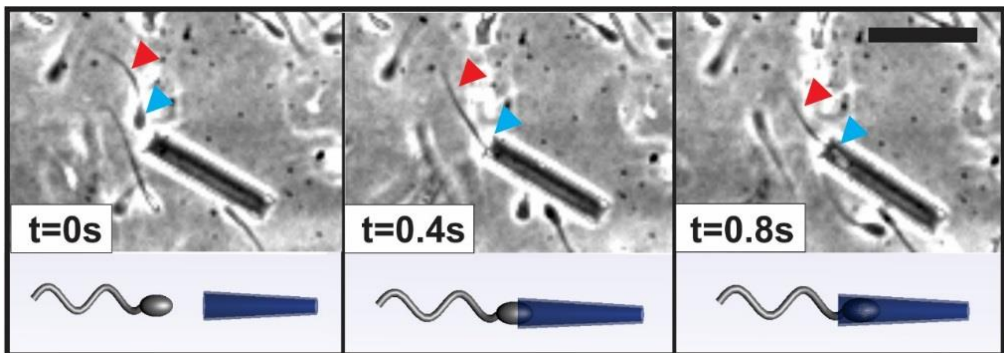


Figure 17: Capturing of bovine spermatozoon inside a microtube over a time span of 0.8 seconds. The red arrow points at the sperm tail and the blue arrow points at the sperm head. Scale bar 50 μm .^[47]

As can be seen in Figure 17, the actively moving bovine sperm cell enters the tube with its head first and becomes trapped in the cavity of the rolled up microtube. The scanning electron microscopic images in Figure 18 illustrate how the spermatozoa fit well inside the cavity of the rolled-up microtubes. They also show the flat head of the bull sperm.

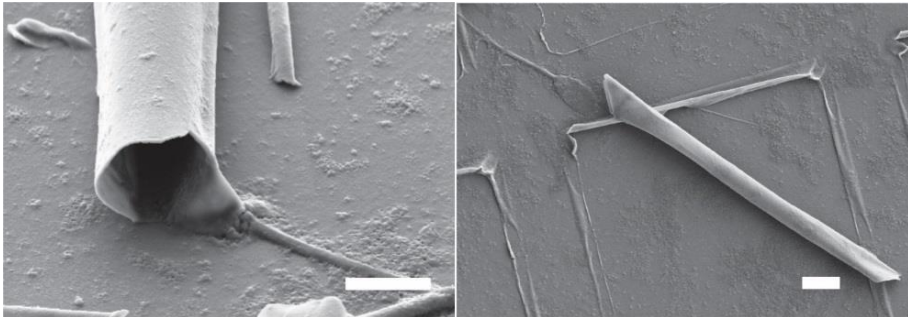


Figure 18: Scanning electron images of rolled-up microtubes and bovine spermatozoa at the tube openings. Scale bars 5 μ m . Modified from [47].

4.1 CHARACTERIZATION OF SPERMBOTS

With the aim of evaluating the performance of the sperm-driven microtubes, the effect of cell penetration, tube radius and velocity of over 40 samples of spermbots depending on the initial velocity of the freely swimming spermatozoon at room temperature were analyzed. The schematic in Figure 19 displays how the radius R_{tube} and the length of the microtube L_{tube} as well as penetration x are defined. The length of the confined cell L_{conf} (0-50 μ m) divided by the total length of the microtube

(50 μm) and multiplied by 100, results in the relative penetration x in percent (Equation 1).

$$x = \frac{L_{conf}}{L_{tube}} \times 100 \tag{1}$$

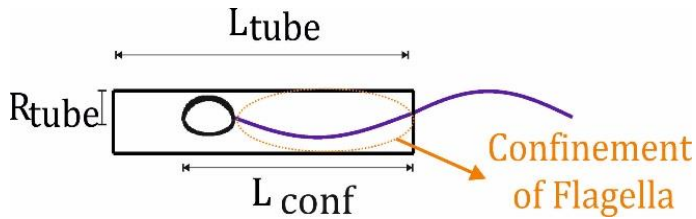


Figure 19: Schematic of sperm cell penetration inside a microtube. [47]

Since the natural variation of swimming velocities of bovine spermatozoa is very high, this variation was accounted for by relating the velocity of our spermbots to the initial cell velocity of each case before entering the microtube. This means, that only spermbots that were recorded during the free cell swimming, the capturing process of the cell inside the microtubes and the motion of the spermbots were considered in this analysis.

The tube radius required for the trapping of the sperm cell is between 2 and 4.5 μm . This range of tube radii results in different cell penetrations inside the tube (see Figure 20). The larger the radius of the microtube, the further the sperm cell enters the tube.

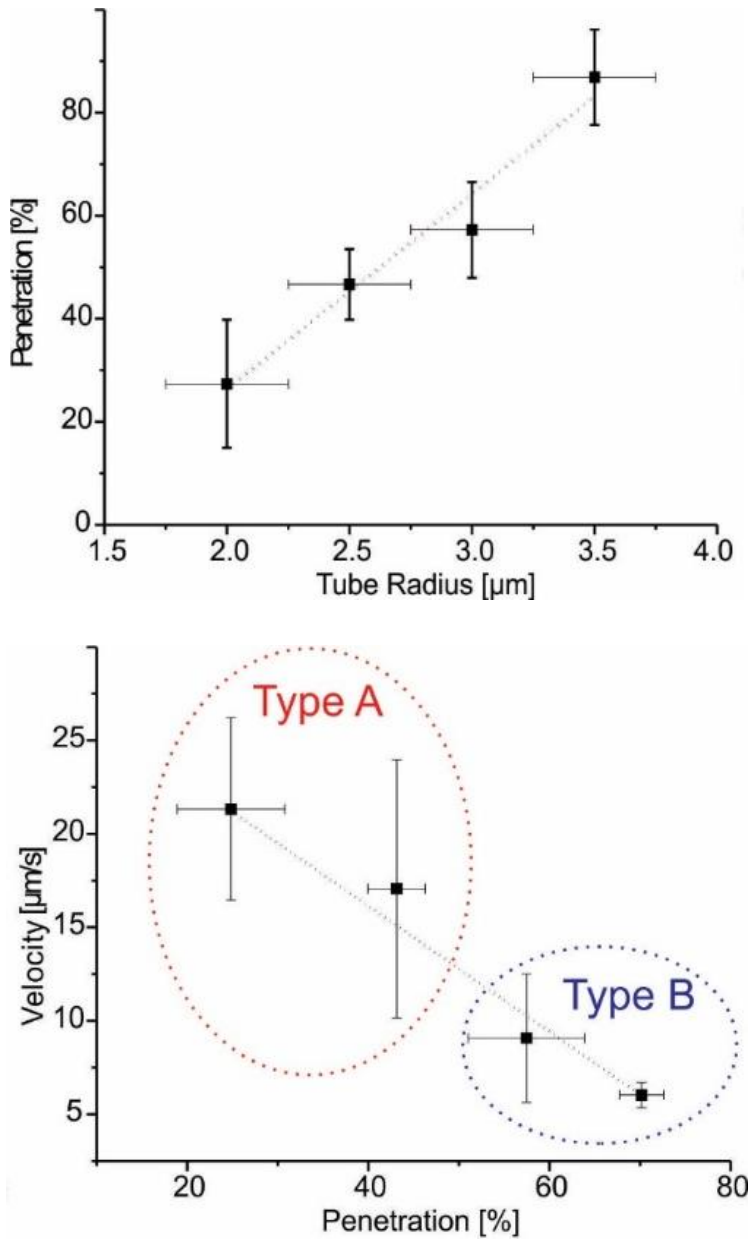


Figure 20: Left: Penetration x [%], calculated according to equation 1, over microtube radius [μm], Right: Velocity of spermbots over penetration x [%] with categorization into type A spermbots (less than

50% penetration) and type B, more than 50% penetration. Error bars are standard deviations of over 70 cases.^[47]

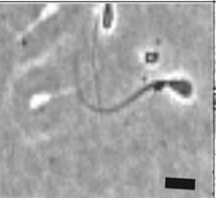
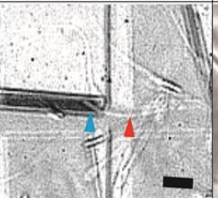
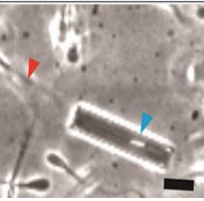
The natural amplitude of a bovine sperm cell ranges from 3-8 μm in each direction of the origin.^[116] The confinement of the cell flagella inside the tube reduces the amplitude of the sperm cell oscillation down to the tube radius. The relation between flagella amplitude and velocity was described in Robert Rikmenspoels work ^[116] as:

$$v \propto \frac{fb^2}{\lambda} \quad (2)$$

wherein v is the velocity, f the frequency, b the amplitude and λ the wavelength of the sperm flagella. Assuming that the frequency and wavelength of the sperm motion stay the same, the amplitude has a significant impact on the change of velocity of the sperm cell during cell capture. With increasing penetration, the flagellum of the sperm cell becomes more restricted in its natural movement. Due to the known relation between flagella amplitude and cell velocity (equation 2, ^[116]), a sperm cell with confined flagella has a reduced velocity compared to a free cell. As expected from these facts, with increasing penetration, the spermbot velocity decreases (see Figure 20, right graph). In order to obtain a better understanding of the large amount of coupling cases, the penetration depth of the spermatozoa inside the magnetic microtube were categorized into 2 groups: type A with a low penetration of 0 - 50 % of the total tube length, and type B with a high penetration of 50 - 100 % of the total tube length, as displayed in

Table 2.

Table 2: Type A (penetration $x < 50\%$, $N=15$) and B (penetration $x > 50\%$, $N=26$) of spermbots inside microtubes. Microscopic images, relative penetration x (as % of total tube length), relative velocity (% of initial free cell speed) and average velocity of free sperm cells as well as type A and type B spermbots. The red arrows point at the sperm tails, the blue arrows point at the sperm heads inside the microtube. Scale bars: $10\ \mu\text{m}$.^[47]

	Free Sperm Cell	Type A	Type B
Microscopic Image			
Penetration x [%]	-	0-50	50 - 100
Relative Velocity [%]	100	18 ± 6	9 ± 3
Average Velocity [$\mu\text{m/s}$]	45 ± 15	10 ± 4	5 ± 3

In conclusion, type A spermbots display in general a higher relative velocity than type B spermbots. The lower velocity is due to the influence

of penetration on the confinement of sperm flagella which in turn reduces the cell speed. The average velocity of type A spermbots is 10 $\mu\text{m/s}$ compared to 5 $\mu\text{m/s}$ for type B. In both cases the speed reduces significantly from the free cell velocity (45 $\mu\text{m/s}$ at room temperature) which can be explained by two phenomena: the cargo the cell is pushing and the confined flagella amplitude.

4.2 TEMPERATURE INFLUENCE

The performance of natural microswimmers such as spermatozoa is influenced by the temperature of the media in which they swim.^[117] Accordingly, the spermbots are sensitive to those changes. The sperm cells, no matter if they are captured or not, display different metabolic activity at different temperatures and therefore their motility changes. In this part of the study, the effect of temperature on the performance of the microbiorobot was analyzed by heating and cooling the sample while recording videos of the moving microtubes. The temperature was kept in the range of 5 – 40 °C, which is the tolerance range of bovine sperm cells. As a representative example, trajectories of a spermbot at 12 °C and 37 °C over a time span of 10 seconds are illustrated in Figure 21.

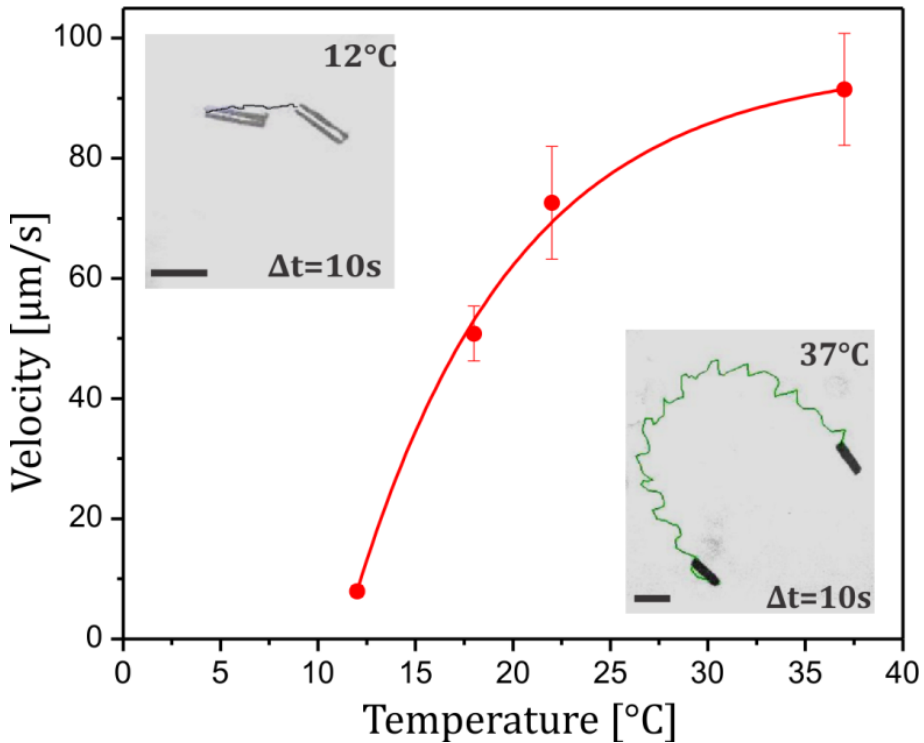


Figure 21: Influence of temperature on the velocity of spermboats. Trajectories of the same spermboat at 12°C (left inset) and 37°C (right inset) over a time interval of 10s. Scale bars 50μm. The graph plots the exemplary spermboat velocity over temperature for spermboats with a tube radius of 4 μm. [47]

Generally, in all 73 observed cases the increase of temperature lead to an increase of velocity. The reason for the increase in velocity at higher temperatures is caused by physiological changes in the metabolism of the sperm cell. As described by Rikmenspoel in 1984, raising the temperature results in a larger flagella frequency and amplitude and

thus an increase in cell velocity.^[117] Furthermore, sperm thermotaxis is a mechanism that takes place *in vivo* to guide the cells along a temperature gradient towards the oocyte in the female body. ^[118] It is a mechanism that, in combination with chemotaxis, leads sperm cells that are ready to fertilize to the oocyte. The response of sperm cells to changing temperature can be used to control the velocity of the spermbots. By increasing the temperature from 12 °C to 37 °C, as illustrated in Figure 21, an acceleration of the spermbot is achieved. When the temperature is decreased again, the spermbot can be slowed down and eventually the sperm cell motion is so slow that the spermbots stops moving. This can be reversed by raising the temperature once more so that the sperm cell starts moving and starts pushing the microtubule forward again. Therefore, a “stop and go” motion control of the spermbots can be performed.

4.3 MAGNETIC CONTROL

Achieving remote directional control over an autonomous system is a crucial requirement for its implementation as microbiorobot. Magnetic fields offer a great way to control a system in a non-invasive and biocompatible manner. The incorporation of magnetic nanoparticles is one attempt to provide magnetic control in a moving system. Although magnetic nanoparticles have been successfully applied to sperm cells for sorting, drug and gene delivery ^[119] as well as tracking and targeting of

other cells *in vivo*, [120,121] their major disadvantage is that they can pass through the cell membrane and might affect vital functions of the cell. As a consequence, depending on the chosen material composition of the nanoparticles, they can display toxic effects to the cells and their biocompatibility is a contentious issue.[122] With the future purpose of using the spermbots for *in vivo* guidance of sperm cells and fertilization, the capture of a sperm cell inside a ferromagnetic microtube seems a more suitable approach as control method without altering the cell. Microtubes are sufficiently large to not be taken up by cells and thus can be combined with sperm cells without any effect on sperm activity or their ability to undergo acrosome reaction.

Once the coupling between the sperm cell and microtube is completed, the spermbot can be steered through the alignment with an external magnetic field, as shown in Figure 22, in a similar fashion as presented in the past with nanoparticles, magnetotactic bacteria and self-propelled microjets.[123-125] In all these experiments, a permanent neodymium magnet with a magnetic field intensity of 540 mT was used, which was applied to the sample at a distance of about 2 cm resulting in a magnetic field intensity of 22 mT. This field intensity is enough to align and guide the microtubes along the external magnetic field lines.

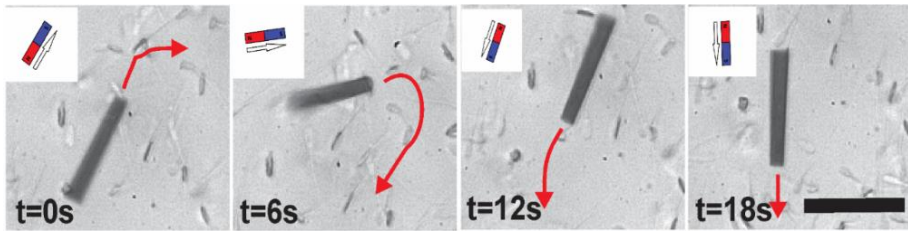


Figure 22: Magnetic remote control of microtube containing a bovine sperm cell. Scale bar: 50 μm .^[47]

In order to quantify the directed motion of the cell once it is trapped inside the microtubes, the directionality of a free cell was measured in comparison to the trapped cell. For the measurement and calculation of the directionality it is referred to the work by Paxton *et al.*^[126] Therein, the directionality factor was defined as $\cos(\theta)$. The angle θ occurs between the directionality vector and the microtube axis (or sperm head axis, respectively, when observing free sperm cells) over one time interval ($t = 0.2$ s in these experiments). Thus, an object that moves straight in axial direction has a directionality factor of 1 ($\cos 0^\circ = 1$), whereas a 90 degree turn means a directionality factor of 0 ($\cos 90^\circ = 0$). Hence, directionality is a measure for how straight a motion is performed.

Figure 23 shows the directionality (white/blue) and the velocity (black) over the time of the coupling process. Prior to the coupling between the sperm cell and microtube, the directionality of the freely swimming cell ranges from 0.65 to 1. This is a result of the natural motion of the sperm cell with two- and three-dimensional rotational and

wavy movements.^[127] Before the coupling, the sperm cell reaches an instantaneous velocity of up to 100 $\mu\text{m/s}$. However, when the sperm cell couples with the microtube, the speed decreases to an average of 10 $\mu\text{m/s}$. After the coupling is completed, the cell inside the tube moves with a high directionality factor of close to 1. This value becomes even more invariable when an external magnet is applied, since the alignment of the tube is induced by the magnetic field lines.

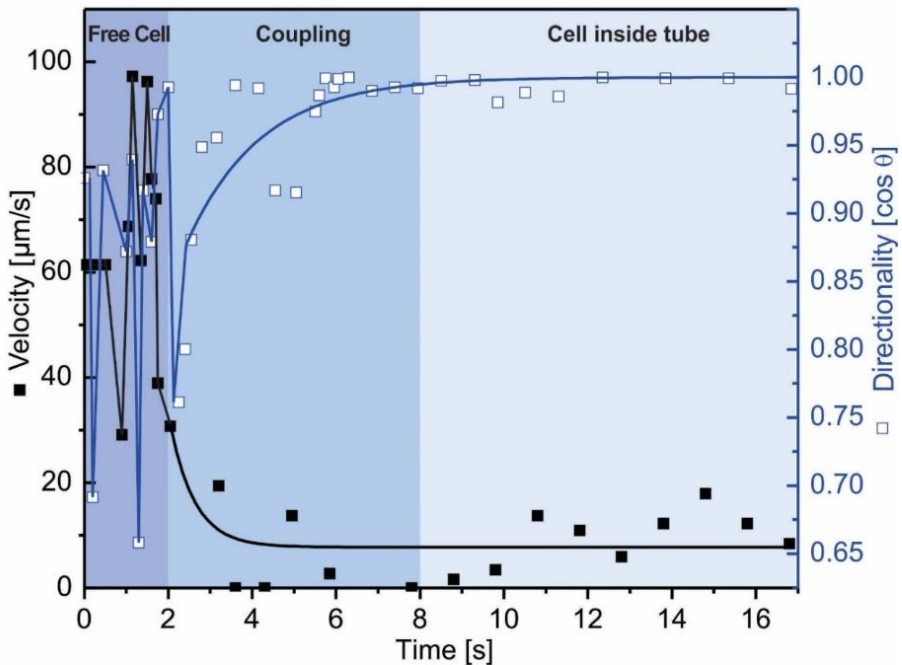


Figure 23: Velocity (left axis, black data points) and directionality (right axis, white data points) over the process of coupling. Directionality is defined as $\cos(\theta)$, where θ is the angle between directionality vector and axis of the sperm head or tube over one time interval ($t = 0.2\text{s}$). During the first 2 s the cell displays a large range of instantaneous velocity and directionality. Coupling of the sperm cell inside the tube takes place at

$t = 2 - 8$ s while the tube and cell velocity reduces. From 8 s to 17 s, magnetic guidance through an external magnet takes place characterized by high directionality of the spermbot. [47]

In cooperation with Sarthak Misra from the University of Twente, the magnetic control of the spermbots was demonstrated by the use of a setup of four electromagnetic coils and a microscope which are connected to an image recognition software for automatic tracking of the microtube (Figure 24, right image). This system provides closed-loop control of the spermbot in two dimensions. Details of this work are described elsewhere.[128]

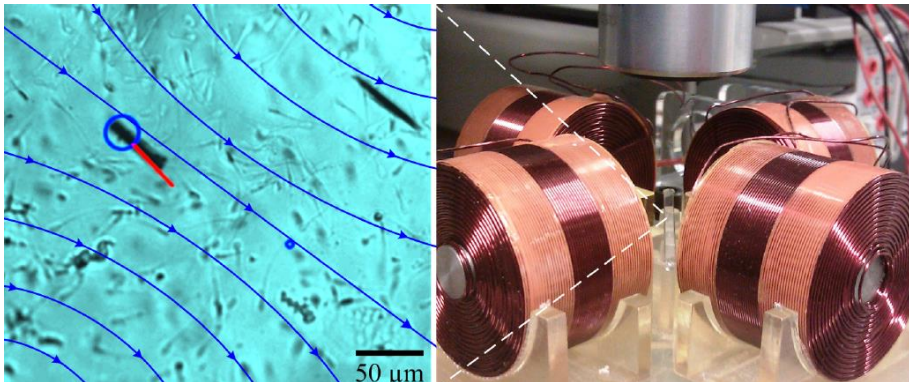


Figure 24: Wireless closed-loop control of a spermbot.[128] The system consists of an orthogonal array of electromagnetic coils. The left image shows a controlled spermbot swimming towards a reference position (small blue circle) under the influence of the controlled magnetic fields (blue lines) and the self-propulsion force. The large blue circle is assigned by the feature tracking algorithm and the red line represents the velocity vector of the spermbot. For more details see reference [128].

As can be seen in Figure 24 in the left image, the microtube aligns along the magnetic field lines. Using this electromagnetic coil setup, the required magnetic field strength for guiding the spermbots could be determined more precisely to be approximately 1.39 mT. The obtained region-of-convergence for the motion control of spermbots that was achieved with this feed-back control system was $90 \pm 40 \mu\text{m}$.^[128]

4.4 SEPARATION ON CHIP

Separation of biological cells from a heterogenous mixture is a desired task for purification and single cell analysis. Generally, these procedures are based on the separation according to size, density (gradient centrifugation), adhesion to surfaces or separation according to surface markers (antibodies for fluorescence activated cell sorting or magnetic-activated cell sorting).^[129]

Semen samples are highly complex cell mixtures that not only contain a high heterogeneity of spermatozoa in terms of quality, morphology and motility, but also mucus, seminal fluid, white blood cells, prostaglandins, decapacitating factors and other components that might interfere with the outcome of artificial insemination.^[130-132] Especially for artificial insemination, sperm selection is a crucial treatment step in the preparation of the semen to achieve successful fertilization. Selection methods for spermatozoa are required to enrich high quality sperm and separate them from any components that could damage the sperm cells or interfere with fertilization. A conventional separation method is the swim-up, in which pre-washed sperm cells are placed on the bottom of a vial containing an overlaying medium and by the active swimming of the sperm cells the most actively moving spermatozoa reach the top of the vial after about 30 minutes.^[133] This is a simple separation method, but has limited outcome. Another method for sperm separation is density gradient centrifugation which is commonly used in IVF clinics. During this procedure the sperm sample is placed on top of a medium

containing an increasing density from top to bottom. During centrifugation, motile sperm reach the bottom of the vial faster than immotile sperm and are concentrated in a pellet.^[134] Other methods for sperm separation and selection include magnetically activated cell sorting,^[135] use of magnetic particles coated with sperm-specific antibodies,^[136] flow cytometry (e.g. for sex sorting)^[137] and several more based on chemotaxis, morphological selection, biochemical binding or other mechanisms.^[138,139] Microfluidic technology research has also put forth sperm selection and enrichment methods on micro-sized platforms.^[140-143]

Herein, a new method of sperm selection and separation is presented by the use of a simple microchip, spermbots and external magnetic fields. The concept is depicted in Figure 25. The microchip consists of two chambers that are connected through a channel.

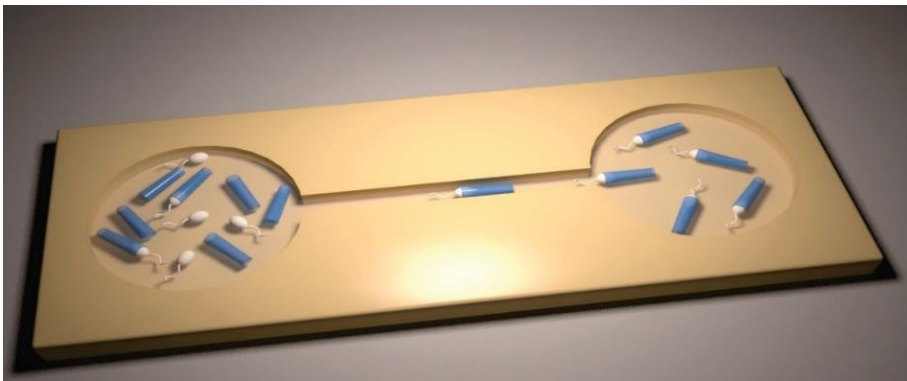


Figure 25: Schematic illustration of separation chip. This simple microchip consists of two chambers that are connected with a channel. In the left chamber is a mixture of microtubes and sperm cells. The captured

sperm cells inside microtubes can be guided by an external magnetic field into the right chamber and thereby selects the motile sperms. (Image source: Dr. R. Träger, IFW Dresden)

A mixture of sperm cells and microtubes is injected in the left chamber of the microchip. After coupling of sperm cells with the ferromagnetic microtubes, the actively moving spermbots can be separated into the right chamber by application of an external magnetic field. Since only the moving spermbots can pass through the middle channel, this approach leads to the selection of motile sperm cells and separation from dead cells, other components of the semen sample and microtube debris.

A commercially available microfluidic chamber from ibidi® (Martinsried, Germany) was used as a platform with 2 chambers that are connected by a narrow channel. The platform, as displayed in Figure 26, consists of two 80 μ L chambers that are connected by a narrow 70 μ m high channel (1 mm wide and 10 mm long). The red circles in Figure 26 mark the position of the spermbot that is guided from the top 80 μ L chamber into the middle channel over a time length of 5 minutes. Using a permanent magnet that is mounted on a rotating stand underneath the sample, the microtube is aligned parallel to the magnetic field lines and the propulsion by the sperm cell leads to the forward motion of the robot. After less than 5 minutes, the selected microtube with the captured sperm cell has reached the channel and is separated from all other microtubes. At this point, the selected spermbot can be removed from the chip by taking out the solution from the middle channel with a

micropipette. The spermbot in this separation process displays an average velocity of $15 \mu\text{m/s}$.

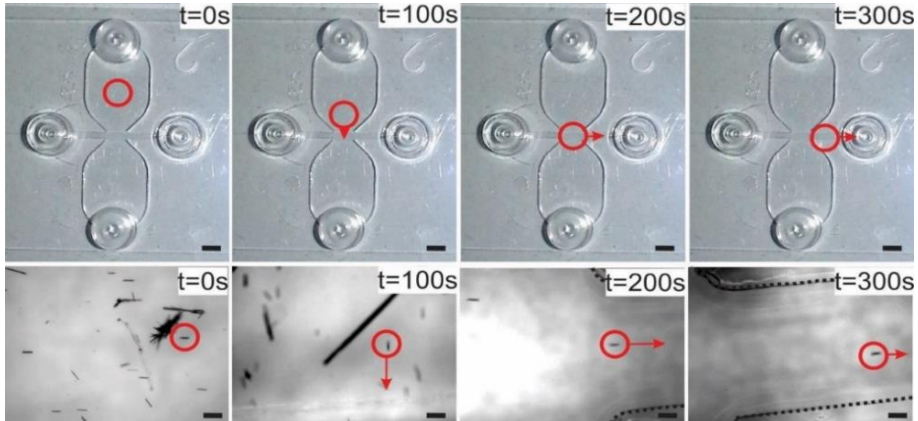


Figure 26: Separation of a spermbot from a mixture of microtubes and sperm cells. Top row: top view of the ibidi® chip used for separation. The red circle marks the position of the guided spermbot. Scale bar 1 mm. Bottom row: close view into the micro-platform during separation process. The red circle marks the selected spermbot. Scale bar 100 μm . (Modified from ^[47])

This method demonstrates that the spermbot is capable of capturing and separating single sperm cells from a mixture of spermatozoa and microtubes. Only the fast moving spermbots will be moved into the separation channel. Thereby, a selection based on cell motility is performed. However, no active pre-selection of spermatozoa is performed and sperm cells are captured on a random basis. Nevertheless, this experiment serves as a proof-of-concept for single cell separation. No further analysis of the selected sperm cell regarding its quality or fertilization capability was conducted. The goal was to

demonstrate the usefulness of spermbots to capture and separate single cells from a mixture. In the framework of sperm selection methods ranging from the morphological selection of single sperm cells for ICSI (which relies on the observation and experience of the andrologist) to selection based on motility, the here presented spermbot selection method is a new approach and has its value.

4.5 EFFECT OF DECREASED MICROTUBE LENGTH

As mentioned in chapter 4.1, the velocity of the spermbots is highly influenced by the confinement of the sperm flagellum inside the microtube. Since the length of the microtube determines how much of the sperm flagella is confined inside the cavity of the tube, one way to improve the spermbot velocity is to fabricate shorter microtubes. This enables the flagellum to move more freely and takes advantage of its full amplitude in contrast to its restriction in long microtubes. To demonstrate this, 20 μm microtubes were fabricated by rolled-up technology, as described in chapter 3.1. Since the full length of a bovine spermatozoon including its head (10 μm long) and flagellum is around 60 μm , the 20 μm tubes capture only the cell head and a maximum of 10 μm of the shaft of the flagellum, if the cell has entered the tube completely. This 20 μm microtube is depicted in the right image in

Figure 27 in comparison to a 50 μm long microtube in Figure 27 on the left.

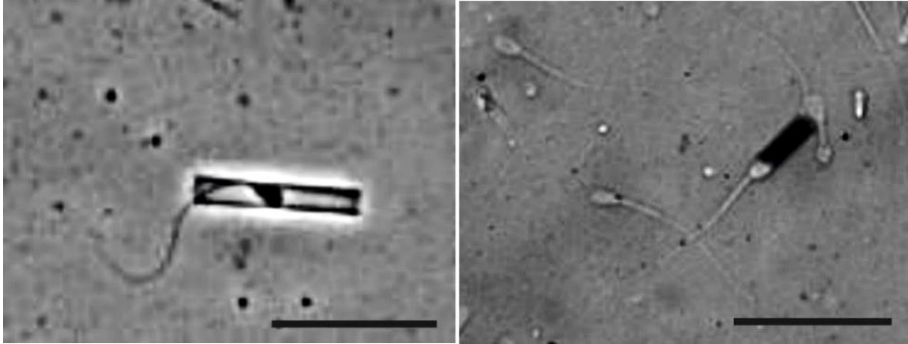


Figure 27: A bovine spermatozoon captured inside the 50 μm (left) and 20 μm (right) rolled up microtube. Scale bars 50 μm . Images modified from [108].

The average spermbot velocity can be improved from 10 $\mu\text{m}/\text{s}$ (in case of 50 μm long spermbots, see chapter 4.1) to 33.3 $\mu\text{m}/\text{s}$ with a velocity relative to the initial free cell speed of 84 % (see graph in Figure 28). This means that when 20 μm long microtubes are used for the cell capture, the initial free cell speed is only reduced by 17 % with a standard deviation of 9 % compared to an average speed reduction for a 50 μm spermbot of 82 %, with a standard deviation of 6 %.

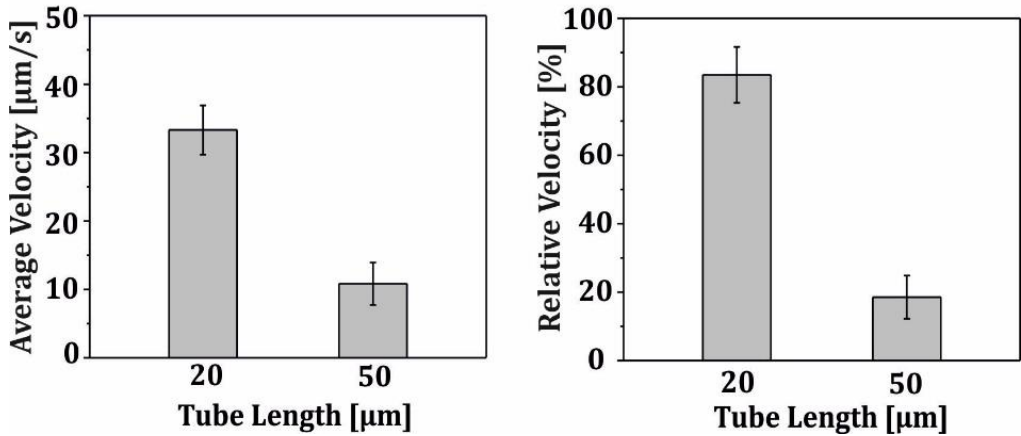


Figure 28: Comparison of spermbot velocity consisting of 50 µm and 20 µm microtubes. Average (left) and relative (right) velocity of the spermbots. The relative velocity is defined as spermbot velocity divided by initial free cell velocity times in percent. ^[108]

4.6 COUPLING EFFICIENCY

The capturing process of the sperm cell inside the microtube is based on the random motion of the spermatozoon and its arbitrary entry into the microtube. The success of capturing is also dependent on the tube architecture, meaning the length and radius of the tube contributes to the entrapment of the cell. For 50 µm microtubes with a diameter of 5 – 8 µm the coupling efficiency is 23.6 ± 1.9 %. The coupling efficiency is defined as follows: an array of at least 200 microtubes is immersed in a solution of sperm cells with a concentration of 10^6 cells/mL and incubated for 30 minutes on the tube array. The number of microtubes with captured sperm cells was then counted and divided by the total

number of microtubes on the array. This results in the coupling efficiency in percentage. It was observed that the coupling efficiency for 20 μm long spermbots with the same range of diameter (5-8 μm) is much lower and lies around 1%. A summary of the average and relative velocities as well as the coupling efficiencies of 20 μm and 50 μm spermbots is displayed in Table 3.

Table 3: Average and relative velocities as well as coupling efficiencies of 50 μm and 20 μm spermbots. The average values displayed are given with the standard error of the mean ($N \geq 5$).^[108]

		50 μm tubes	20 μm tubes
Average velocity [$\mu\text{m/s}$]		10.4 \pm 0.2	33.3 \pm 3.6
Relative velocity [%]		18.3 \pm 0.4	83.5 \pm 3.4
Coupling efficiency [%]	Bare microtubes (control)	23.6 \pm 1.9	1.1 \pm 0.2
	Fibronectin on Au or SiO ₂ <i>via</i> surface chemistry	38.6 \pm 3.6	4.8 \pm 1.6
	Fibronectin on SiO ₂ <i>via</i> microcontact printing	58.7 \pm 2.2	8.0 \pm 1.7

Even though the velocity of spermbots is increased by using shorter microtubes, their coupling efficiency is significantly decreased. The cause for the lower chance of entrapping cells in 20 μm tubes is that the length of the microtube contributes to the confinement of the cell. The shorter the microtube is, the higher the chance that the sperm cell can slip through. There is only little contact area between the flagella and the tube walls. The microtube is slightly larger than the sperm cell head and due to the vigorous motion of the spermatozoa, it is easier to escape from shorter tubes.

In an approach to improve the coupling efficiency, in addition to the physical entrapment of the cell inside the microtube, the cell-tube binding is supported by attaching biomolecules on the inner tube surface which interact with the sperm cell membrane. There are several candidates of biomolecules that are able to bind to sperm cells such as fibronectin, hyaluronic acid and others. [144-150] The glycoprotein fibronectin is a component of the extracellular matrix and also present in the surroundings of the oocyte.[145] Spermatozoa possess cellular adhesion molecules, also called integrins, on their cell membrane that can bind to fibronectin. The integrins connect the external environment with the interior cytoskeleton of the cell and act as mediators.[145,146] Fibronectin was recently utilized in a high throughput platform to attach and analyze single spermatozoa to a planar surface.[147] Hyaluronic acid binds specifically to mature spermatozoa.[148-150] Hyaluronic acid was also tested as a sperm coupling agent inside microtubes, but did not increase the coupling significantly. A fluorescently labelled form of

hyaluronic acid was used as characterization method of the two functionalization approaches, see section 3.3.

Hyaluronic acid was tested in 20 μm microtubes and improved the coupling from 1.1 % to 3.3 % (standard error of the mean (SEM): 1.3 %). The lower coupling increase of hyaluronic acid compared to fibronectin (see below) can be explained by the specific binding of only matured spermatozoa to hyaluronic acid. It is known that hyaluronic acid is a natural component of the extracellular matrix surrounding the egg cell and cumulus cells and that it is involved in the selection process of spermatozoa prior to fertilization *in vivo*.^[151] Only spermatozoa that have undergone the necessary maturation steps for fertilization (e.g. formation of zona pellucida binding sites) and are still viable, contain high DNA integrity and have not yet acrosome reacted are able to bind to hyaluronic acid.^[148-150] The percentage of mature cells in a population of spermatozoa is generally around 10 % which explains why the increase in coupling success rate is fairly low.^[118]

This work focuses on the use of fibronectin as sperm binding agent for improving coupling efficiency, because it addresses the general population of sperm cells. Every sperm cell independent of its maturation state is expected to exhibit active fibronectin binding receptors on its surface. Figure 29 shows that for FN-containing 20 μm microtubes the coupling efficiency was improved from 1.1 % (control, non-functionalized, SEM = 0.2 %) to 4.8 % by surface chemistry (SEM = 1.6 %) and to 8.0 % by microcontact printing (μCP) (SEM = 1.7 %). In 50

μm microtubes, the coupling efficiency is improved from 23.6 % (control, non-functionalized tubes, SEM = 1.9 %) to 38.6 % by surface chemistry with a SEM of 3.6 % and to 58.7 % by the μCP method (SEM = 2.2 %). In general, the coupling of spermatozoa inside microtubes occurs solely due to mechanical trapping of the cell inside the tube in case of the non-functionalized microtubes. Both methods, μCP and EDC/NHS surface chemistry, improve the coupling efficiency by adding a binding component on the inner tube surface. Microcontact printing results in a better coupling efficiency compared to NHS/EDC chemistry, because it deposits a large amount of target molecule exactly on the nanomembranes before roll-up. Thereby, the local concentration of target molecules is significantly higher inside the tube resulting in a higher number of binding events of spermatozoa inside the microtube. The EDC/NHS method functionalizes the whole array but does not offer a pre-concentration of the target molecule inside the microtube. However, it also causes an increased number of coupling events due to the biochemical linking of the target molecule FN on the inside of the tube which binds the spermatozoa.

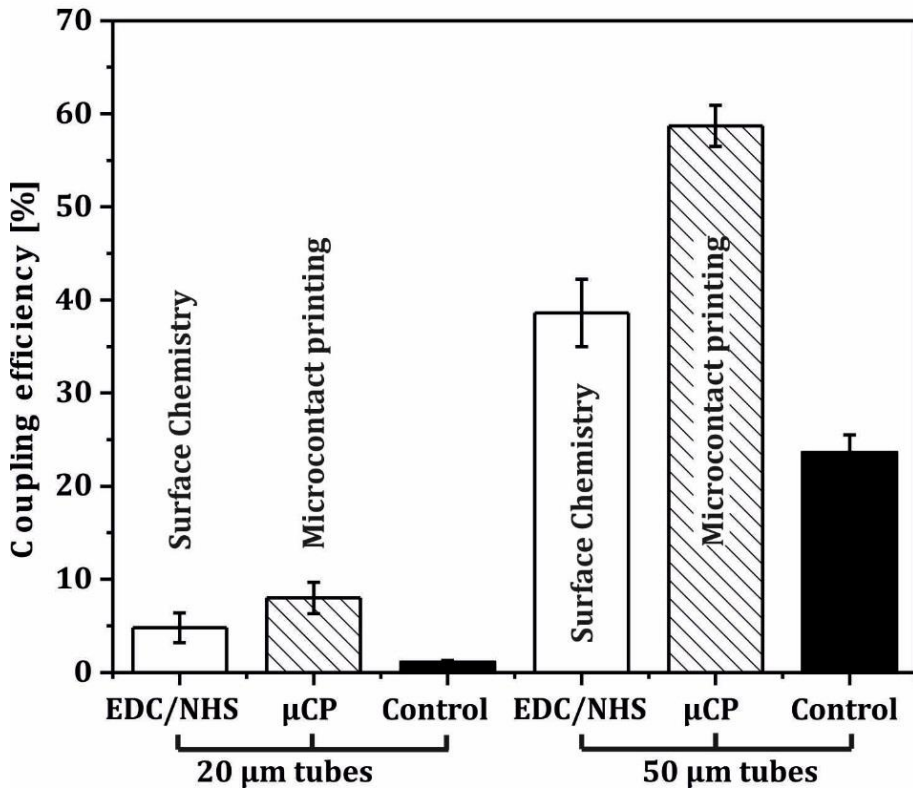


Figure 29: Coupling efficiency of bovine spermatozoa in 20 μm and 50 μm rolled up microtubes with surface modification by surface chemistry or microcontact printing. The coupling efficiency is defined as the number of microtubes with captured sperm cells divided by the total number of microtubes on the array. The controls are microtubes without surface modification.^[108]

The coupling efficiency in 50 μm microtubes is generally higher than in the short 20 μm microtubes. This matter of fact is originated in the stronger confinement effect on the sperm flagellum in 50 μm tubes. The short tail confinement in 20 μm microtubes was mentioned in section 4.5

as a reason for higher sperm velocity. It is also the reason for the decreased coupling success in 20 μm microtubes. In 20 μm microtubes, spermatozoa are more likely to slip through the tube and do not remain captured. This phenomenon might be illustrated by comparing the sperm cell inside the tube to rotating a rope in circular and wavy motion through a tube. The rope keeps hitting the inner walls of the tube and this causes an impact force on the rope. This impact force is stronger, the longer the tube is. The microtubes are large enough that the sperm heads can fit through the opening and escape the tubes. This also means that the sperm cells are trapped inside the tubes in a dynamic way without locking the sperm head and that the confined flagella motion contributes to the entrapment of the cell. The influence of the tube radius can be neglected in this context because both, 20 μm and 50 μm microtubes, were fabricated to have the same range of diameter of 5 - 8 μm .

4.7 THERMORESPONSIVE POLYMERIC MICROTUBES FOR CELL RELEASE

Although the previous chapters showed that single sperm cells can be captured and guided in rolled-up metallic microtubes, these microstructures do not offer the possibility to release the cell in a controlled way. In this section, the stimuli-responsive polymer PNIPAM is used to fabricate a dynamic structure for remote-controlled release of single sperm cells. In section 2.5, it was explained how the polymer PNIPAM swells and shrinks upon small temperature changes and how this can be used to induce conformational changes of polymeric microstructures. Figure 30 illustrates how 40 μm PNIPAM circles,

fabricated by photolithographic processes as described in section 3.4.3, swell and shrink when the temperature is cycled. It also shows how the films with thin passive layers of metals form microtubes that can open and close when the temperature of the solution is heated above or cooled below the LCST.

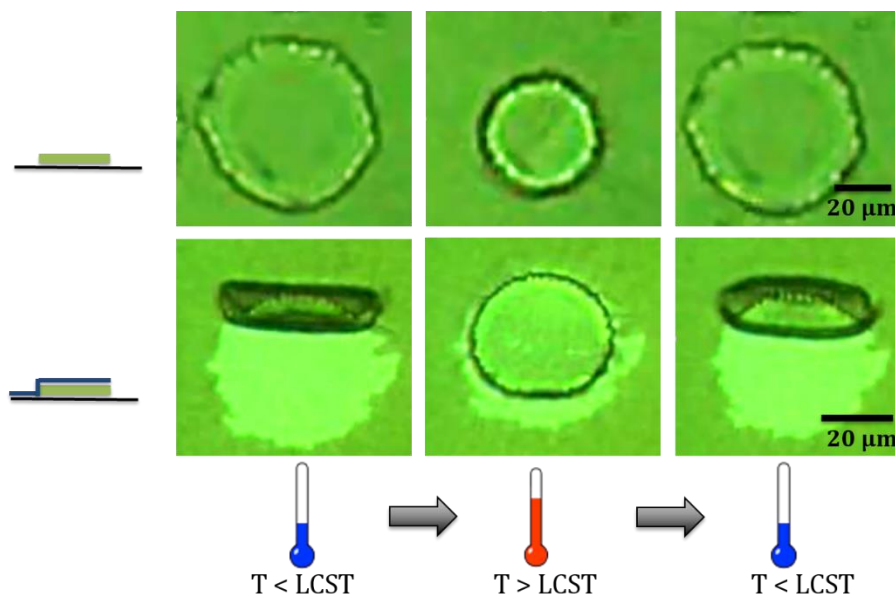


Figure 30: Reversible swelling and shrinking of PNIPAM-co-ABP polymer films without (top row) and with passive layer (bottom row) on a silicon wafer as substrate. The temperature increase leads to a collapse of the polymer film which is reversed when the temperature is reduced again. The bottom row shows that the shrinking leads to the unfolding and refolding of the microtubes when a passive layer is present.

This concept was proven to be useful to create stimuli-responsive microjets. Microjets are small autonomous motors consisting of

microtubes which move by jet propulsion through the generation of oxygen bubbles on their inner platinum layer due to catalytic reactions of hydrogen peroxide. PNIPAM films with an inner platinum layer create microjets that can speed up and slow down depending on their tube radius which is changing when different temperatures are applied. Figure 31 demonstrates cycles of temperature which lead to reversible folding and unfolding of the microjet and thereby changing of the speed of the microjet. This stimuli-response leads to a reconfiguration of the shape of the microjet and demonstrates a remote-controlled speed control mechanism achieved by small temperature changes.

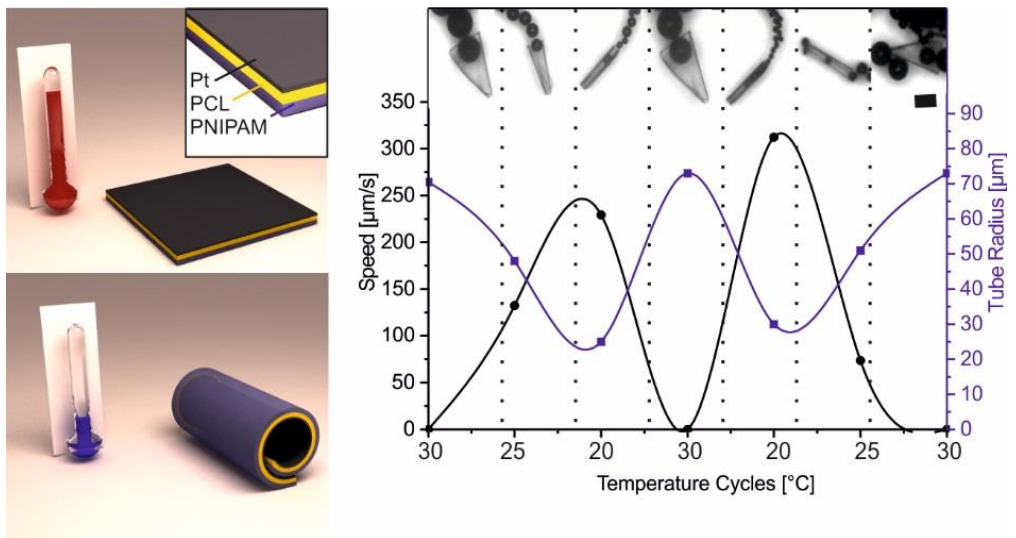


Figure 31: Stimuli-responsive microjets made from poly(N-isopropylacrylamide) (PNIPAM), polycaprolactone (PCL) and an inner platinum layer. The jets unfold at high temperatures (top left) and unfold at lower temperatures (bottom left).The graph on the right shows

temperature cycles with according microjet speed (left axis) and microtube radius (right axis). Scale bar 100 μm . Modified from [90].

Similar to stimuli-responsive tubular microjets^[90] that open and close and thereby change their speed accordingly, this concept was used in this work for the first time for sperm cell release. Rolled-up nanometer-thin polymeric films based on the thermoresponsive material poly(*N*-isopropylacrylamide-co-acryloylbenzophenone-co-acrylic acid) (PNIPAM-co-ABP-AAc) and thin layers of titanium and iron as ferromagnetic passive elements were fabricated to capture and release sperm cells in a physiological temperature range upon an external temperature stimulus.^[152]

Crucial for the stimuli-response of this tubular polymeric microstructure is the preservation of its thermoresponse resulting in folding and unfolding of the structure. In order to tailor the polymer poly(*N*-isopropylacrylamide) (PNIPAM) for the sperm capture and release, two main modifications were made. At first, in order to directly photopattern the thin polymeric films, the photosensitive monomer 4-acryloylbenzophenone (ABP) was synthesized. Xiao et al.^[113] reported the synthesis of this photosensitive monomer and this protocol was followed closely, see experimental section 3.4. This modification enables the use of a photomask and deep UV (254 nm) photolithography to obtain the fine-structured patterns of these polymer films. The resulting polymer films made from PNIPAM-co-ABP were able to fold and unfold at 28 °C. This temperature is lower than the LCST of pure PNIPAM

(~32 °C) due to the addition of the monomer ABP which is directly associated to the swelling properties of the polymer.

Secondly, with the aim of increasing the shrinking temperature (which leads to opening of the tubes) to temperatures that are optimum for bovine sperm cells (38 °C), Acrylic acid was added as a second monomer to the polymerization. Acrylic acid increases the amount of hydrophilic monomers in the copolymer and therefore shifts the LCST to higher temperatures.^[153] Hence, acrylic acid was co-polymerized with the photosensitive monomer ABP and NIPAM resulting in the photopatternable, thermoresponsive polymer PNIPAM-co-ABP-AAc with a lower critical solution temperature around 38°C. The folding temperature was determined by measuring the radius of the polymeric structures containing a passive layer of Ti/Fe for folding, at different temperatures during the folding. As shown in Figure 32, the resulting temperature at which PNIPAM-co-ABP-AAc microtubes containing an inner passive layer unfold is about 38 °C, compared to the photopatternable polymer without acrylic acid, PNIPAM-co-ABP, with a folding temperature of 28 °C. Consequently, the addition of acrylic acid to the polymerization of NIPAM and ABP offers a physiological temperature for the sperm cell capture and release experiments.

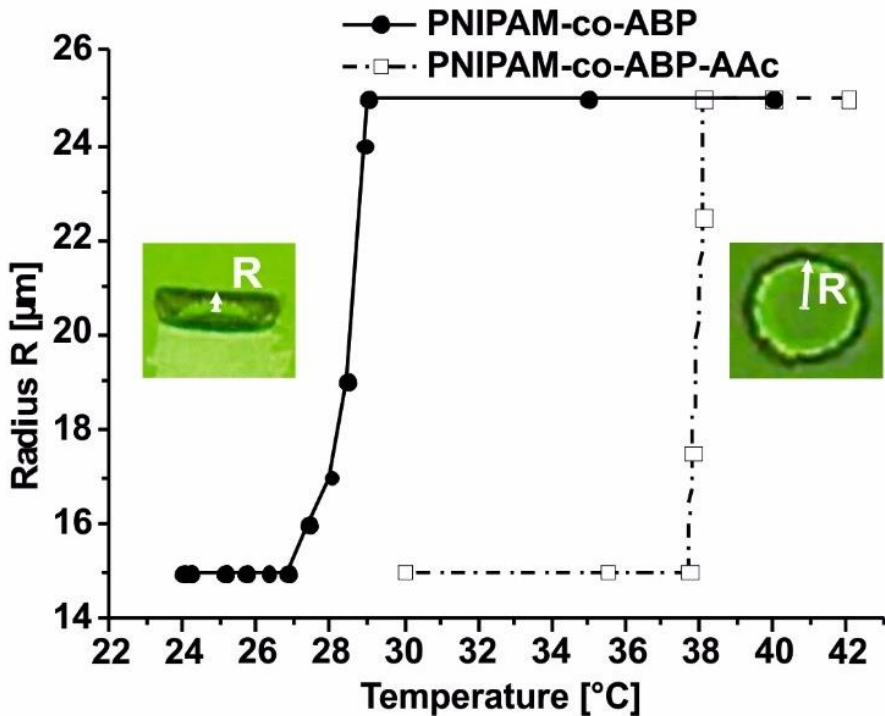


Figure 32: Swelling temperature of PNIPAM-co-ABP and PNIPAM-co-ABP-AAc layers displayed as radius change of the folding microtube depending on the temperature.^[152]

In order to verify the reversible thermo-responsiveness of the synthesized polymer, cycles of temperature between 20 - 55°C were applied to the polymer films. Figure 33 illustrates the highly reversible swelling process of the polymer films during heating and cooling cycles. When there is no passive layer deposited on top of the PNIPAM-co-ABP-AAc, the film swells and contracts during temperature cycles, but does not fold. In this way, the change in size of the circles can be measured, as illustrated in Figure 33. The diameter of ten polymeric circles without

passive layer were measured for each data point at different temperatures and normalized to the maximum diameter of the circles in the swollen state in order to obtain a normalized size. The change in diameter of the photopatterned 40 μm polymer microcircles during such temperature cycles is around 25 %. The swelling is sufficient to cause a reversible folding of the PNIPAM-co-ABP-AAc films into the desired microtubes.

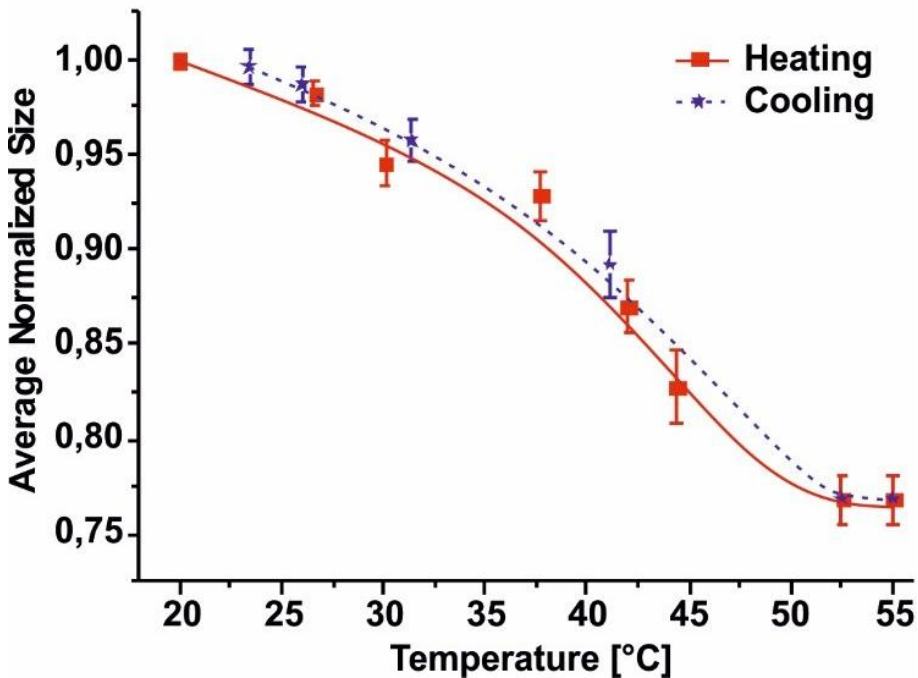


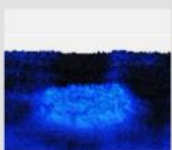
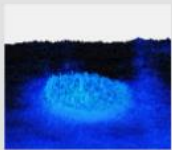
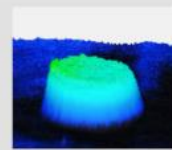
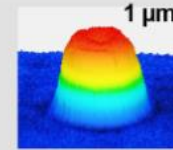
Figure 33: Reversible swelling process of PNIPAM-co-ABP-AAc film. The red data curve resulted from a heating process from 20 °C to 55°C, the blue data curve was obtained from cooling the samples from 55 °C to 23°C. The average normalized size of the polymer films were obtained from measuring the diameter of 10 circular 40 μm polymer structures for each

data point and normalizing them over the initial, maximum swollen state of the film.^[152]

Once the passive layers of Ti (2 nm, adhesive) and Fe (10 nm, ferromagnetic) are deposited, the 20 μm circular films swell and result in 30 μm long microtubes after being immersed in aqueous solution at temperatures below 38 $^{\circ}\text{C}$ (see left inset in Figure 32).

As the last step of the fabrication, thin layers of Ti and Fe were deposited by electron beam evaporation on top of the PNIPAM-co-ABP-AAc, as the layers will only fold when a passive, non-swelling layer is present. Table 4 illustrates how the folding behavior of the polymer changes depending on the layer thickness. The images in the morphology row are obtained from confocal microscopic measurements of 20 μm circles and the color code illustrates the different heights of the structures. The schematic on the bottom left illustrates the composition of the microtubes with an outer PNIPAM-co-ABP-AAc layer and thin films of Ti (2 nm) and Fe (10 nm) as passive layer. The bottom row displays optical images of the folded microtubes for the polymer concentrations 5 %, 10 % and 20 %.

Table 4: Folding behavior of the polymer films depending on the concentration of PNIPAM-co-ABP-AAc.^[152]

Concentration of PNIPAM-co-ABP-AAc	<5%	5%	10%	20%	
Film thickness	<100nm	108 ± 13 nm	209 ± 25 nm	782 ± 40 nm	
Folding	No folding	Folding ok, no unfolding	Folding ok, only few unfold	Folding & unfolding good	
Morphology (20 μm circles)					
Diameter	-	Too small (<7μm)	Ok (6-15μm)	Best (6-12μm)	
					

Below 5 % concentration of PNIPAM-co-ABP-AAc in ethanol, no folding was observed (only wrinkling) due to the fact that adhesion to the substrate dominates at low thicknesses and therefore, the films cannot release and fold into three-dimensional shapes. 5 % layers result in microtubes that fold too tight for sperm capture (less than 7 μm outer diameter) and do not unfold. The inability to unfold may be due to the tight rolling which results in multiple windings. 10 % and 20 % layers gave best results for folding, 20 % PNIPAM-co-ABP-AAc being the best

for sperm cell capture and release. Presumably, there is a minimum layer thickness that maintains the reversible folding mechanism.

The folded tubes can then be used to capture bovine sperm cells and are propelled forward by the motion of the cells. The images in Figure 34 on the left demonstrate the different scenarios of moving spermbots. Depending on how the circular polymer layer folds, straight, conical or tubes with curved edges and triangular shaped tubes were obtained, as illustrated by the optical images and schematics in Figure 34. The graph on the right displays the maximum forward velocity of spermbots observed for the different cases. The straight spermbot shows the lowest velocity with $5 \mu\text{m/s}$ which is due to the tight flagella confinement. How the flagella confinement plays a decisive role for the resulting spermbot velocity is described in Section 4.1. The conical tubes and curved tubes show higher velocities of almost $30 \mu\text{m/s}$. In these two cases, the flagella are less confined and have more space to beat with their full amplitude. The triangular tube performs rotational motion and therefore the forward motion is decreased. For the capturing and propulsion event, all four cases are useful. It was observed that it is not as easy to release cells from the triangular or straight tubes when they do not unfold properly. The straight tubes do not unfold when they consist of more than 1.5 windings, while the triangular tubes often stay folded in one corner and thereby keep the cell captured.

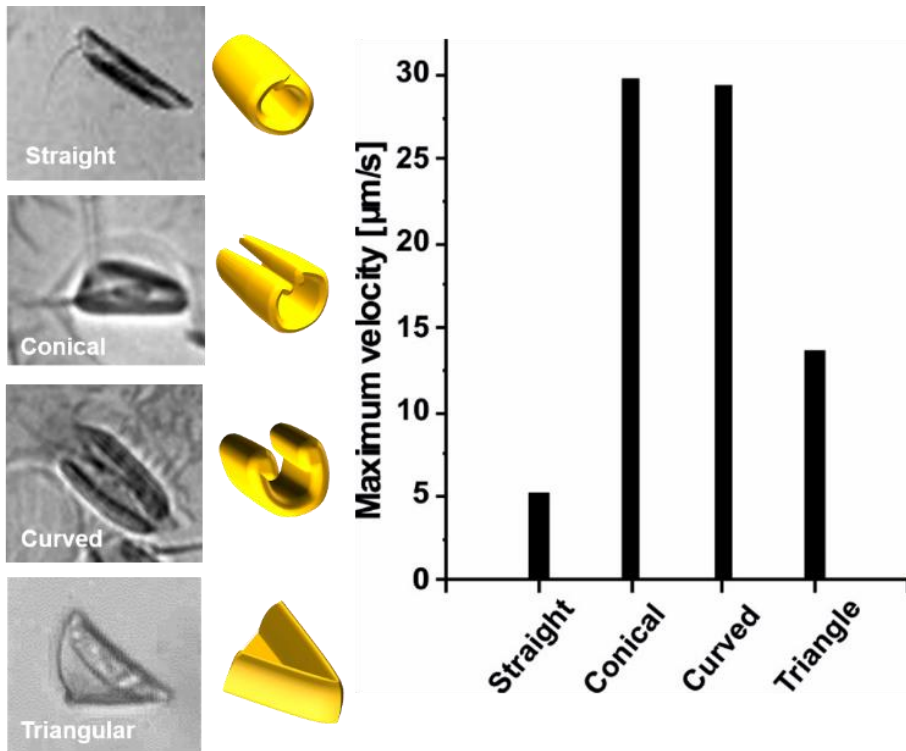


Figure 34: Polymeric spermbots. The left row of images displays four scenarios of spermbots folded from PNIPAM-co-ABP-AAC structures with according schematics to illustrate the folding cases. The graph of the right shows the observed maximum forward velocities of the polymeric spermbots.^[152]

The release of the sperm cells from the microtubes is performed by increasing the temperature, e.g. from a working temperature of 30 °C to 38 °C (optimum temperature of sperm cells). Thereby, the polymer layer collapses and this results in the increase of the radius and final opening of the tube. Figure 35 illustrates the process of the cell release.

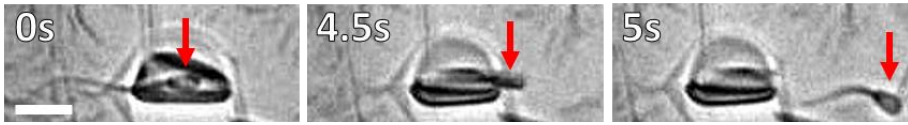


Figure 35: Image series of single bovine sperm cell release from an attached microtube over a time interval of 5 s. The red arrows point at the sperm head. Scale bar 20 μm .^[152]

The red arrows in the image series are pointing at the sperm cell head. At 4.5 s, the tube unfolds and the cell is released. On average, it takes 4.8 ± 0.9 s to release the cell from the microtube once they unfold. The graph in Figure 36 illustrates the velocity of the polymeric spermbot. The instantaneous velocity of the spermbot ranges from 2 - 47 $\mu\text{m/s}$ and is on average 15 $\mu\text{m/s}$ at a temperature of 30 °C. Once the temperature increases, the tube starts unfolding at 33 °C and releases the cell at 35 °C. The exact release temperature varies between 35 - 38 °C as these tubes are dynamic structures and unfold in a slightly different way, but also the motion of the individual sperm plays a role for the exact release event. Upon cell release, it was observed that the freely swimming sperm cell has a velocity of about 50 $\mu\text{m/s}$. The decreased spermbot velocity compared to the free cells is known from metallic microtube-sperm hybrids (section 4.1) and is mainly due to the cargo they are pushing and the flagella confinement.

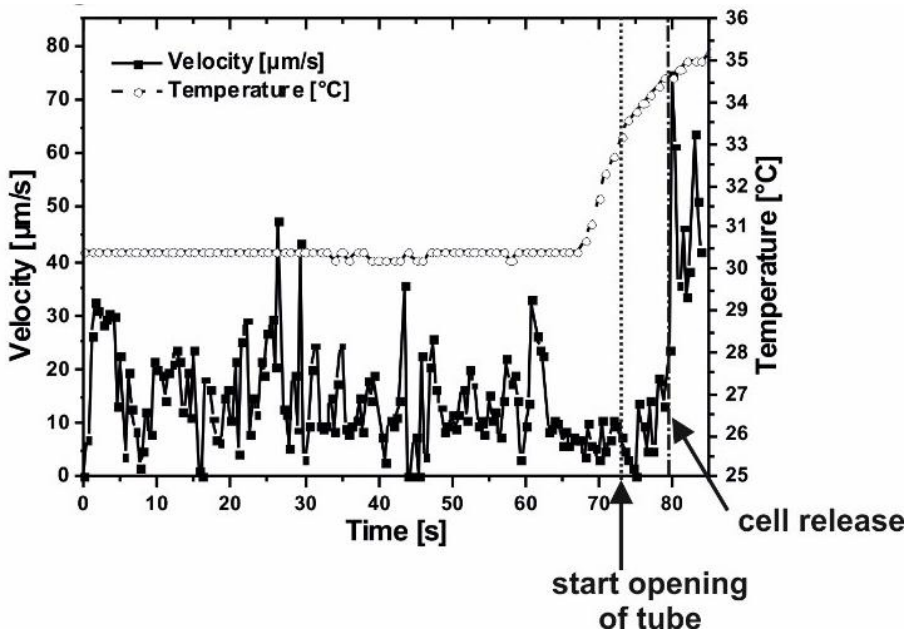


Figure 36: Cell release process: Sperm cell velocity (left axis) and temperature (right axis) over time for a representative example of a sperm cell. For $t > 79$ s (sperm cell release), the free cell velocity is displayed.^[152]

Finally, it is briefly shown that the incorporated iron layer can be used for external magnetic steering of the polymeric sperm cell for guidance purposes. Figure 37 illustrates how the sperm cell is aligned to the external magnet and can be guided over time. At 40 s, the cell is released from the sperm cell due to temperature increase to 38 °C.

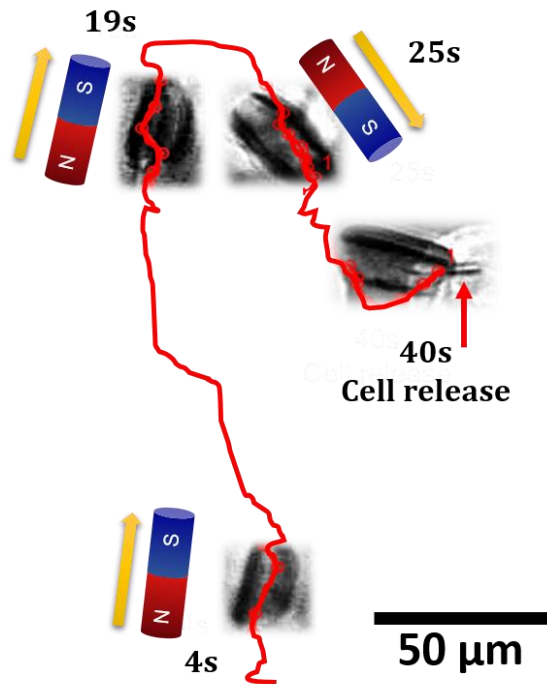


Figure 37: Magnetic guidance of a polymeric spermbot and release of cell. The red line shows the tracking of the spermbot over 40 s. The schematics of the magnets illustrate the direction of the external magnetic field. At $t = 40$ s the cell is released from the spermbot due to temperature increase. Modified from [152].

In summary, the remote-controlled temperature-induced release of single sperm cells from dynamic microtubular structures was demonstrated. The polymeric microtubes are tailored to fit single bovine sperm cells and modified to release them at physiological temperatures around 38 °C. The release process is fast and biocompatible. The slight temperature changes during capture and release do not harm the cells and as a matter of fact could be exploited in sperm thermotaxis. It has

been shown that sperms are exposed to a temperature gradient *in vivo* between the isthmus and the fertilization site of the oocyte and it is believed that this temperature gradient of 2 - 3 °C attracts the sperm cells to the oocyte location with the mechanism of thermotaxis.^[118] This draws an analogy between sperm thermotaxis *in vivo* and the here presented temperature-triggered cell release. Finally, this represents the first example of a remote-controlled single sperm cell release from a microstructure. This work demonstrates thermo-responsive microtubes that are tailored to capture single sperm cells, guide their motion and release them at physiological temperatures. This is an important step towards the development of new assisted fertilization techniques as well as, in a broader view, single motile cell release.

4.8 SPERM VIABILITY TESTS

Compatibility of the involved materials is a very important fact when targeting biomedical applications. Sperm compatibility of the involved materials (PNIPAM-co-ABP-AAc, Ti and Fe) was verified in sperm viability tests. Flat films of PNIPAM-co-ABP-AAc with and without Ti and Fe cover were compared in terms of sperm viability with a glass surface as the control sample. The results are displayed in Figure 38.

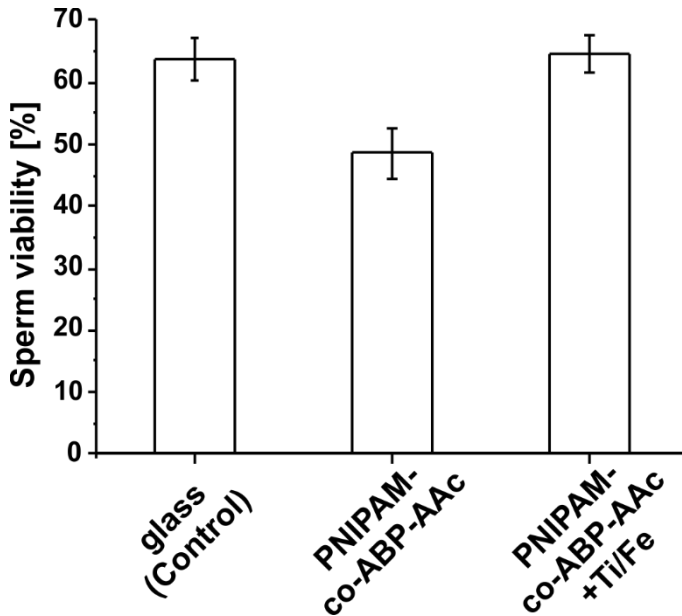


Figure 38: Sperm viability test performed with SYBR 14 (live cells) and propidium iodide (dead cells) in SP-TALP on glass surface (control), PNIPAM-co-ABP-AAc and PNIPAM-co-ABP-AAc with Ti (2nm) and Fe (10nm) coating.

According to the performed t-test at the 95% probability level (where M is the average corresponding to the sperm viability value, SEM the standard error of the mean, N the count, and P the P-value), the results in Figure 38 show that the cell viability on the polymer with metal coating as passive layer ($M = 64.6\%$, $SEM = 3.0\%$, $N = 3$) is comparable to the viability on glass ($M = 63.6\%$, $SEM = 3.3\%$, $N = 3$, $P = 0.9 > 0.05$). However, the viability on the polymer PNIPAM-co-ABP-AAc without metal layer is reduced ($M = 48.5\%$, $SEM = 4.0\%$, $N = 3$, $p = 0.19 > 0.05$) compared to the control sample, but not in a significant amount. The reduced viability on PNIPAM-co-ABP-AAc without metal layer can be

explained by possible remains of monomers of NIPAM inside the polymer layer which can cause toxic effects on the cells.^[154] The t-test confirmed the significance in difference to be $p = 0.9$ and $p = 0.19$ (both >0.05) and therefore these values can be considered to show no significant difference.

5 SUMMARY AND CONCLUSIONS

In summary, this doctoral thesis presents a novel type of microbiorobot which is generated by the self-assembly of a motile sperm cell and a rolled up magnetic microtube. The motion of this tubular microbiorobot is based on the powerful propulsion by the sperm flagellum. The spermbot moves in physiological conditions and, accompanied by an external magnet, can be guided by magnetic directional control to desired locations. The performance of the microbiorobot was investigated regarding the influence of tube radius, penetration of cell inside the microtube and temperature on the velocity of the spermbot. It was shown that the more the cell is confined, the lower is the resulting velocity of the spermbot. Also, the larger the tube radius, the larger is the penetration of the cells inside the tube. Cells can be captured in tubes with 2 – 4.5 μm radius. By increasing the temperature within the range of 5 °C to 37 °C, the spermbot velocity can be increased. This increase is originated in the accelerated metabolic activity of spermatozoa which leads to faster ATP generation. In turn, this results in increased sperm flagella amplitude and frequency and hence faster sperm motion. Upon temperature reduction, the spermbots are slowed down, which again is due to the reduced sperm velocity at lower temperatures. The temperature dependence of spermbot performance is a reversible mechanism. As a proof-of-concept experiment, the separation of a selected sperm-driven microbiorobot by remote magnetic guidance from

a chamber with microtubes and spermatozoa into a separate chamber was demonstrated on-chip. Improving the design of the microtubes by decreasing the length of the microtubes from 50 μm to 20 μm further improved the velocity of the spermbot. Rolled up technology offers the opportunity to tune the dimensions of the microtubes simply by adjusting the dimensions of the photomask patterns. Therefore, 20 μm microtubes could easily be obtained for the capture of single bovine spermatozoa. The reduced confinement of the flagella inside the short 20 μm microtubes leads to increased spermbot velocities. Furthermore, two surface modification methods were applied to improve the coupling success between the spermatozoa and the microtubes. The extracellular matrix protein fibronectin is known to attach to the membranes of spermatozoa. Surface chemistry was applied to attach fibronectin covalently to the inner layer of the microtube *via* NHS/EDC as linkers. Also, microcontact printing was applied to print fibronectin from a PDMS stamp onto the patterned nanomembranes before rollup. Both methods resulted in increased coupling between microtubes and spermatozoa. Microcontact printed microtubes lead to higher coupling success due to more concentrated placement of the protein on the inner tube surface. A cell release mechanism was implemented by the use of thermoresponsive polymeric microtubes. The thermoresponsive microtubes were fabricated from patterned films of PNIPAM-co-ABP-AAc and thin passive layers of titanium and iron. The polymer layer is swollen and leads to rolled up microtubes at temperatures below their lower critical solution temperature. Thereby, they are designed to

capture single spermatozoa. The thin ferromagnetic layer guarantees the remote directional control of the microtubes while they are propelled by the spermatozoa. When the temperature of the medium is increased to 38 °C, the spermatozoa can be released again because the thermoresponsive polymer layers start shrinking and thereby opening the microtubes. The release mechanism is crucial for the sperm-driven microbiorobot to become a promising device for alternative reproduction methods where fertilization takes place *in vivo* once the spermbots loaded with selected sperm cells are remotely guided to the oocyte.

The involved materials PNIPAM-co-ABP-AAc in combination with titanium and iron were tested regarding their biocompatibility and it was proven that the polymeric microtubes covered with titanium and iron have little effect on the cell viability compared to the control sample on glass.

In conclusion, the combination of rolled up microtubes and single spermatozoa lead to a microbiorobot that uses the sperm as propulsion force for this biohybrid device. It is a biocompatible system that can swim under physiological conditions. Influencing factors on the performance of the spermbot such as temperature, tube design and binding to biomolecules were analyzed and discussed in this work. It is the first example of guiding single spermatozoa by an external magnetic field simply by mechanical trapping inside a microtube. Finally, stimuli-responsive microtubes offer a way to remotely release single cells by

temperature increase. Even if this approach leaves much room for improvement, it is a unique initial step towards innovative research aiming at assisted *in vivo* fertilization technology.

6 OUTLOOK

In general, biohybrid microrobotic devices demonstrate potential for various applications in medicine, such as micromanipulation, minimally invasive operations, diagnostics, therapeutics and targeted drug delivery. If the specific potential of spermrobots is considered to be in the field of reproductive medicine, a number of future research subjects come to mind that are prerequisites for the application in such a medical field. In the current work, sperm cells enter the microtube randomly. The development of a method for the controlled capturing of specifically selected sperm cells will be an important feature. As pointed out in section 2.2 of this thesis, the state-of-the-art assisted reproduction technologies, e.g. ICSI, bypass the natural sperm selection stages that occur *in vivo* by injecting the sperm cell directly into the oocyte. Nonetheless, the sperm selection by the female reproductive system which includes sperm passage through different parts of the reproductive tract, sperm binding to the oviductal epithelium and local storage, capacitation and release of sperm, passage through the cumulus cells and the zona pellucida and final fusion with the oocyte, seems to be a crucial procedure that leads to successful reproduction. Mimicking such a multi-step sperm selection *in vitro* would be a great way to replace the sperm selection method before the cells are captured in the microtubes for the delivery to the oocyte. This selection method could for instance include the selection of spermatozoa regarding their motility,

their ability to pass through microchannels with similar topography as found in the *in vivo* reproductive tract, sperm attachment to and release from oviductal cells and insurance of capacitation of spermatozoa. However, these biochemical processes are not fully elucidated yet, so further studies are necessary to ensure the proper mimicking of these processes in an *in vitro* setup.

For the tracking and visualization during *in vivo* applications, it would be necessary to develop a setup that allows the three-dimensional remote control of the spermbots in combination with a non-visual detection method. It is clear that, for biomedical applications, non-invasive imaging techniques are required. One option to make the microtubes visible in the body could be with the use of high-resolution ultrasound machines. Ultrasound is able to penetrate into deep tissue without harm and is used in medical examinations to image organs and tissues. It was recently demonstrated that ultrasound can be used to image and guide microparticles and microjets and is also used for the guidance of needles in blood vessels.^[155-157] The current machines reach a lower resolution in the large micrometer range and it would be exciting to adapt these machines for the imaging of the microtubes. However, it remains questionable if ultrasound is able to image microtubes in real tissue samples. Near-infrared imaging might be another option for the detection of microtubes. It offers higher resolution than ultrasound, even so its ability to penetrate into deep tissue is lower. Currently, the penetration of near-infrared light into the tissue reaches only a few millimeters.^[158] Other techniques such as magnetic resonance imaging,

which is also already widely used in medicine, might be an alternative approach for the tracking of the magnetic microstructures.

The further improvement of spermbot performance in physiological environments and their testing in *in vivo*-like scenarios, e.g. in complex three-dimensional channel structures needs to be conducted. There are plenty of obstacles in the female reproductive system that spermbots need to overcome on their way to the oocyte. First, some parts of the female reproductive tract offer a hostile environment for sperm with acidic pH and narrow branched channels. There are parts of the fallopian tubes in which sperm cells are likely to adhere to the surface, e.g. in the isthmus temporary sperm adhesion selects hyperactivated sperm. Only hyperactivated sperm are able to detach from the isthmus and are able to promote to the oocyte location. The interaction between spermbots and oviductal cells needs to be tested. Once the sperm cells have reached the oocyte, they need to get through the cumulus layer around the oocyte. Furthermore, the oocyte is surrounded by the zona pellucida which is a thick membrane that sperms adhere to before they are able to enter to the inside of the oocyte. It remains questionable how the spermbots can overcome these obstacles. When the remote guidance and delivery to the oocyte are achieved, the cell release mechanism at the fertilization site is a necessary step. In the present study, the whole solution is heated to 38 °C in order to release the sperm cells from the thermoresponsive tubes. For a remote controlled release without heating the entire environment, magnetic nanoparticles could be incorporated into the thermoresponsive polymer film. By applying an alternating magnetic

field to the polymer tubes, the hyperthermia effect^[159] caused by the nanoparticles would lead to the local heating and thereby unfolding of the microtubes.

Still unknown is the immune response that will be triggered by the introduction of such biohybrid device. As it is the case for most microbiorobots, this is a field that has not yet been studied in detail. There are two aspects regarding the immune response: the response to the microtube as artificial component and to the sperm cell as a foreign biological entity to the body. There have been studies on resorption of biomaterials^[160] (including metals, glasses and polymers). Due to the corrosive nature of body fluids, nanometer thin membranes of biocompatible material can be assumed to be dissolved in the human body over time. This process is supposed to have no toxic effect on the tissue as long as the composition of the material systems is biocompatible. Another option of limiting the long-term effect of the microtubes would be the remote controlled removal of the magnetic tube from the body with a strong magnetic field. In any case, it needs to be ensured that the involved materials express no harm to the sperm cell, oocyte, embryo or the surrounding tissue.

Sperm cells contain mechanisms that can inhibit the immune response and therefore prolong their lifetime in a foreign body. Prostatosomes are extracellular organelles present in human semen that display immunosuppressive behavior.^[161] Furthermore, sperm cells contain membrane-bound proteins that have antibody-blocking abilities which

protect them against attacks by white blood cells.^[162] Without these defense mechanisms they would have no chance to remain in the human body and reach the fertilization site. Nevertheless, this remains one field worth studying in the future.

Moreover, the spermbot might display an interesting approach for diagnostic purposes. The pathways of sperm cells during their journey to the oocyte *in vivo* involve several obstacles and still raise a lot of questions. In unknown infertility cases it is often not clear why sperm cells do not reach the fertilization site and if for example anatomical abnormalities are the reason for sperm cells to get stuck in certain passages or where conditions in the female body lead to the elimination of sperm cells. Therefore, a tracking method for single sperm cells or swarms of such cells would be an interesting tool for studies on sperm cell behavior *in vivo*. In addition, they could be equipped with sensors that send a certain signal e.g. about pH change or other biochemical changes in the *in vivo* environment in which they are located. This would offer a non-invasive procedure for diagnostic procedures in reproductive medicine.

Albeit the above defined goal of spermbots for assisted fertilization is far-fetched, there are other fields in which spermbots can offer useful applications. One potential application that is shared with most approaches of micro- and nanomotors is the use as a drug carrier. A drug that is loaded onto the spermbot could be transported and delivered to a target location. The active autonomous motion in the blood or brain

vessels remains a challenging task. The spermbots offer different interesting aspects for drug carriers: the microtube can be functionalized on its surface with target molecules. Also the sperm cell itself could be loaded with proteins. The strength of this system is its biocompatibility and swimming ability in biological fluids. The microtubes are able to capture single cells and transport them in a directed manner. This is an interesting aspect for applications of single cell sorting and analysis. Since the microtube acts as an envelope for the cell it can be potentially made visible *in vivo* and used to facilitate detection and tracking of single cells. The sperm-tube hybrid system provides more flexibility regarding the type of organism that can be integrated. One could imagine that also other motile cells can be captured and used as power sources. One advantage of using sperm cells for the microbiorobot actuation is that these cells are readily available, easy to handle, don't need to be cultivated, and are completely harmless.

A concern that exists regarding the spermbot application in assisted reproduction as well as for drug delivery is the cooperative application of such microrobots. Of course, it will be much more useful to guide a swarm of spermbots to the oocyte in order to achieve fertilization rather than trying to maneuver a single robot. In the same way, it would make more sense to deliver drugs to a diseased tissue by a collection of microrobots, maybe even fulfilling different tasks. The topic of swarming is starting to become a matter of scientific interest, but will remain hard to tackle in the near future.

7 LIST OF FIGURES

Figure 1: Schematic image of vision of spermbot potential for assisted fertilization techniques.	9
Figure 2: Schematic image of morphology of a bovine sperm cell. The sperm cell consists of a head, midpiece and tail.	16
Figure 3: Female reproductive tract.	17
Figure 4: Rolled-up technology for the fabrication of microtubes from thin nanomembranes.	30
Figure 5: 50x50 μm nanomembranes before (left) and after (right) rollup.	31
Figure 6: Schematic of surface chemistry functionalization.....	37
Figure 7: Fluorescein-hyaluronic acid functionalized microtubes.....	38
Figure 8: Schematic procedure of microcontact printing onto nanomembranes.....	40
Figure 9: Left: Scanning electron microscopic image of the PDMS stamp used for microcontact printing with 20 x 20 μm pillars. Inset shows magnification of a single pillar structure. Right: fluorescent image of microcontact print of PDMS stamp onto a glass substrate.....	42

Figure 10: Microcontact printing.43

Figure 11: 4-benzophenone and acryloylchloride react to 4-acryloylbenzophenone in methylene chloride and N,N-diisopropylethylamine.....45

Figure 12: Thickness of spin-coated PNIPAM-co-ABP-AAc layers depending on concentration of PNIPAM-co-ABP-AAc (w/v%) in ethanol.....50

Figure 13: N-isopropylacrylamide polymerizes with 4-acryloylbenzophenone to poly(N-isopropylacrylamide-co-acryloylbenzophenone) in dioxane with AIBN as radical starter.....47

Figure 14: Thicknesses of spin-coated PNIPAM-co-ABP-AAc layers depending on the concentration of PNIPAM-co-ABP-AAc (w/v%) in ethanol.....50

Figure 15: Live/dead staining of bovine spermatozoa.....51

Figure 16: Optical image of a bovine spermatozoon.....54

Figure 17: Capturing of bovine spermatozoon inside a microtube over a time span of 0.8 seconds.....54

Figure 18: Scanning electron images of rolled-up microtubes and bovine spermatozoa at the tube openings.....55

Figure 19: Schematic of sperm cell penetration inside a microtube.....56

Figure 20: Left: Penetration x [%], calculated according to equation 1, over microtube radius [μm], Right: Velocity of spermbots over penetration [%] with categorization into type A spermbots (less than 50% penetration) and type B, more than 50% penetration.....	57
Figure 21: Influence of temperature on the velocity of spermbots.....	61
Figure 22: Magnetic remote control of microtube containing a bovine sperm cell.....	64
Figure 23: Velocity (left axis, black data points) and directionality (right axis, white data points) over the process of coupling.....	65
Figure 24: Wireless closed-loop control of a spermbot.....	66
Figure 25: Schematic illustration of separation chip.....	69
Figure 26: Separation of a spermbot from a mixture of microtubes and sperm cells.....	71
Figure 27: A bovine spermatozoon captured inside the 50 μm (left) and 20 μm (right) rolled up microtube.....	73
Figure 28: Comparison of spermbot velocity consisting of 50 μm and 20 μm microtubes.....	74

Figure 29: Coupling efficiency of bovine spermatozoa in 20 μm and 50 μm rolled up microtubes with surface modification by surface chemistry or microcontact printing.....79

Figure 30: Reversible swelling and shrinking of PNIPAM-co-ABP polymer films without (top row) and with passive layer (bottom row) on a silicon wafer as substrate. The temperature increase leads to a collapse of the polymer film which is reversed when the temperature is reduced again. The bottom row shows that the shrinking leads to the unfolding and refolding of the microtubes when a passive layer is present.....81

Figure 31: Stimuli-responsive microjets made from poly(N-isopropylacrylamide) (PNIPAM), polycaprolactone (PCL) and an inner platinum layer.....82

Figure 32: Swelling temperature of PNIPAM-co-ABP and PNIPAM-co-ABP-AAc layers displayed as radius change of the folding microtube depending on the temperature.....85

Figure 33: Reversible swelling process of PNIPAM-co-ABP-AAc film.....86

Figure 34: Polymeric spermbots. The left row of images displays four scenarios of spermbots folded from PNIPAM-co-ABP-AAc structures with according schematics to illustrate the folding cases. The graph of the right shows the observed maximum forward velocities of the polymeric spermbots.....90

Figure 35: Image series of single bovine sperm cell release from an attached microtube over a time interval of 5 s.....	91
Figure 36: Cell release process: Spermbot velocity (left axis) and temperature (right axis) over time for a representative example of a spermbot.....	92
Figure 37: Magnetic guidance of a polymeric spermbot and release of cel.....	93
Figure 38: Sperm viability test performed with SYBR 14 (live cells) and propidium iodide (dead cells) in SP-TALP on glass surface (control), PNIPAM-co-ABP-AAc and PNIPAM-co-ABP-AAc with Ti (2nm) and Fe (10nm) coating.....	95

8 LIST OF TABLES

Table 1: Conditions and molar concentrations of components for polymerizations.....	48
Table 2: Type A (penetration $x < 50\%$, $N=15$) and B (penetration $x > 50\%$, $N=26$) of spermbots inside microtubes.....	59
Table 3: Average and relative velocities as well as coupling efficiencies of $50\ \mu\text{m}$ and $20\ \mu\text{m}$ spermbots.....	75
Table 4: Folding behavior of the polymer films depending on the concentration of PNIPAM-co-ABP-AAc.....	88

9 ABBREVIATIONS

ABP	Acryloylbenzophenone
AIBN	Azobisisobutyronitrile
ATP	Adenosine triphosphate
DNA	Deoxyribonucleic acid
EDC	1-Ethyl-3-(3- dimethylaminopropyl) carbodiimide
FN	Fibronectin
IVF	<i>in vitro</i> fertilization
ICSI	intracytoplasmic sperm injection
LCST	Lower critical solution temperature
M	molar
m	mean
μ CP	microcontact printing
μ L	microliter
mL	milliliter
μ m	micrometer
mT	millitesla
mbar	millibar
MHz	megahertz

9 ABBREVIATIONS

mol	moles
N	sample size
NHS	N-Hydroxysuccinimide
NIPAM	N-isopropylacrylamide
nm	nanometer
NMR	nuclear magnetic resonance
p	p-value, probability
PDMS	Polydimethylsiloxane
PNIPAM	Poly(N-isopropylacrylamide)
PNIPAM-co-ABP	Poly(N-isopropylacrylamide-co-acryloylbenzophenone)
PNIPAM-co-ABP-AAc	Poly(N-isopropylacrylamide-co-acryloylbenzophenone-co-acrylic acid)
R	radius
rpm	rounds per minute
s	seconds
SAM	self-assembling monolayer
SEM	standard error of the mean
SP-TALP	modified Tyrode's Albumin-Lactate-Pyruvate Medium
UV	ultraviolet
w/v	weight to volume

10 CURRICULUM VITAE

Personal Information

Name: Magdanz
First Name: Veronika
Maiden name: Sasse
Date of birth: April 18, 1985
Place of birth: Rathenow, Germany
Nationality: German

Education

2004 Highschool Diploma with Honours

2004 - 2010 Studies of Biotechnology at the TU Braunschweig, Germany

2007 - 2008 Exchange student, DAAD/ISAP scholarship, Chemical Engineering, University of Waterloo, Canada

Summer 2008 Thesis about "RT-PCR of Antibody-Producing Cells" at the Carl Hansen Laboratory at the University of British Columbia, Vancouver, Canada

2009 Final Diploma Thesis about "Continuous Cultivation of *S.cerevisiae* DSM 2155 in a microbioreactor" at the Institute for Biochemical Engineering, TU Braunschweig, Germany

Work experience

2005	Tutor in physics laboratory at University of Technology, Braunschweig, Germany
2010	Research Assistant at the Institute of Surface Technology, TU Braunschweig, Germany
2010 - 2012	Self-employed as Translator (English-German) and Technical Writer in Germany/Canada
2012 - current	Research Scientist at the Institute for Integrative Nanosciences at the Leibniz Institute for Solid State and Materials Research (IFW) Dresden, Germany

11 LIST OF PUBLICATIONS

JOURNAL ARTICLES

2016

V. Magdanz, M. Guix, F. Hebenstreit, O. G. Schmidt: *Dynamic polymeric microtubes for the remote-controlled capture, guidance and release of sperm cells*, Advanced Materials 2016, 28, 21, pp. 4084-4089.

2015

C. Pacchierotti, **V. Magdanz**, M. Medina-Sánchez, O. G. Schmidt, D. Prattichizzo, S. Misra: *Intuitive control of self-propelled microjets with haptic feedback*, Journal of Micro-Bio Robotics 2015, 10, 1, pp. 37-53.

V. Magdanz, M. Medina-Sanchez, Y. Chen, M. Guix, O.G. Schmidt: *How to Improve SpermBot Performance*, Advanced Functional Materials 2015, 25, 18, pp. 2763-2770.

V. Magdanz, B. Koch, S. Sanchez, O.G. Schmidt: *Sperm dynamics in tubular confinement*, Small 2015, 11, pp. 781-785.

I.S.M. Khalil, **V. Magdanz**, S. Sanchez, O.G. Schmidt, S. Misra: *Precise localization and control of catalytic janus micromotors using weak magnetic fields*, International Journal of Advanced Robotic Systems 2015, 12, 2, pp. 1-7.

2014

V.M. Fomin, M. Hippler, **V. Magdanz**, L. Soler, S. Sanchez, O.G. Schmidt: *Propulsion mechanism of catalytic microjet engines*, IEEE Transactions on Robotics 2014, 30, 1, pp. 40-48.

I.S.M. Khalil, **V. Magdanz**, S. Sanchez, O.G. Schmidt, S. Misra: *Biocompatible, accurate, and fully autonomous: A sperm-driven micro-bio-robot*, Journal of Micro-Bio Robotics 2014, 9, 3-4, pp. 79-86.

I.S.M. Khalil, **V. Magdanz**, S. Sanchez, O.G. Schmidt, S. Misra: *Wireless magnetic-based closed-loop control of self-propelled microjets*, PLOS one 2014, 9, 2, pp. e83053/1-6.

V. Magdanz, O.G. Schmidt: *Spermbots: Potential impact for drug delivery and assisted reproductive technologies (Editorial)*. Expert Opinion on Drug Delivery 2014, vol. 11, 8, Informa Healthcare, pp. 1125-1129.

V. Magdanz, G. Stoychev, L. Ionov, S. Sanchez, O.G. Schmidt: *Stimuli-responsive microjets with reconfigurable shape*, Angewandte Chemie International Edition 2014, 53, 10, pp. 2673-2677.

V. Magdanz, M. Guix, O.G. Schmidt: *Tubular micromotors: from microjets to spermbots*, Robotics and Biomimetics 2014, 1, 11, pp. 1-10.

J. Simmchen, **V. Magdanz**, S. Sanchez, S. Chokmaviroj, D. Ruiz-Molina, A. Baeza, O.G. Schmidt: *Effect of surfactants on the performance of tubular and spherical micromotors - A comparative study*, RSC Advances 2014, 4, pp. 20334-20340.

2013

I.S.M. Khalil, **V. Magdanz**, S. Sanchez, O.G. Schmidt, S. Misra: *Three-dimensional closed-loop control of self-propelled microjets*, Applied Physics Letters 2013, 103, pp. 172404/1-5.

V. Magdanz, S. Sanchez, O.G. Schmidt: *Development of a sperm-flagella driven micro-bio-robot*, Advanced Materials 2013, 25, pp. 6581-6588.

L. Soler, **V. Magdanz**, V.M. Fomin, S. Sanchez, O.G. Schmidt: *Self-propelled micromotors for cleaning polluted water*, ACS nano 2013, 7, 11, pp. 9611-9620.

CONTRIBUTIONS TO COLLECTED EDITIONS/PROCEEDINGS

2014

A. Sanchez, **V. Magdanz**, O.G. Schmidt, S. Misra: *Magnetic control of self-propelled microjets under ultrasound image guidance*, 5th IEEE RAS and EMBS International Conference on Biomedical Robotics and

Biomechatronics (BioRob) 2014, Sao Paulo/ Brazil, 12.-15.8.14, in: Proceedings, pp. 169-174.

S. Sanchez, W. Xi, A.A. Solovev, L. Soler, **V. Magdanz**, O.G. Schmidt: *Tubular micro-nanorobots: Smart design for bio-related applications*, in: Small-Scale Robotics. From Nano-to-Millimeter-Sized Robotic Systems and Applications. Lecture Notes in Computer Science, Berlin: Springer-Verl., 2014, I. Paprotny, S. Bergbreiter (eds.), 8336, pp. 16-27.

S. M. Khalil, **V. Magdanz**, S. Sanchez, O. G. Schmidt, S. Misra: *The control of self-propelled microjets inside a microchannel with time-varying flow rates*, IEEE Transactions on Robotics 2014, 30, pp. 49-58.

V. M. Fomin, M. Hippler, **V. Magdanz**, L. Soler, S. Sanchez, O. G. Schmidt: *Propulsion mechanism of catalytic microjet engines*, IEEE Transactions on Robotics 2014, 30, pp. 40-48.

2013

I.S.M. Khalil, **V. Magdanz**, S. Sanchez, O.G. Schmidt, S. Misra: *Magnetotactic bacteria and microjets: A comparative study*, 2013 IEEE/RSJ International Conference on Intelligent Robots and Systems (IROS) 2013, Tokyo/ Japan, 3.-7.11.13, in: Proceedings, pp. 2035-2040.

12 ACKNOWLEDGEMENTS

I would like to thank a number of people for their support in many ways during the time of my PhD: First of all, Prof. Dr. Oliver G. Schmidt for entrusting me with such an exciting PhD topic and letting me explore this field on my own, continuously providing valuable feedback and guidance. I thank Prof. Dr. Stefan Diez for agreeing to be the official supervisor of my PhD thesis. I am also grateful for Dr. Samuel Sanchez who gave me guidance during the first year of my PhD, for teaching me how to write and publish articles and for many inspiring discussions. My two desk neighbours Dr. Maria Guix and Mariana Medina Sanchez for their daily smiles, positive outlook on life and continuous motivation. Franziska Hebenstreit for taking good care of the biolab and her assistance with many little things, Dr. Anne Meyer, Lukas Schwarz, Britta Koch, Sonja Weiz, Haifeng Xu, Yan Chen for simply being great team members. I thank Ronny Engelhardt, Dr. Stefan Harazim, Sandra Nestler, Martin Bauer, Stephan Rölz, Cindy Kupka for providing excellent assistance with deposition machines and clean room equipment. Dr. Lluís Soler, Dr. Juliane Simmchen, Dr. Xi Wang, Laura Restrepo, Anka Kempe, Linda Helbig for the good times we shared at the lab. I also thank the people that have brought my attention to the 'micro-stuff' in science years ago, especially Prof. Dr. Rainer Krull (TU Braunschweig) and Prof. Dr. Carl Hansen (UBC Vancouver). Last but not least I thank my family for supporting me in my work. My Mom for always encouraging me to

continue and my Dad for his appreciation of my scientific work. I am forever grateful for my husband who left his home country behind so that we could be here in Dresden for me to pursue my PhD; for his continuous support and (career) sacrifices during the last years. I thank everyone that has stirred my passion for this research and that I have met during the journey of this project. Thank you!

13 REFERENCES

- [1] R. Feynman: *There's Plenty of Room at the Bottom - An Invitation to Enter a New Field of Physics*, *Engineering and Science* magazine 1960, vol. XXIII, no. 5, February 1960.
- [2] H. Kleiner: „*Fantastic Voyage*“ Science Fiction movie 1966, Directed by Richard Fleischer, 20th Century Fox Film Corporation.
- [3] E.M. Purcell: *Life at low Reynolds Number*. *American Journal of Physics* 1977, vol. 45, 1, pp. 3-11.
- [4] M.Kim, A.A. Julius, E. Steager: *Microbiorobotics, Biologically inspired microscale robotic systems*. 1st edition 2012, Elsevier Inc., ISBN 978-4557-7891-1.
- [5] M.G.R. Hull, C. M. A. Glazener, N.J. Kelly, D.I. Conway, P.A. Foster, R.A. Hinton, C. Coulson, P.A. Lambert, E.M. Watt, K.M. Desai: *Population study of causes, treatment and outcome of infertility*. *British Medical Journal* 1985, vol. 291, 6510, pp.1693-1697.
- [6] V. Magdanz, S. Sanchez, O.G. Schmidt: Inside front cover page. *Micro-robots: Development of a Sperm-Flagella Driven Micro-Bio-Robot*. *Advanced Materials* 2013, vol. 45, 25, p. 6470.
- [7] T.E. Mallouk, A. Sen: *Powering nanorobots*. *Scientific American* 2009, vol. 300, pp. 72-77.

[8] J. Wang, W. Gao: *Nano/Microscale Motors: Biomedical Opportunities and Challenges*. ACS Nano 2012, vol. 6, 7, pp. 5745-5751.

[9] W.F. Paxton, S. Sundararajan, T.E.Mallouk, A. Sen: *Chemical Locomotion*. Angewandte Chemie International Edition 2006, vol. 45, 33, pp, 5420-5429.

[10] J. Wu, Balasubramanian, S., D.Kagan, K.M. Manesh, S. Campuzano, J. Wang: *Motion-based DNA detection using catalytic nanomotors*. Nature Communications 2010, vol. 1, 36.

[11] S. Sengupta, M.E.Ibele, A. Sen: *Fantastic Voyage: Designing Self-Powered Nanorobots*. Angewandte Chemie International Edition 2012, 51, 34, pp. 8434-8445.

[12] Y.F. Mei, A. A. Solovev, S. Sanchez, O. G. Schmidt: *Rolled-up nanotech on polymers: from basic perception to self-propelled catalytic microengines*. Chemical Society Reviews 2011, vol. 40, 5, pp. 2109-2119.

[13] G. Zhao, E.J.E Stuart, M. Pumera: *Enhanced diffusion of pollutants by self-propulsion*, Physical Chemistry Chemical Physics 2011, 13, pp. 12755-12757.

[14] M.M. Hanczyc, T. Toyota, T. Ikegami, N. Packard, T.Sugawara: *Fatty acid chemistry at the oil-water interface: self-propelled oil droplets*. Journal of American Chemical Society 2007, vol. 1, 129, pp. 9386-9391.

-
- [15] W. Wang, S. Li, L. Mair, S. Ahmed, T.J. Huang, T. E. Mallouk: *Acoustic propulsion of nanorod motors inside living cells*. *Angewandte Chemie International Edition* 2014, vol. 53, 12, pp. 3201-3204.
- [16] Z. Wu, T. Li, J. Li, W. Gao, T. Xu, C. Christianson, W. Gao, M. Galarnyk, L. Zhang, J. Wang: *Turning Erythrocytes into Functional Micromotors*, *ACS Nano* 2014, vol. 8, 12, pp. 12041-12048.
- [17] A. Gosh, P. Fischer: *Controlled Propulsion of Artificial Magnetic Nanostructured Propellers*. *Nano Letters* 2009, vol. 9, 6, pp, 2243-2245.
- [18] L. Zhang, J.J. Abbot, D. Dong, B.E. Kratochivil, D. Bell, B.J. Nelson: *Artificial bacterial flagella: Fabrication and magnetic control*. *Applied Physics Letters* 2009, 94, 064107.
- [19] S. Tottori, L. Zhang, F. Qiu, K.K. Krawczyk, A. Franco-Obregon, B.J. Nelson: *Magnetic helical micromachines: fabrication, controlled swimming, and cargo transport*. *Advanced Materials* 2012, vol. 24, 6, pp. 811-816.
- [20] G. Loget, A. Kuhn: *Electric field-induced chemical locomotion of conducting objects*. *Nature Communications* 2011, vol. 2, 535.
- [21] G. Loget, A. Kuhn: *Propulsion of Microobjects by Dynamic Bipolar Self-Regeneration*. *Journal of American Chemical Society* 2010, vol. 132, 45, pp. 15918-15919.

- [22] W. Xi, A.A.Solovev, A.Ananth, D. Gracias, S. Sanchez, O. G. Schmidt: *Rolled-up magnetic microdrillers: towards remotely controlled minimally invasive surgery*. *Nanoscale* 2013, vol. 5, 4, pp. 1294-1297.
- [23] D. Kagan, M. J. Benchimal, J. C. Claussen, E. Chuluun-Erdene, S. Esener, J. Wang: *Acoustic droplet vaporization and propulsion of perfluorocarbon-loaded microbullets for targeted tissue penetration and deformation*. *Angewandte Chemie International Edition* 2012, vol. 51, 30, pp. 7519-7522.
- [24] A. A. Solovev, W. Xi, D. Gracias, S. M. Harazim, C. Deneke, S. Sanchez, O. G. Schmidt: *Self-Propelled Nanotools*. *ACS Nano* 2012, vol. 6, 2, 1751-1756.
- [25] W. Gao, R. Dong, S. Thamphiwatana, J. Li, W. Gao, L. Zhang, J. Wang: *Artificial Micromotors in the Mouse's Stomach: A Step toward in Vivo Use of Synthetic Motors*. *ACS Nano* 2015, vol. 9, 1, pp. 117-123.
- [26] R. Dreyfus, J. Baudry, M.L. Roper, M. Fermigier, H.A. Stone, J. Bibette: *Microscopic artificial swimmers*. *Nature* 2005, vol. 437, pp. 862-865.
- [27] I. S. M. Khalil, H. C. Dijkslag, L. Abelmann, S. Misra: *MagnetoSperm: A microrobot that navigates using weak magnetic fields*. *Applied Physics Letters* 2014, vol. 104, 22, 223701.

-
- [28] M. Medina-Sánchez, L. Schwarz, A. K. Meyer, F. Hebenstreit, O.G. Schmidt: *Cellular Cargo Delivery: Toward Assisted Fertilization by Sperm-Carrying Micromotors*. Nano Letters 2016, vol. 16, 1, pp. 555-561.
- [29] H. Hess, G. Bachand: *Biomolecular motors*. Materials Today 2005, vol. 8, 12, pp. 22-29.
- [30] S. Diez, C. Reuther, C. Dinu, R. Seidel, M. Mertig, W. Pompe, J. Howard: *Stretching and Transporting DNA Molecules Using Motor Proteins*, Nano Letters 2003, vol. 3, 9, pp. 1251–1254.
- [31] A. Goel, V. Vogel: *Harnessing biological motors to engineer systems for nanoscale transport and assembly*. Nature Nanotechnology 2008, vol. 3, pp. 465 – 475.
- [32] R.K. Soong, G.D. Bachand, H.P. Neves, A.G. Olkhovets, H.G. Craighead, C.D. Montemagno: *Powering an inorganic nanodevice with a biomolecular motor*. Science 2000, vol. 290, 5496, pp.1555-1558.
- [33] B.J. Williams, S. V. Anand, J. Rajagopalan, M. T. A. Saif: *A self-propelled biohybrid swimmer at low Reynolds number*. Nature Communications 2014, vol. 5, 3081.
- [34] S. Martel, Sylvain, C.C. Tremblay, S. Ngakeng, G. Langlois: *Controlled manipulation and actuation of micro-objects with magnetotactic bacteria*. Applied Physics Letters 2006, 89, 23, 233904.

[35] B. Behkam, M. Sitti: *Bacterial flagella-based propulsion and on/off motion control of microscale objects*. Applied Physics Letters 2007, vol. 90 , 2, pp. 23902-23904.

[36] J. Xi, J.J. Schmidt, C.D. Montemagno: *Self-assembled microdevices driven by muscle*. Nature Materials 2005, vol. 4, 2, pp. 180-184.

[37] R. Di Leonardo, L. Angelani, D. Dell'Arciprete, G. Ruocco, V. Iebba, S. Schippa, M.P. Conte, F. Mecarini, F. De Angelis, E. Di Fabrizio: *Bacterial ratchet motors*. Proceedings of the National Academy of Sciences of the United States of America, 2010, vol. 107, 21, pp. 9541-9545.

[38] N. Darnton, L. Turner, K. Breuer, H.C. Berg: *Moving fluid with bacterial carpets*. 2004, vol. 86, 3, pp. 1863-1870.

[39] B. Behkam and M. Sitti: *Towards hybrid swimming microrobots: bacteria assisted propulsion of polystyrene beads*. Proceedings of the IEEE International Conference of Engineering in Medicine and Biology Society 2006, New York, NY, 30 August–3 September 2006 (IEEE, New York, 2006), p. 2421.

[40] S. Martel: *Bacterial microsystems and microrobots*. Biomedical Microdevices 2012, vol. 14, 6, pp. 1033-1045.

[41] S. Martel, M. Mohammadi, O. Felfoul, Z. Lu, P. Pouponneau: *Flagellated Magnetotactic Bacteria as Controlled MRI-trackable Propulsion and Steering Systems for Medical Nanorobots Operating in the*

Human Microvasculature. International Journal for Robotics Research 2009, vol. 28,4, pp. 571-582.

[42] P. Pouponneau, J.-C. Leroux, G. Soulez, L. Gaboury, S. Martel: *Co-encapsulation of magnetic nanoparticles and doxorubicin into biodegradable microcarriers for deep tissue targeting by vascular MRI navigation*. Biomaterials 2011, vol. 32 ,13, pp. 3481-3486.

[43] S. Martel, C.C. Tremblay, S. Ngakeng, G. Langlois : *Controlled manipulation and actuation of micro-objects with magnetotactic bacteria*. Applied Physics Letters 2006, vol. 89, 233904.

[44] D. Kim, A. Liu, E. Diller, M. Sitti: *Chemotactic steering of bacteria propelled microbeads*. Biomed. Microdevices, 2012, vol. 14, 6, pp. 1009-1017.

[45] J. Zhuang, R. W. Carlsen, M. Sitti: *pH-Taxis of Biohybrid Microsystems*. Scientific Reports 2015, vol. 5, 11403.

[46] E.B. Steager, M.S. Sakar, D.H. Kim, V. Kumar, G.J. Pappas, M. J. Kim: *Electrokinetic and optical control of bacterial microrobots*. Journal of Micromechanics and Microengineering 2011, vol. 21, 3, 035001.

[47] V. Magdanz, S. Sanchez, O. G. Schmidt: *Development of a sperm-flagella driven micro-bio-robot*, Advanced Materials 2013, vol. 25, 45, pp. 6581-6588.

[48] C. Van Duijn: *Mensuration of the heads of bull spermatozoa*. Mikroskopie 1960, 14, pp. 265-276.

[49] E.A. Gaffney, H. Gadelha, D.J. Smith, J.R. Blake, J.C. Kirkman-Brown: *Mammalian Sperm motility: Observation and Theory*. Annual Review in Fluid Mechanics 2011, 43, pp. 501-528.

[50] D.W. Fawcett: *The Mammalian Spermatozoon*. Developmental Biology 1975, 44, pp. 394-436.

[51] T.J. Mitchison, H.M. Mitchison: *Cell Biology: How cilia beat*. Nature 2010, vol. 463, pp. 308-309.

[52] V. Magdanz, O.G. Schmidt: *Spermbots: Potential impact for drug delivery and assisted reproductive technologies* (Editorial), Expert Opinion on Drug Delivery 2014, Informa Healthcare, vol. 11, 8, pp. 1125-1129.

[53] S.S. Suarez, A.A. Pacey: *Sperm transport in the female reproductive tract*. Human Reproduction Update 2006, vol. 12, 1, pp. 23-37.

[54] M. Ikawa, N. Inoue, A. M. Benham, M. Okabe: *Fertilization: a sperm's journey to and interaction with the oocyte*. Journal of Clinical Investigation 2010, vol.120, 4, pp. 984-994.

[55] P.E. Patton, D.E. Battaglia: *Office Andrology 2005*. Chapter 16, p. 242, Humana Press, Totowa, New Jersey.

-
- [56] C.H. Muller: *Rationale, Interpretation, Validation, and Uses of sperm function tests*. Journal of Andrology 2000, vol. 21, 1, pp. 10-30.
- [57] M.N. Mascarenhas, S. R. Flaxman, T. Boerma, S. Vanderpoel, G.A. Stevens: *National, Regional, and Global Trends in Infertility Prevalence Since 1990: A Systematic Analysis of 277 Health Surveys*. PLoS Medicine 2012, 9, 12, e1001356.
- [58] <http://www.who.int/reproductivehealth/topics/infertility/perspective/en/>, accessed 27.7.2015
- [59] M.B. Goldman, R. Troisi, K. M. Rexrode: *Women and Health (Second Edition)* 2013. Academic Press, *Chapter 17: Infertility*. pp. 251–270.
- [60] A. Jungwirth, A. Giwercman, H. Tournaye, T. Diemer, Z. Kopa, G. Dohle, C. Krausz: *European Association of Urology Guidelines on Male Infertility: The 2012 Update*. European Urology 2012, vol. 62, 2, pp. 324-332.
- [61] M. A. Hassan, S.R. Killick: *Negative lifestyle is associated with a significant reduction in fecundity*. Fertility and Sterility 2004, vol. 81, 2, pp. 384-392.
- [62] F. Hammiche: *Preconception care: The influence of nutrition and lifestyle on fertility*. Erasmus MC: University Medical Center Rotterdam, 2012. Retrieved from <http://hdl.handle.net/1765/38822>.

[63] P.C. Steptoe, R.G. Edwards: *Birth after reimplantation of a human embryo*. The Lancet 1978, vol. 312, 8085, p. 366.

[64] R.M. Kamel: *Assisted Reproductive Technology after the Birth of Louise Brown*. Journal of Reproduction and Infertility 2013, vol. 14, 3, pp. 96-109.

[65] I. Natali: *Sperm Preparation Techniques for Artificial Insemination - Comparison of Sperm Washing, Swim Up, and Density Gradient Centrifugation Methods*. Artificial Insemination in Farm Animals 2011, Dr. Milad Manafi (Ed.), ISBN: 978-953-307-312-5, InTech, doi: 10.5772/17026.

[66] <http://www.who.int/reproductivehealth/topics/infertility/new/en/>, accessed 30.7.2015

[67] E. G. Brown, S. T. Shahrooz, S. S. Vasaya, S. Shadman, G. I. Gallicano: *Assessment of the Field of Assisted Reproductive Technology: Improvements and the Future of Human In Vitro Fertilization*. Journal of Fertilization: In vitro, IVF-Worldwide, Reproductive Medicine, Genetics & Stem Cell Biology 2015, vol. 3, 3, 1000156.

[68] V. Blumenauer, U. Czeromin K. Fiedler, C. Gnoth, L. Happel, J.S. Krüssel, M.S. Kupka, A. Tandler-Schneider: *German IVF Registry, Annual Report 2013*. Journal of Reproductive Medicine and Endocrinology 2014, vol. 11, 5-6, pp. 236-273.

-
- [69] A. Khademhosseini, J. Borenstein, M. Toner, S. Takayama: *Micro and nanoengineering of the cell microenvironment*. Artech House, Norwood, USA; 2008.
- [70] J.W. Gordon, B. E. Talansky: *Assisted fertilization by zona drilling: a mouse model for correction of oligospermia*. The Journal of Experimental Zoology 1986, 239, pp. 347-354.
- [71] J. Nilsson, M. Evander, B. Hammarström, T. Laurell: *Review of cell and particle trapping in microfluidic systems*. Analytica Chimica Acta 2009, vol. 649, 2, pp. 141-157.
- [72] H. Zhang, K.-K. Liu: *Optical tweezers for single cells*. Journal of The Royal Society Interface 2008, vol. 5, 24, pp. 671-690.
- [73] R. N. Zare, S. Kim: *Microfluidic platforms for single-cell analysis*. Annual review of biomedical engineering 2010, vol. 12, pp. 187-201.
- [74] S. Hou, H. Zhao, L. Zhao, Q. Shen, K. S. Wei, D. Y. Suh, A. Nakao, M. A. Garcia, M. Song, T. Lee, B. Xiong, S.-C. Luo, H.-R. Tseng, H.-H. Yu: *Capture and Stimulated Release of Circulating Tumor Cells on Polymer-Grafted Silicon Nanostructures*. Advanced Materials 2013, vol. 25, 11, pp. 1547-1551.
- [75] Z. Zhang, N. Chen, S. Li, M. R. Battig, Y. Wang: *Programmable hydrogels for controlled cell catch and release using hybridized aptamers*

and complementary sequences. Journal of the American Chemical Society 2012, vol. 134, 38, pp. 15716-15719.

[76] R.L. Nebel, J.H. Bame, R.G. Saacke, F. Lim: *Microencapsulation of bovine spermatozoa.* Journal of Animal Science 1985, vol. 60, 6, pp. 1631-1639.

[77] T.W. Munkittrick, R.L. Nebel, R.G. Saacke: *Accessory sperm numbers for cattle inseminated with protamine sulfate microcapsules,* Journal of Dairy Science 1992, vol. 75, 3, pp. 725-731.

[78] J.S. Randhawa, T.G. Leong, N. Bassik, B.R. Benson, M.T. Jochmans, D.H. Gracias: *Pick-and-place using chemically actuated microgrippers.* Journal of the American Chemical Society 2008, vol. 130, 51, pp. 17238-17239.

[79] T.G. Leong, C. L. Randall, B. R. Benson, N. Bassik, G.M. Stern, D.H. Gracias: *Tetherless thermobiochemically actuated microgrippers.* Proceedings of the National Academy of Sciences of the United States of America 2009, vol. 106, 3, pp. 703–708.

[80] N. Bassik, A. Brafman, A. M. Zarafshar, M. Jamal, D. Luvsanjav, F. M. Selaru, D. H. Gracias: *Enzymatically triggered actuation of miniaturized tools.* Journal of American Chemical Society 2010, vol. 132, 46, pp. 16314–16317.

-
- [81] K. Malachowski, M. Jamal, Q. Jin, B. Polat, C.J. Morris, D.H. Gracias: *Self-folding single cell grippers*. Nano Letters 2014, vol. 14, 7, pp. 4164-4170.
- [82] K. Malachowski, J. Breger, H.R. Kwag, M.O. Wang, J.P. Fisher, F.M. Selaru, D.H. Gracias: *Stimuli-responsive theragrippers for chemomechanical controlled release*. Angewandte Chemie International Edition 2014, vol. 53, 31, pp. 8045-8049.
- [83] G. Stoychev, N. Puretskiy, L. Ionov: *Self-folding all-polymer thermoresponsive microcapsules*. Soft Matter 2011, vol. 7, 7, pp. 3277-3279.
- [84] M. A. C. Stuart, W. T.S. Huck, J. Genzer, M. Müller, C. Ober, M. Stamm, G.B. Sukhorukov, I. Szleifer, V.V. Tsukruk, M. Urban, F. Winnik, S. Zauscher, I. Luzinov, S. Minko: *Emerging applications of stimuli-responsive polymer materials*, Nature materials 2010, vol. 9, pp.101—113.
- [85] D. Schmaljohann, *Thermo- and pH-responsive polymers in drug delivery*, Advanced Drug Delivery Reviews 2006, vol. 58, p. 1655-1670.
- [86] B. Simpson, G. Nunnery, R. Tannenbaum, K. Kalaitzidou: *Capture/release ability of thermo-responsive polymer particles*, J. Mater. Chem. 2010, vol. 20, 17, pp.3496-3501.
- [87] H.G. Schild: *Poly(N-isopropylacrylamide): experiment, theory and application*, Progress in Polymer Science 1992, vol. 17, 2, pp. 163-249.

[88] S. Zakharchenko, N. Puretskiy, G. Stoychev, M. Stamm, L. Ionov: *Temperature controlled encapsulation and release using partially biodegradable thermo-magneto-sensitive self-rolling tubes*, *Soft Matter* 2010, vol. 6, 7, pp. 2633-2636.

[89] D. H. Gracias: *Stimuli responsive self-folding using thin polymer films*, *Current Opinion in Chemical Engineering* 2013, vol. 2, 1, p.112-119.

[90] V. Magdanz, G. Stoychev, L. Ionov, S. Sanchez, O.G. Schmidt: *Stimuli-responsive microjets with reconfigurable shape*, *Angewandte Chemie - International Edition* 2014, vol. 53, 10, pp. 2673-2677.

[91] X. Yin, A. S. Hoffman, P.S. Stayton: *Poly(N-isopropylacrylamide-co-propylacrylic acid) Copolymers That Respond Sharply to Temperature and pH*, *Biomacromolecules* 2006, vol. 7, 5, pp.1381-1385.

[92] Y.F. Mei, G. Huang, A.A. Solovev, E.B. Urena, I. Mönch, F. Ding, T. Reindl, R.K.Y. Fu, P.K. Chu, O.G. Schmidt: *Versatile approach for integrative and functionalized tubes by strain engineering of nanomembranes on polymers*. *Advanced Materials* 2008, vol. 20, 21, pp. 4085-4090.

[93] S.M. Harazim, W. Xi, C.K. Schmidt, S. Sanchez, O.G. Schmidt: *Fabrication and applications of large arrays of multifunctional rolled-up SiO/SiO₂ microtubes*. *Journal of Materials Chemistry* 2012, 22, 7, pp. 2878-2884.

-
- [94] D. Grimm, C. C. Bof Bufon, C. Deneke, P. Atkinson, D. J. Thurmer, F. Schäffel, S. Gorantla, A. Bachmatiuk, O. G. Schmidt: *Rolled-up nanomembranes as compact 3D architectures for field effect transistors and fluidic sensing applications*. Nano Letters 2013, vol. 13, 1, pp.213-218.
- [95] H.-X. Ji, X.-L. Wu, L.-Z. Fan, C. Krien, I. Fierung, Y.-G. Guo, Y. Mei, O.G. Schmidt: *Self-Wound Composite Nanomembranes as Electrode Materials for Lithium Ion Batteries*. Advanced Materials 2010, vol. 22, 41, pp. 4591-4595.
- [96] C. Yan, W. Xi, W. Si, J. Deng, O. G. Schmidt: *Highly Conductive and Strain-Released Hybrid Multilayer Ge/Ti Nanomembranes with Enhanced Lithium-Ion-Storage Capability*. Advanced Materials 2013, vol. 25, 4, pp. 539–544.
- [97] J. Deng, H. Ji, C. Yan, J. Zhang, W. Si, S. Baunack, S. Oswald, Y. F. Mei, O. G. Schmidt: *Naturally rolled-up C/Si/C trilayer nanomembranes as stable anodes for Lithium-ion batteries with remarkable cycling performance*. Angewandte Chemie International Edition 2013, vol. 52, 8, pp. 2326-2330.
- [98] S. Böttner, S. Li, M. R. Jorgensen, O. G. Schmidt: *Vertically aligned rolled-up SiO₂ optical microcavities in add-drop configuration*. Applied Physics Letters 2013, vol. 102, 251119

[99] A. Madani, M. Kleinert, D. Stolarek, L. Zimmermann, L. Ma, O. G. Schmidt: *Vertical optical ring resonators fully integrated with nanophotonic waveguides on silicon-on-insulator substrates*. Optics Letters 2015, 40, 16, 3826-3829.

[100] S. M. Harazim, V. A. Bolaños Quiñones, S. Kiravittaya, S. Sanchez, O. G. Schmidt: *Lab-in-a-tube: On-chip integration of glass optofluidic ring resonators for label-free sensing applications*. Lab on a Chip 2012, vol. 12, 15, pp. 2649-2655.

[101] C. S. Martinez-Cisneros, S. Sanchez, W. Xi, O. G. Schmidt: *Ultracompact three-dimensional tubular conductivity microsensors for ionic and biosensing applications*. Nano Letters 2014, vol. 14, 4, pp. 2219-2224.

[102] V. Magdanz, M. Guix, O.G. Schmidt: *Tubular micromotors: from microjets to spermboats*. Robotics and Biomimetics 2014, vol. 1, 11, pp. 1-10.

[103] S. Sanchez, A.A. Solovev, Y.Meï, O.G. Schmidt: *Dynamics of biocatalytic microengines mediated by variable friction control*. Journal of American Chemical Society 2010, vol. 132, 38, pp. 13144-13145.

[104] W. Xi, C. K. Schmidt, S. Sanchez, D. H. Gracias, R. E. Carazo-Salas, S. P. Jackson, O. G. Schmidt: *Rolled-up functionalized nanomembranes as three-dimensional cavities for single cell studies*. Nano Letters 2014, vol. 14, 8, pp. 4197-4204.

-
- [105] B. Koch, S. Sanchez, C. K. Schmidt, A. Swiersy, S. P. Jackson, O. G. Schmidt: *Confinement and deformation of single cells and their nuclei inside size-adapted microtubes*. *Advanced Healthcare Materials* 2014, vol. 3, 11, pp. 1753-1758.
- [106] R. A. Sperling, W. J. Parak: *Surface modification, functionalization and bioconjugation of colloidal inorganic nanoparticles*. *Philosophical Transactions of the Royal Society A* 2010, vol. 368, pp.1333-1383.
- [107] J. Conde, J.T. Dias, V. Grazu, M. Moros, P.V. Baptiste, J.M. de la Fuente: *Revisiting 30 years of biofunctionalization and surface chemistry of inorganic nanoparticles for nanomedicine*. Review, *Frontiers in Chemistry* 2014, vol. 2, 48.
- [108] V. Magdanz, M. Medina-Sanchez, Y. Chen, M. Guix, O.G. Schmidt: *How to improve spermbot performance*. *Advanced Functional Materials* 2015, vol. 25, 18, pp. 2763-2770.
- [109] J. L. Wilbur, A. Kumar, H. A. Biebuyck, E. Kim and G.M. Whitesides: *Microcontact printing of self-assembled monolayers: Application in microfabrication*. *Nanotechnology*, 1996, vol. 7, pp. 452–457.
- [110] J-H. Pai , Y. Wang, G. T. A. Salazar, C. E. Sims, M. Bachman, G. P. Li , N. L. Allbritton: *Photoresist with low fluorescence for bioanalytical applications*. *Analytical Chemistry* 2007, 79, vol. 22, pp. 8774–8780.

[111] H. D. Inerowicz, S. Howell, F. E. Regnier, R. Reifengerger: *Multiprotein Immunoassay Arrays Fabricated by Microcontact Printing*. Langmuir 2002, vol. 18, 13, pp. 5263–5268.

[112] U. S. Schwarz, C. M. Nelson, P. Silberzan: *Proteins, cells, and tissues in patterned environments*. Soft Matter 2014, 10, pp. 2337-2340.

[113] P. Xiao, Y. Wang, M. Dai, G. Wu, S. Shi, J. Nie: *Synthesis and photopolymerization kinetics of benzophenone piperazine one-component initiator*. Polymers for Advanced Technologies 2008, vol. 19, 5, pp. 409-413.

[114] G. Stoychev, S. Zakharchenko, S. Turcaud, J.W.C. Dunlop, L. Ionov: *Shape-programmed folding of stimuli-responsive polymer bilayers*. ACS Nano 2012, vol. 6, 5, pp. 3925-3934.

[115] M. A. Van Dilla, B. L. Gledhill, S. Lake, P. N. Dean, J. W. Gray, V. Kachel, B. Barlogie, W. Göhde: *Measurement of mammalian sperm deoxyribonucleic acid by flow cytometry. Problems and approaches*. Journal of Histochemistry & Cytochemistry 1977, vol. 25, 7, pp. 763-773.

[116] R. Rikmenspoel: *The tail movement of bull spermatozoa. Observations and model calculations*. Biophysical Journal 1965, vol. 5, 4, pp. 365–392.

-
- [117] R. Rikmenspoel: *Movements and active movements of bull sperm flagella as a function of temperature and viscosity*. Journal of Experimental Biology 1984, vol. 108, pp. 205-230.
- [118] M. Eisenbach, L. C. Giojalas: *Sperm guidance in mammals — an unpaved road to the egg*. Nature Reviews Molecular Cell Biology 2006, vol. 7, pp. 276-285.
- [119] J. Dobson: *Gene therapy progress and prospects: magnetic nanoparticle-based gene delivery*. Gene Therapy 2006, vol. 13, pp. 283-287.
- [120] Y. Pan, X. Du, F. Zhao, B. Xu: *Magnetic nanoparticles for the manipulation of proteins and cells*. Chemical Society Reviews 2012, vol. 41, pp. 2912-2942.
- [121] K. E. Scarberry, E.B. Dickerson, J. F. McDonald, Z. J. Zhang: *Magnetic nanoparticle-peptide conjugates for in vitro and in vivo targeting and extraction of cancer cells*. Journal of American Chemical Society 2008, vol. 130, 31, pp. 10258-10262.
- [122] A. Nel, T. Xia, L. Maedler, N. Li: *Toxic Potential of materials at the nanolevel*. Science 2006, vol. 311, 5761, pp. 622-627.
- [123] A. Senyei, K. Widder, G. Czerlinski: *Magnetic guidance of drug-carrying microspheres*. Journal of Applied Physics 1978, 49, pp. 3578-3583.

[124] R.B. Frankel: *Magnetic guidance of organisms*. Annual Review of Biophysics and Bioengineering 1984, 13, pp. 85-103.

[125] I. S. M. Khalil, V. Magdanz, S. Sanchez, O. G. Schmidt, L. Abelmann, S. Misra: *Magnetic control of potential microrobotic drug delivery systems: nanoparticles, magnetotactic bacteria and self-propelled microjets*. Proceedings of the IEEE Engineering in Medicine and Biology Society (EMBC) 2013, 3-7 July, Osaka, Japan, pp. 5299-5302.

[126] W. F. Paxton, K. C. Kistler, C. C. Olmeda, A. Sen, S. K. St. Angelo, Y. Cao, T. E. Mallouk, P. Lammert, V.H. Crespi: *Autonomous Movement of Striped Nanorods*. Journal of American Chemical Society 2004, 126, pp. 13424-13431.

[127] R. Nosrati, A. Driouchi, C. M. Yip, D. Sinton: *Two-dimensional slither swimming of sperm within a micrometer of a surface*. Nature Communications 2015, vol. 6, 8703.

[128] I.S.M. Khalil, V. Magdanz, S. Sanchez, O.G. Schmidt, S. Misra: *Biocompatible, accurate, and fully autonomous: A sperm-driven micro-bio-robot*. Journal of Micro-Bio Robotics 2014, vol. 9, 3-4, pp. 79-86.

[129] D.J. Recktenwald, A. Radbruch: *Cell Separation Methods and Applications*. Chapter 1, CRC Press 1998, ISBN: 0-8247-9864-3, Marcel Dekker, Inc. New York.

[130] P.E. Patton, D.E. Battaglia: *Office Andrology 2005*. Chapter 3, p. 41, Humana Press, Totowa, New Jersey.

[131] Wolff, H., J. A. Politch, A. Martinez, F. Haimovici, J. A. Hill, D. J. Anderson: *Leukocytospermia is associated with poor semen quality*. *Fertility and Sterility* 1990, vol. 53, 3, pp. 528-536.

[132] C. De Jonge: *Biological basis for human capacitation*. *Human Reproduction Update* 2005, vol. 11, 3, pp. 205-214.

[133] M. Mahadevan, G. Baker: *Assessment and preparation of semen for in vitro fertilization*. In: *Clinical In Vitro Fertilization* Edited by: Wood C, Trounson A. Springer-Verlag, Berlin, 1984, pp. 83-97.

[134] R. R. Henkel, W.-B. Schill: *Sperm preparation for ART*. *Reproductive Biology and Endocrinology* 2003, vol. 1, 108, pp. 1-22.

[135] E. K. Dirican, O. D. Özgün, S. Akarsu, K. Okhan Akin, Ö. Ercan, M. Uğurlu, Ç. Çamsarı, O. Kanyılmaz, A. Kaya, A. Ünsal: *Clinical outcome of magnetic activated cell sorting of non-apoptotic spermatozoa before density gradient centrifugation for assisted reproduction*. *Journal for Assisted Reproduction Genetics* 2008, 25, pp. 375-381.

[136] K. Anslinger, B. Bayer, S.M. Danilov, R. Metzger: *Application of sperm-specific antibodies for the separation of sperm from cell mixtures*. *Forensic Science International: Genetics Supplement Series* 1, 2008, vol. 1, 1, pp. 394-395.

[137] D.L. Garner, B.L. Gledhill, D. Pinkel, S. Lake, D. Stephenson, M.A. van Dilla, L.A. Johnson: *Quantification of the X- and Y-chromosome-bearing spermatozoa of domestic animals by flow cytometry*. *Biology of Reproduction* 1983, vol. 28, 2, pp. 312-321.

[138] B. Bartoov, A. Berkovitz, F. Eltes, A.Kogosowski, Y. Menezes, Y. Barak: *Real-Time Fine Morphology of Motile Human Sperm Cells is Associated With IVF-ICSI Outcome*. *Journal of Andrology* 2002, vol. 23, pp. 1-8.

[139] J. Attila, D. Sakkas, E. Delpiano, S. Cayli, E. Kovanci, D. Ward, A. Ravelli, G. Huszar: *Intracytoplasmic sperm injection: a novel selection method for sperm with normal frequency of chromosomal aneuploidies*. *Fertility and Sterility* 2005, vol. 84, 6, pp. 1665-1673.

[140] T.G. Schuster, B. Cho, L.M. Keller, S. Takayama, G.D. Smith: *Isolation of motile spermatozoa from semen samples using microfluidics*. *Reproductive BioMedicine Online* 2003, 7, 1, pp. 75-81.

[141] L. Xie, R. Ma, C. Han, K. Su, Q. Zhang, T. Qiu, L. Wang, G. Huang, J. Qiao, J. Wang, J. Cheng: *Integration of Sperm Motility and Chemotaxis Screening with a Microchannel-Based Device*. *Clinical Chemistry* 2010, vol. 56, 8, pp. 1270-1278.

[142] D. Shibata, H. Ando, A. Iwase, T. Harata, F. Kikkawa, K. Naruse: *Analysis of sperm motility and fertilization rates after the separation by*

microfluidic sperm sorter made of quartz. Fertility and Sterility 2007, 88, p.S110.

[143] Y.-J. Ko, J.-H. Maeng, B.-C. Lee, S. Lee, S. Y. Hwang, and Y. Ahn: *Separation of progressive motile sperm from mouse semen using on-chip chemotaxis*. Analytical Sciences 2012, vol. 28, 1, pp. 27–32.

[144] P. Bansal, S.K. Gupta: *Binding characteristics of sperm with recombinant human zona pellucida glycoprotein-3 coated beads*. Indian Journal of Medical Research 2009, vol. 130, pp. 37-43.

[145] E.S. Diaz, M. Kong, P. Morales: *Effect of fibronectin on proteasome activity, acrosome reaction, tyrosine phosphorylation and intracellular calcium concentrations of human sperm*. Human Reproduction 2007, vol. 22, 5, pp. 1420-1430.

[146] G. Wennemuth, P.J. Schiemann, W. Krause, A.M. Gressner, G. Aumüller: *Influence of fibronectin on the motility of human spermatozoa*. International Journal of Andrology 1997, vol. 20, 1, pp. 10-16.

[147] J.-P. Frimat, M. Bronkhorst, B. de Wagenaar, J.G. Bomer, F. Van der Heijden, A. Van den Berg, L. I. Segerink: *Make it spin: individual trapping of sperm for analysis and recovery using micro-contact printing*. Lab on a Chip 2014, vol. 14, 15, pp. 2635-2641.

[148] G. Huszar, C.C. Ozenci, S. Cayli, Z. Zavaczki, E. Hansch, L. Vigue: *Hyaluronic acid binding by human sperm indicates cellular maturity*,

viability and unreacted acrosome status. Fertility and Sterility 2003, vol. 79, 3, pp. 1616-1624.

[149] A. Yagci, W. Murk, J. Stronk, G. Huszar: *Spermatozoa Bound to Solid State Hyaluronic Acid Show Chromatin Structure With High DNA Chain Integrity: An Acridine Orange Fluorescence Study*. Journal of Andrology 2010, vol. 31, 6, pp. 566-572.

[150] L. Parmegiani, G.E. Cognigni, S. Bernardi, E. Troilo, S. Taraborrelli, A. Arnone, A.M.Maccarini, M. Filicori: *Comparison of two ready-to-use systems designed for sperm-hyaluronic acid binding selection before intracytoplasmic sperm injection: PICSI vs. Sperm Slow: A prospective, randomized trial*. Fertility and Sterility 2012, vol. 98, 3, pp. 632-637.

[151] L. Parmegiani, G.E. Cognigni, S. Bernhardt, E.Troilo, W. Ciampaglia, M. Filicori: *"Physiologic ICSI": Hyaluronic acid (HA) favors selection of spermatozoa without DNA fragmentation and with normal nucleus, resulting in improvement of embryo quality*. Fertility and Sterility 2010, vol. 93, 2.

[152] V. Magdanz, M. Guix, F. Hebenstreit, O.G. Schmidt: *Dynamic polymeric microtubes for the remote-controlled capture, guidance and release of sperm cells*. Advanced Materials 2016, Advanced Materials 2016, vol. 28, 21, pp. 4084-4089.

[153] H. Feil, Y.H. Bae, J. Feijen, S. W. Kim: *Effect of comonomer hydrophilicity and ionization on the lower critical solution temperature of*

N-isopropylacrylamide copolymers. *Macromolecules* 1993, vol. 26, 10, pp. 2496-2500.

[154] M. A. Cooperstein, H. E. Canavan: *Assessment of cytotoxicity of (N-isopropyl acrylamide) and Poly(N-isopropyl acrylamide)-coated surface*. *Biointerphases* 2013, vol. 8, 1, 19.

[155] I. S. M. Khalil, P. Ferreira, R. Eleutério, C. L. de Korte, and S. Misra: *Magnetic-based closed-loop control of paramagnetic microparticles using ultrasound feedback*. *Proceedings of the IEEE International Conference on Robotics and Automation (ICRA) 2014, Hong Kong, China*, pp. 3807-3812.

[156] A. Sánchez, V. Magdanz, O. G. Schmidt, S. Misra: *Magnetic control of self-propelled microjets under ultrasound image guidance*. *Proceedings of the IEEE RAS/EMBS International Conference on Biomedical Robotics and Biomechatronics (BioRob) 2014, Sao Paulo, Brazil*, pp. 169-174.

[157] G. J. Vrooijink, M. Abayazid, S. Patil, R. Alterovitz, S. Misra: *Needle path planning and steering in a three-dimensional non-static environment using two-dimensional ultrasound images*. *International Journal of Robotics Research* 2014, vol. 33,10, pp. 1361-1374.

[158] G. Hong, J. C. Lee, J. T. Robinson, U. Raaz, L. Xie, N. F. Huang, J. P. Cooke, H. Dai: *Multifunctional in vivo vascular imaging using near-infrared II fluorescence*. *Nature Medicine* 2012, vol. 18, pp.1841-1846.

[159] R. K. Gilchrist, R. Medal, W. D. Shorey, R. C. Hanselman, J. C. Parrott, C. B. Taylor: *Selective Inductive Heating of Lymph Nodes*. Annals of Surgery 1957, vol. 146, 4, pp. 596-606.

[160] D. Debarun, Z. Zhang, T. Winkler, M. Mour, C. I. Günter, M. M. Morlock, H.-G. Machens, A. F. Schilling: *Bioresorption and degradation of biomaterials*. Springer Berlin Heidelberg, 2012, In Tissue Engineering III: Cell-Surface Interactions for Tissue Culture, pp. 317-333.

[161] R. W. Kelly, P. Holland, G. Skibinski, C. Harrison, L. McMillan, T. Hargreave: *Extracellular organelles (prostasomes) are immunosuppressive components of human semen*. Clinical and Experimental Immunology 1991, vol. 86, 3, pp. 550-556.

[162] I. A. Rooney, T. J. Oglesby, J. P. Atkinson: *Complement in Human Reproduction: Activation and Control*. Journal of Immunology Research 1993, 12, pp. 276-294.